NASA TECHNICAL NOTE

NASA TN D-2841

NASA TN D-2841

FACILITY FORM 602

N65-24381 (ACCESSION NUMBER)

72 (PAGES)

(NASA CR OR TMX OR AD NUMBER)

1 (THRU)

(CODE)

30 (CATEGORY)

ANALYSIS OF MARS ENTRY WITH CONSIDERATION OF SEPARATION AND LINE-OF-SIGHT RELAY COMMUNICATION FOR BUS-CAPSULE COMBINATIONS

by E. Brian Pritchard and Edwin F. Harrison

Langley Research Center

Langley Station, Hampton, Va.

GPO PRICE $ _____

OTS PRICE(S) $ 3.00

Hard copy (HC) 1.25

Microfiche (MF) _____

NATIONAL AERONAUTICS AND SPACE ADMINISTRATION • WASHINGTON, D. C. • MAY 1965

NASA TN D-2841

ANALYSIS OF MARS ENTRY WITH CONSIDERATION OF SEPARATION AND LINE-OF-SIGHT RELAY COMMUNICATION FOR BUS-CAPSULE COMBINATIONS

By E. Brian Pritchard and Edwin F. Harrison

Langley Research Center
Langley Station, Hampton, Va.

NATIONAL AERONAUTICS AND SPACE ADMINISTRATION

For sale by the Clearinghouse for Federal Scientific and Technical Information
Springfield, Virginia 22151 – Price $3.00

ANALYSIS OF MARS ENTRY WITH CONSIDERATION OF SEPARATION AND LINE-OF-SIGHT RELAY COMMUNICATION FOR BUS-CAPSULE COMBINATIONS

By E. Brian Pritchard and Edwin F. Harrison
Langley Research Center

24381 ABST

SUMMARY

An analytical study of the deceleration loads, stagnation-point heating, communication time after blackout, and parachute-deployment conditions encountered during Mars atmospheric entry was conducted for several Mars model atmospheres with surface pressures from 10 to 40 millibars. Both steep and shallow entry angles were considered for entry velocities from 20 000 to 32 000 fps, for values of the ballistic parameter from approximately 0.1 to 1.0 slug/ft^2, and values of lift-drag ratio of 0 and 0.5. The requirements for separation and line-of-sight relay communication for the combinations of a fly-by bus and entry capsule were studied in terms of capsule aerodynamics, Martian atmospheric structure, separation distance, bus periapsis distance, hyperbolic excess velocity, and the angle at which the separation-velocity increment was applied.

The results indicate that for a vertical entry requirement the maximum allowable value of the ballistic parameter is less than 0.2 slug/ft^2 for unmanned ballistic entry vehicles capable of either communication with the Earth between blackout and Mars impact for 60 seconds or a soft landing with parachute-deployment velocities of 1000 fps or less. The utilization of a vehicle with a lift-drag ratio of 0.5 was shown to allow a significant increase in the maximum allowable ballistic parameter to values of about 0.3 slug/ft^2. If a terminal guidance system capable of obtaining entry corridors of about 5° is available for such missions, it may be possible to extend the maximum allowable values of the ballistic parameter to about 0.66 and 0.9 slug/ft^2 for the ballistic and lifting vehicles, respectively.

Separation of the entry capsule from the fly-by bus at a distance of 300 Mars radii from the planet requires a separation-velocity increment from about 100 to 300 fps. For steep entry, an effective line-of-sight communication can be maintained from the end of blackout to capsule impact with an increase in the separation-velocity increment of about 15 fps or less. A large increase in this velocity is shown to be required for soft-landing vehicles requiring vertical entry with surface lifetimes of approximately 1 hour if a relay communications link is employed. This velocity increment is reduced by approximately two-thirds by employing shallow entry.

Author

INTRODUCTION

Prior to any manned Mars landing mission it will be necessary to accomplish successfully an unmanned Mars mission program in order to define the characteristics of the Martian atmosphere and surface. The information to be obtained from such an unmanned program is necessary to the design of a safe and efficient manned entry module. An additional objective will be an attempt to determine the existence of life on the planet.

Many studies of the Mars entry problem have been conducted for the model atmospheres with surface pressures from 80 to 120 millibars which, for many years, were thought to be representative of the Martian atmosphere. However, the recent findings of Kaplan (ref. 1), indicative of a Mars atmospheric surface pressure from 10 to 40 millibars, have necessitated new investigations of the Mars entry problem. See, for example, references 2 and 3, which are primarily concerned with the vertical entry of ballistic capsules.

It is the purpose of this study to investigate Mars atmospheric entry from shallow entry to vertical entry with the objective of defining the entry-vehicle requirements based on the present knowledge of the Martian atmosphere. Although the primary emphasis is placed on ballistic entry, the effects of a lifting capability on the entry-capsule requirements are assessed for a vehicle having a lift-drag ratio of 0.5. The results were obtained for values of the ballistic parameter from 0.1 to 1.0 slug/ft^2.

The primary assumptions utilized for this analysis were that the planet is spherical and nonrotating and that the atmosphere could be approximated by a constant lapse rate of the troposphere and an isothermal stratosphere extending from the tropopause to the altitude at which entry is initiated. In addition, it is arbitrarily assumed for the purposes of this study that terminal guidance systems could be developed with the capability of restricting the Mars entry corridor to about 5° or 10°. It is realized, of course, that some additional spacecraft weight would be required to attain this capability. Thus, the weight available for the entry-capsule system would be reduced to some extent and trade-off studies would become necessary in order to define the best system or mode.

It is also the purpose of the present report to analyze the separation and the maintenance of line-of-sight contact of those missions involving the combination of a fly-by bus and an entry capsule. This combination may be desirable for early missions, as pointed out in reference 4 where some of the general problems are discussed. The requirements for separation of the two vehicles and injection of the entry capsule onto a Martian impacting trajectory are assessed in terms of the separation-velocity increment. The effects of parametric variations in the time of separation, angle of separation, and point of closest passage of the bus to the planet on the separation velocity requirements are also defined.

The choice of a relay or a direct communications link between the capsule and Earth depends on many factors such as the particular mission objectives and

restrictions. Thus, in order to maintain flexibility, no attempt is made in this report to define the missions for which the relay system would be superior to the direct system. Rather, the approach taken here is to define only the conditions for which a clear line of sight between the bus and the capsule may be maintained to capsule impact for relay-communication purposes. Furthermore, it was desired to determine the additional constraints placed on two typical missions if a short surface life were required of the capsule.

SYMBOLS

A	cross-sectional area of capsule
a	semimajor axis of a hyperbolic trajectory
C_D	drag coefficient
e	eccentricity of a hyperbolic trajectory
G	deceleration load
g	local acceleration due to gravity
g_e	acceleration due to gravity at Earth's surface
h	altitude
L/D	lift-drag ratio
m	mass of capsule
$\frac{m}{C_D A}$	ballistic parameter
P_o	Mars atmospheric surface pressure
p	semilatus rectum of a hyperbolic trajectory
Q_c	convective stagnation-point heat load
Q_r	radiative stagnation-point heat load
$\dot{q}_c$	convective stagnation-point heating rate
$\dot{q}_r$	radiative stagnation-point heating rate
R_N	capsule nose radius
r	radial distance to center of Mars

t	time
V	velocity
$\Delta V_{s,b}$	velocity decrement applied to bus at separation
$\Delta V_{s,c}$	separation velocity increment required to inject entry capsule on desired course of a specified entry angle (fig. 1)
γ	flight-path angle relative to local horizontal
$\Delta\gamma_E$	entry corridor obtainable with terminal guidance
$\Delta\gamma_s$	difference in flight-path angles of bus and capsule at separation (fig. 1)
Θ	range angle measured from point of entry
θ	orbital central angle (fig. 1)
λ_s	separation angle between bus and capsule (fig. 1)
μ	Mars gravitational constant, 1.5144×10^{15} ft^3/sec^2
ρ	atmospheric density

Subscripts:

b	bus
c	capsule
d	parachute-deployment conditions
E	entry conditions at an altitude of 360 000 feet
h	entry conditions at any arbitrary altitude
i	impact conditions
max	maximum
min	minimum
0	overshoot boundary
p	periapsis conditions
s	separation
∞	conditions where r is infinite

ANALYSIS

Separation

Separation of a fly-by bus and an entry capsule must occur at relatively large distances from the planet in order to insure that separation velocities are not excessive, with the restriction that the fly-by bus must not impact the planet. A primary concern of the present study was, therefore, the determination of the velocity increment $\Delta V_{s,c}$ required to inject an entry capsule on the desired course of entry at a given angle γ_E. The geometry and parameters associated with this separation maneuver, as well as the bus and capsule trajectories, are presented in schematic form in figure 1.

It is assumed in this phase of the analysis that the vehicles are acted upon only by the Martian gravitational field and that the vehicle trajectories are hyperbolic in form (the effect of the solar gravitational field on the trajectories is discussed in the section entitled "Results and Discussion").

In order to define the trajectories of the fly-by bus and the entry capsule, a number of conditions are required. (See fig. 1.) The conditions required for the bus trajectory are:

(1) Vehicle hyperbolic excess velocity V_∞ at Mars

(2) Distance from Mars at which vehicles separate r_s

(3) Periapsis distance of fly-by trajectory $r_{p,b}$

The conditions required for the capsule trajectories are:

(1) Distance from Mars at which vehicles separate r_s

(2) Capsule entry angle γ_E

(3) Distance from Mars center to edge of atmosphere r_E

(4) Resultant velocity of the capsule at separation $V_{s,c}$

In the present analysis, a set of nominal conditions was selected, and each parameter was systematically varied about the nominal value to determine its influence on the problem. These nominal conditions were:

$r_{p,b}$ = 2.5 Mars radii (5283 int. statute miles)

r_s = 300 Mars radii (633 900 int. statute miles)

V_E = 26 000 fps

V_∞ = 20 323 fps

$$\lambda_s = 90^\circ$$

The equations necessary to the solution of the problem are very well known (e.g., see ref. 5) and, therefore, are presented in the appendix with a minimum of discussion.

Entry

In the analysis of atmospheric entry, two factors are of primary interest; these are the velocities with which a spacecraft might be reasonably expected to encounter a planet, and the physical characteristics of the planet and its atmosphere.

The velocity at which a spacecraft encounters the atmosphere of Mars is dependent on the trip time and the location of Mars in its orbit, as indicated by figure 2. (See ref. 6.) Although minimum velocities as low as about 19 000 fps are possible for long trip times, short trip times are highly desirable from the standpoint of reliability and communications. On this basis, a nominal entry velocity of 26 000 fps was selected for study. The effects of a variation in entry velocity were obtained, however, by considering, to a limited extent, the additional entry velocities of 20 000 fps and 32 000 fps.

The Martian model atmospheres employed in this study (fig. 3) represent the results of the analysis of reference 7, which is based on the observations of Kaplan (ref. 1). Reference 7 recommends that these models be used in future studies, sponsored by the NASA, of Mars entry in order to facilitate the interpretation of the results of such studies. Since any vehicle design must be based on the extreme conditions represented by the upper and lower atmospheres (40 and 10 millibars, respectively), the mean model atmosphere was not utilized in this investigation Of the two lowest atmospheres shown in figure 3(b), the primary emphasis has been placed on the atmosphere having a surface temperature of 540° R (model atmosphere 4) since this temperature has been postulated by a number of astronomers to be the equatorial dayside temperature. The advantages of dayside landings are numerous, and it appears reasonable that an entry-capsule mission would be designed on such a basis.

Entry is assumed to be initiated at an altitude of 360 000 feet for the low-density atmospheres where the magnitude of the atmospheric density is approximately equivalent to the Earth's atmosphere at an altitude of 400 000 feet. A specific entry altitude is required since the free-space trajectories and the entry trajectories must be matched at the altitude where atmospheric effects become of importance. Figure 3 indicates that atmospheric effects become important at much higher altitudes for model atmospheres 1 and 2 than for model atmospheres 3 and 4. Thus, the entry and free-space trajectories must be matched at altitudes in excess of 700 000 feet for model atmosphere 1. In order to compare the results obtained for entry into the several atmospheres considered, it is necessary to relate the entries to a common set of initial conditions (i.e., initial entry velocity and entry angle). Thus, an altitude of 360 000 feet was chosen as the altitude at which the entry angle is to be defined for all atmospheres. The equivalent vacuum entry angle at an altitude

of 360 000 feet is obtained in terms of the entry angle at the altitude for which atmospheric effects are first encountered from the relation

$$\cos \gamma_E = \frac{\cos \gamma_h}{\bar{V}_E}\sqrt{\frac{2r_h}{r_E} + \frac{r_h^2}{r_E^2}\left(\bar{V}_E^2 - 2\right)}$$

where $\bar{V}_E$ is the ratio of the entry velocity to the local circular velocity and is approximately constant for the range of entry altitudes considered.

In the present analysis, the overshoot boundary is defined by entry at that angle for which the entry capsule pulls out and "skips" to a maximum altitude equal to the initial entry altitude but does not exit the atmosphere. No limitation or definition has been placed on the undershoot boundary since unmanned capsules could be designed for vertical entry.

The trajectories traversed by the entry capsule during atmospheric flight were obtained by numerical integration with a high-speed digital computer of the well-known equations of motion in the following form:

$$\frac{1}{g}\frac{dV}{dt} = -\frac{\rho V^2}{2g}\frac{1}{m/C_D A} - \sin \gamma$$

$$\frac{1}{g}\frac{d\gamma}{dt} = \frac{\rho V}{2g}\frac{L/D}{m/C_D A} - \frac{\cos \gamma}{V}\left(1 - \frac{V^2}{rg}\right)$$

$$\frac{dh}{dt} = V \sin \gamma$$

and

$$\frac{d\Theta_c}{dt} = \frac{V}{r}\cos \gamma$$

In the present study, both ballistic and lifting vehicles have been considered. It is assumed that control over the lifting vehicle is asserted only to the extent that the lift is always directed upward (positive) with respect to the planet and the pitch and roll attitudes remain unchanged during entry. This assumption is important since the full potential of the use of lift can not be realized because of the lack of a maneuvering capability. However, for simplicity of the entry capsule, only a constant lift coefficient was selected for study with the realization that later, more sophisticated entry vehicles could utilize lift modulation or control to a far greater advantage.

The purpose here is only to determine whether a simple lifting entry capsule can alleviate the two primary problems associated with the entry of early

unmanned vehicles into a shallow planetary atmosphere. These two problems are the communication-time problem for impacting capsules and the parachute-deployment problem for soft-landing capsules. It is not the purpose of this study to minimize the heating loads or heating rates, the result of which could be obtained if the lift were controlled during entry. Thus, in order to offset the tendency of the vehicle with constant lift coefficient to skip out of the atmosphere, the present use of lift will require much steeper entry at the overshoot boundary than either the ballistic vehicle or the vehicle with controlled lift.

Heating

In a study such as this, it is highly desirable to maintain a generality of results. For this reason, only stagnation-point heating rates and loads have been assessed.

In reference 8 it is indicated that the stagnation-point convective heating rates may be approximated by the same equations for both Mars and Earth atmospheric entry. Thus, in this study the following expression was used:

$$\dot{q}_c\sqrt{R_N} = \left(20.4 \times 10^{-9}\right)\rho^{1/2}V^3$$

where $\dot{q}_c$ is given in units of Btu/ft^2-sec and R_N, in units of feet.

In an attempt to define the radiative stagnation-point heating, the experimental results obtained in reference 9 were analyzed for a hypothetical atmosphere having a composition of 10.5 percent CO_2 and 89.5 percent N_2. It is assumed for this analysis that the ratio of the shock detachment distance to the nose radius has a value of 0.045. In reference 8 a value of unity for the density exponent is utilized in the analysis; also pointed out is the fact that nonequilibrium radiation heating may occur for shallow entry. In the present analysis, a density exponent of 0.85 is chosen in an attempt to account, at least partially, for both nonequilibrium and ablation-product radiation. The results presented here should therefore be considered to be only a rough estimate because of the restricted range of validity of the experimental data on which they are based. The equation obtained in this analysis for the radiative stagnation-point heating is:

$$\frac{\dot{q}_r}{R_N} = \left(2.34 \times 10^4\right)\rho^{0.85}\left(\frac{V}{10^4}\right)^{7.25}$$

where $\dot{q}_r$ is in terms of Btu/ft^2-sec.

Of course, much more definitive experimental and theoretical analyses are required in order to resolve the present uncertainties regarding the radiative-heating environment for Mars atmospheric entry.

Communication

An important requirement of the relay communication system between the bus and capsule is that line-of-sight transmission be available between the two vehicles. The limiting condition for line-of-sight communication is defined in the present analysis as the condition for which the angle between the planetary radius vector and the transmission line between the bus and capsule is equal to 90° at impact of the capsule on the Martian surface. A necessary assumption is, of course, that the planet be spherical and nonrotating.

The procedure for the determination of those conditions for which a clear line-of-sight transmission is available to capsule impact is as follows:

(1) Select values for γ_E, $\frac{m}{C_D A}$, and L/D. The time of flight from separation to entry may be computed from equation (A8) or (A13). The time from entry to impact is obtained from the numerical integration of the well-known equations of motion on a high-speed digital computer. It is also necessary to define the angle $\theta_{c,i}$ from the general equation (A7) and the entry program.

(2) For this time of flight from separation to impact of the capsule, it is necessary to determine the corresponding location of the bus. Its location is obtained in terms of θ_b and r_b, corresponding to the flight time computed in step (1).

(3) Obtain a value of $\Delta\theta = \theta_{c,i} - \theta_b$.

(4) Plot this value against r_b for each entry angle and entry vehicle to obtain a carpet plot, as shown in sketch (a).

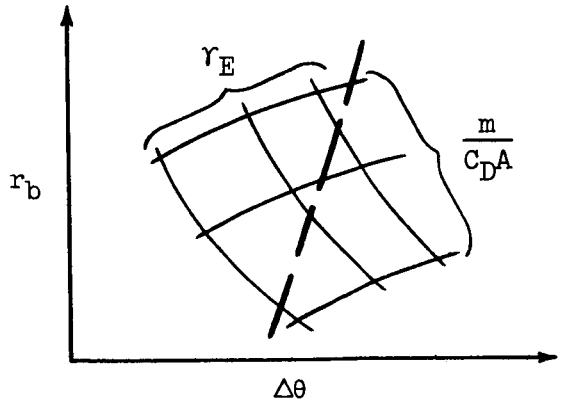

Sketch (a)

(5) The limiting line-of-sight condition is defined from geometry by $\Delta\theta = \cos^{-1}\frac{r_{c,i}}{r_b}$ (dashed line in sketch (a)).

(6) The conditions to the left of the dashed line in sketch (a) allow line-of-sight transmission between the fly-by bus and the capsule at impact; the conditions to the right do not.

Curves may then be obtained of $\frac{m}{C_D A}$ plotted against γ_E for various separation conditions. Thus, the lowest value of $\frac{m}{C_D A}$ may be obtained for which relay communication between the fly-by bus and the entry capsule is available until the point of impact of the capsule with the planet surface.

An important assumption in the preceding analysis is that the planet is spherical and nonrotating. Since a point on the Martian equator rotates at about 15° per hour, it is apparent that the effect of planetary rotation on the problem of line-of-sight relay communication is important in the consideration of communication time after landing of a capsule. Thus, in the study of a particular mission it would be desirable to include a more detailed analysis of the line-of-sight problem which would consider probable landing sites as well as the effects of planetary rotation.

RESULTS AND DISCUSSION

Separation

There are many factors to be considered in the definition of the time, or point, at which separation of an entry capsule from the fly-by bus should be accomplished. One prime factor is that adequate time must be available after separation and before entry in order that reorientation of the spacecraft, check-out of the instrumentation, and testing of the communications link may be completed. A typical time history of the bus trajectory (fig. 4) indicates that for reasonable separation distances from about 100 to 500 Mars radii (ref. 10) adequate time is probably available without further restricting the problem. Of primary importance, then, is the effect of the trajectory factors on the propulsive-velocity increment required to carry out the separation maneuver. Thus, the effects of separation distance, bus periapsis distance, hyperbolic excess velocity, separation angle, and entry angle on the required separation velocity have been determined and are presented in figures 5 to 8.

The effect of the separation distance (i.e., distance from the planet to the spacecraft at the time of separation) is shown in figure 5. The required increase in separation velocity is approximately inversely proportional to the decrease in the available separation distance attained for a particular value of entry angle. The effect of entry angle on the propulsive velocity required for the separation maneuver is shown to be large; the separation velocity must be doubled for an increase in entry angle from 10° to 110°.

It should be noted at this point that, for an actual mission, the spread in entry angle will be due to a combination of uncertainties in the knowledge of the bus periapsis distance, separation distance, and separation angle, all

of which depend on the accuracy of the guidance system. In the present study it was considered more desirable to investigate each parameter in turn and determine its effect on the separation problem rather than to attempt an error analysis necessarily based on state-of-the-art or hardware considerations.

It should also be noted that the radius of the Martian sphere of activity for trajectory considerations has been estimated at about 170 Mars radii. Thus, the validity of the assumption that the spacecraft are influenced only by the Martian gravitational field is open to question. Preliminary estimates indicate, however, that the solar influence, while significant in single vehicle considerations, may be neglected when considering the motion of one vehicle relative to another for the range of conditions considered in this study. For instance, a maximum error in the separation-velocity increment between the bus and capsule of about 2 percent is obtained by neglecting the solar influence.

Although small separation velocities are required for separation at extreme distances from the planet, the position of the vehicle, with respect to Mars, is known to a lesser degree of accuracy than for vehicles near Mars. Hence, for subsequent results, a nominal separation distance of 300 Mars radii was selected. This distance corresponds to a travel time of about 1.9 days from separation to Mars encounter (fig. 4) and requires separation velocities from 100 to 220 fps for the entry-angle range considered.

The effect of bus periapsis distance on the separation velocity requirements is shown in figure 6 for the nominal separation distance of 300 Mars radii and a typical entry velocity of 26 000 fps with separation normal to the initial flight path. Small changes in bus periapsis distance are shown to result in large changes in entry angle for a given separation velocity. Note also that the effect of entry angle on the velocity requirement, for a given value of $r_{p,b}$, is greatest for the closest passage to the planet.

Another important factor influencing the separation-velocity requirement is the hyperbolic excess velocity, which dictates the vehicle velocity at the separation point. Figure 7 demonstrates the effect of a variation in this parameter which is equivalent to a variation in nominal entry velocity from 20 000 to 32 000 fps. Reductions in V_∞ are shown to allow reductions in the separation velocity. For the range of V_∞ considered, it is shown that the effects of entry angle (from 10° to 110°) are slightly greater than the effects of hyperbolic excess velocity.

The results of figures 5 to 7 were obtained for a separation angle λ_s of 90°. The effect of this parameter was investigated in some detail, and the results are presented in figure 8 for the nominal conditions. As shown, minimum separation velocity is obtained for a separation angle of about 90°. As expected, a slight variation in the minimum point (less than 2°) with entry angle is obtained. Since the effect of λ_s on the separation velocity is large at angles much away from 90°, it is apparent that the separation angle should be maintained near 90°. The ratio of the separation velocities for two given entry angles is essentially independent of λ_s. For instance, the ratio of the separation velocity required for an entry angle of 10° to the separation velocity required for an entry angle of 90° is about 1.9.

The effects of the primary factors influencing the separation velocity requirement which have been demonstrated in figures 5 to 8 indicate that the most important factor is the location of the spacecraft with respect to Mars and, in particular, $r_{p,b}$. Also of importance is the angle at which the separation-velocity increment is applied.

Overshoot Boundary

In this study of Mars atmospheric entry it has been assumed that unmanned vehicles, capable of vertical entry, are feasible. Consequently, an undershoot boundary is not required. The overshoot boundary, defined by entry at the angle γ_0 for which the vehicle enters, pulls out, and skips to an altitude equal to the assumed height of the sensible atmosphere, is shown in the sketch in figure 9. The actual values of the overshoot entry angle are presented in figure 9 for the range of $\frac{m}{C_D A}$ of interest. Only the two lower atmospheric models are considered since the overshoot boundary must logically be defined by the thinner atmospheres. As one might anticipate, lower values of the overshoot entry angle are obtained for atmosphere 4 than for atmosphere 3 because of the higher densities at high altitudes for this atmospheric model. Note also that the effect of $\frac{m}{C_D A}$, at least in the range investigated, is relatively minor.

The effects of entry velocity and lift are presented only for atmosphere 4, the low-density dayside model atmosphere. As expected, an increase in entry velocity accompanies an increase in the overshoot-boundary entry angle. The utilization of a lifting vehicle ($L/D = 0.5$) is shown to increase this boundary greatly. If, however, modulation of the lift during entry were allowed, the overshoot entry angle for the lifting case shown would be somewhat less than that for the ballistic entry case.

The values of $-\gamma_0$ presented in figure 9 are used hereafter in discussing the effects of a terminal guidance capability utilized to obtain some nominal entry corridor. As shown in the sketch in figure 9, the entry corridor may be defined in terms of $\Delta\gamma_E$ and is always measured from the overshoot boundary. Thus, when a nominal entry corridor of $\Delta\gamma_E$ is considered, the range of entry angle which must be considered is from $-\gamma_0$ to $-(\gamma_0 + \Delta\gamma_E)$. The results of this study are presented for entry at the angles $-\gamma_0$ and $-(\gamma_0 + \Delta\gamma_E)$ for terminally guided vehicles and at the angles $-\gamma_0$ and -90° for vehicles without terminal guidance.

Deceleration Loads

The maximum deceleration loads encountered during Mars atmospheric entry are presented in figures 10 to 12. First, consider the effect of model atmosphere on the maximum deceleration loads for the ballistic entry case shown in figure 10. Here, it is seen that the largest effect of model atmosphere is

exhibited for the vertical-entry case. It should be noted that analytical solutions are available for the determination of the maximum deceleration load encountered during ballistic entry at steep angles into exponential atmospheres. Reference 11, for example, points out that, if the maximum deceleration loads are encountered in the isothermal layer of the atmosphere, the maximum loads will be independent of the value of the ballistic parameter $\frac{m}{C_D A}$. The maximum deceleration loads will then be affected by $\frac{m}{C_D A}$ only if the maximum deceleration occurs in the troposphere. For the vertical-entry case, as shown in figure 10, the peak deceleration loads occur within the troposphere for model atmosphere 4 and for the range of $\frac{m}{C_D A}$ considered. For model atmosphere 3, the peak deceleration loads occur within the troposphere for $\frac{m}{C_D A} > 0.15$ slug/ft^2 and within the stratosphere for $\frac{m}{C_D A} < 0.15$ slug/ft^2. In the case of model atmosphere 1, the maximum deceleration occurs in the stratosphere for the range of $\frac{m}{C_D A}$ shown and is therefore only a function of the density gradient, entry velocity, and entry angle. The difference between the curves for atmospheres 3 and 4 is predominantly due to the differences in the effective density gradient at the point of maximum deceleration.

If a terminal guidance capability is available to the spacecraft, the maximum deceleration loads can obviously be greatly reduced. In this study, therefore, it has been arbitrarily assumed for comparative purposes that systems could be developed with the capability of restricting the vacuum corridor to 5° or 10° at an altitude of 360 000 feet. The effectiveness of terminal guidance in the reduction of maximum deceleration is illustrated in figure 10 by the curves for a nominal corridor width $\Delta\gamma_E$ of 5° measured from the overshoot boundary. The effect of $\frac{m}{C_D A}$ on G_{max} is also reduced somewhat by entry-corridor reduction.

The influence of both the degree of terminal guidance and the lift-drag ratio on the maximum deceleration loads is presented in figure 11 for atmosphere model 4. For vertical entry, increasing the L/D of the capsule from 0 to 0.5 results in only a moderate increase in G_{max}. However, for a corridor width of either 5° or 10°, the same increase in L/D results in large increases in the maximum deceleration loads. This effect is produced by the relatively steep overshoot entry angle required for the capsule with L/D = 0.5. The reduction in the influence of $\frac{m}{C_D A}$ on G_{max} by decreasing the corridor width is also demonstrated in figure 11.

The final factor influencing the magnitude of G_{max} is the entry velocity. As shown in figure 12, the deceleration loads are increased by an increase in the entry velocity. The influence of entry velocity is seen here to be more

pronounced for low values of $\frac{m}{C_D A}$ inasmuch as the maximum deceleration occurs at higher altitudes where the effective density gradient is greater.

In application to manned entry, it appears, for the vehicles considered here, that reducing the entry velocity may be a more effective means of reducing the deceleration loads to human tolerances than decreasing the entry corridor, unless very small corridors can be attained. It should be pointed out, however, that the overshoot entry angle and therefore the overshoot-boundary deceleration loads for the lifting vehicle could be reduced below the overshoot values obtained for the ballistic vehicle if a lifting vehicle which has the capability of lift modulation by either roll or pitch control were utilized.

Aerodynamic Heating

A knowledge of both maximum stagnation-point heating rates and total heat loads is required for heat-shield design. The results of the present approximate heating analysis are presented in terms of these quantities in figures 13 to 22.

First, consider the effect of atmospheric model on the maximum radiative heating rates, as shown in figure 13, for both vertical entry and shallow entry with terminal guidance. As one might expect, the atmospheric models with the steepest density gradient produce the highest heating rates. Atmosphere 4 produces lower heating rates than atmosphere 3 at all but the lowest values of $\frac{m}{C_D A}$ because maximum heating does not occur for entry into atmosphere 4 until the capsule has penetrated the isothermal layer and is traveling through the troposphere where the average density gradient is greatly reduced. Also, a reduction in the entry corridor greatly decreases the maximum radiative heating rate, a well-known effect.

The effect of lift on the maximum radiative heating rate is presented in figure 14 for atmosphere 4. A similar effect to that indicated for the maximum deceleration loads is obtained. That is, the utilization of a capsule with $L/D = 0.5$ results in a moderate increase in the radiative heating rate for vertical entry and in a large increase for shallow entry. This effect for shallow entry is essentially due to the difference in the overshoot entry angle required for the ballistic and lifting vehicles. Decreasing the corridor width is also shown to reduce the influence of $\frac{m}{C_D A}$ on the radiative heating rate and, as expected, minimum values of $\frac{m}{C_D A}$ result in minimum heating rates.

Radiative heating rates are shown in figure 15 to increase rapidly with increasing entry velocity. Since the heating rate also increases rapidly with $\frac{m}{C_D A}$, there appears to be some possibility of trading off $\frac{m}{C_D A}$ for entry velocity while maintaining the same maximum heating rate.

At the nominal entry velocity of 26 000 fps, the convective stagnation-point heating rate is indeed the dominant contributor to the total heating rate

for a vehicle with a nose radius of 1 foot, as may be seen by comparing figures 16 and 13. Of course, the actual value of the nose radius plays an important role in the definition of total stagnation-point heating rates and loads and in the determination of the dominant heating mechanism.

The general effect of atmospheric model on the convective heating rate is essentially the same as that obtained for the radiative heating rate. However, reducing the entry corridor to 5° brings about a reduction in the maximum convective heating rate by only a factor of 2, whereas the radiative heating is reduced by a factor of 3. Also, the convective heating rate is shown to be slightly less influenced by $\frac{m}{C_D A}$ than was the radiative heating.

The influence of lift on the convective heating rates is shown in figure 17 to be essentially the same as it was on the deceleration loads and radiative heating rates. A moderate increase is obtained for a capsule with $L/D = 0.5$ that enters the atmosphere at 90° in comparison with a ballistic capsule. For shallow entry, the increase in convective heating rate becomes large for the same reason as discussed previously; that is, the difference required in the overshoot angle for the ballistic and lifting vehicles. This figure also indicates a reduction in the influence of $\frac{m}{C_D A}$ on the convective heating rates by a reduction in corridor.

A comparison of figures 15 and 18 demonstrates that a variation in entry velocity does not influence the convective heating rates to as great an extent as the radiative heating rates. This variation is, nonetheless, a significant influence since an increase of some 570 Btu/ft^2-sec (or over 300 percent) is obtained for an increase in entry velocity from 20 000 to 32 000 fps for a capsule with $R_N = 1$ foot and $\frac{m}{C_D A} = 1.0$ $slug/ft^2$. (See fig. 18.) Again, note that the effect of $\frac{m}{C_D A}$ is reduced by reducing the entry velocity. Also, entry-velocity reduction may be more advantageous than entry-corridor reduction beyond the first large reduction from vertical entry to shallow entry. (See figs. 17 and 18.) For instance, reducing the corridor from 10° to 5° (fig. 17) reduces the maximum convective heating rate from 403 to 337 Btu/ft^2-sec for $\frac{m}{C_D A} = 1.0$ $slug/ft^2$ and $R_N = 1$ foot. However, the same result can be obtained by an entry-velocity reduction of about 1400 fps. (See fig. 18.) A detailed systems analysis is, of course, required to determine which method might be the more attractive.

Maximum heating loads will be obtained for entry into model atmosphere 1 since this atmosphere has the lowest value of the density gradient. For this reason, model atmosphere 1 is the only atmosphere which is considered in the following discussion concerning stagnation-point heat load.

The total radiative heating load is presented in figure 19 for an entry velocity of 26 000 fps and for both ballistic and lifting vehicles. Since maximum heat loads were obtained for entry at the overshoot boundary, only the overshoot and vertical entry cases are shown. The major factor influencing

the radiative heat load, insofar as capsule design is concerned, appears to be $\frac{m}{C_D A}$, and not L/D. Only relatively minor effects are obtained by increasing the vehicle L/D, a result which is predominantly due to the difference in the overshoot entry angle. Note that for vertical entry, Q_r appears to be independent of L/D, at least to L/D = 0.5.

The effect of entry velocity is very large, as indicated by figure 20, and the variation is essentially the same as that obtained for the maximum heating rates.

The convective heat loads presented in figure 21 demonstrate a greater dependence on L/D than does the radiative heat load. Also, the heat loads are decreased to a greater extent by the use of a vertical entry mode where L/D effects appear to be negligible. Though demonstrating a reduction in heat load, the results obtained for L/D = 0.5 at the overshoot boundary are available only at the expense of increased heating rates and deceleration loads.

The influence of entry velocity on the convective heat loads is presented in figure 22 for model atmosphere 1, L/D = 0, and $-\gamma_E = \gamma_0$. A comparison of figures 20 and 22 demonstrates the greater dependence of Q_r on the entry velocity. The following table presents a comparison of the results of these figures for a ballistic vehicle with R_N = 1 foot and for several values of $\frac{m}{C_D A}$.

V_E, fps	Values of Q_r/Q_c for $m/C_D A$, slug/ft^2, of -		
	0.25	0.5	1.0
20 000	0.04	0.05	0.06
26 000	.12	.15	.19
32 000	.30	.37	.45

The effect of vehicle nose radius on the stagnation-point heating loads for a typical ballistic vehicle with $\frac{m}{C_D A} = 0.5$ slug/ft^2 is presented in the following table:

R_N, ft	Values of Q_r/Q_c for V_E, fps, of -			Values of $Q_r + Q_c$, Btu/ft^2, for V_E, fps, of -		
	20 000	26 000	32 000	20 000	26 000	32 000
0.25	0.0063	0.019	0.046	12 880	22 417	32 840
.5	.0177	.0537	.130	9 210	16 405	23 075
1.0	.050	.152	.366	6 720	12 670	21 450
[a]1.231			.50			[a]21 220
2.0	.1414	.430	1.035	5 165	11 120	22 600
[a]2.215		.50			[a]11 100	
4.0	.40	1.215	2.93	4 480	12 180	30 850
[a]4.65	.50			[a]4 462		

[a]Nose radius for which minimum stagnation-point total heat load is obtained.

Note that the value of the nose radius for which the minimum total heat load is obtained decreases with increasing entry velocity (the ratio of Q_r to Q_c is always 0.50 for the minimum total heat load). Thus, it is necessary to decrease the vehicle nose radius if the anticipated entry velocity is increased for a single value of $\frac{m}{C_D A}$. It should be pointed out, however, that the optimum conditions from the standpoint of stagnation-point heating are not necessarily the conditions for which minimum total heat-shield weights are obtained.

The aerodynamic heating is strongly influenced by entry velocity, ballistic parameter, model atmosphere, and entry angle. In general, increasing $\frac{m}{C_D A}$ results in increased stagnation-point heating rates and loads. The use of terminal guidance to reduce the entry corridor is advantageous in reducing the maximum stagnation-point heating rates, even though entry-velocity reduction may be a more effective means. In particular, the use of shallow entry is of no advantage for stagnation-point heat-load reduction, whereas entry-velocity reduction is most effective.

Communication Time

The concept of a minimum mission type of Mars atmospheric probe allows the vehicle to be destroyed on impact. The information obtained during entry must then be transmitted during the period between the cessation of blackout and impact (blackout ends at about 10 000 fps). The time available for this transmission of information is defined as the communication time and is presented in figures 23 to 25. Several studies have considered this communication problem for simple atmospheric probes. Reference 2 indicates that about 15 seconds of communication time should be adequate, whereas reference 12 indicates that 30 seconds or more may be required to obtain a significant amount of information. Because of this uncertainty, it appears not unreasonable to assume that

a communication time of 1 minute may be required for the capsule to reestablish contact with the fly-by bus and transmit the accumulated data. On this basis then, as shown in figure 23, the value of $\frac{m}{C_D A}$ for the entry capsule must be less than 0.2 slug/ft^2 if the capsule is to be capable of vertical entry into model atmospheres 3 and 4. A considerable increase in communication time is gained if a terminal guidance capability allows an entry corridor of 5°. For the worst atmosphere (model atmosphere 3), a 1-minute communication time is available for a capsule with terminal guidance and with $\frac{m}{C_D A} = 1.0$ slug/ft^2.

The use of a capsule with a lift-drag ratio of 0.5 also gains an increase in communication time, as shown in figure 24. For vertical entry, a 1-minute communication time is available with $\frac{m}{C_D A} = 0.36$ slug/ft^2 for $L/D = 0.5$ as compared with $\frac{m}{C_D A} = 0.18$ for $L/D = 0$. The increase in available time for communication is even more pronounced for shallow entry when detailed atmospheric measurements could be obtained and transmitted in real time.

Since the capsule must decelerate to a velocity of about 10 000 fps before communicating with the bus, the initial entry velocity has a relatively minor influence on the communication time. (See fig. 25.)

It is readily apparent from figures 23 to 25 that reasonable communication times need not require very low values of $\frac{m}{C_D A}$. On the contrary, a ballistic vehicle utilizing a terminal guidance system capable of a 10° entry corridor can yield reasonable communication times with an $\frac{m}{C_D A}$ of about 0.8 slug/ft^2. (See fig. 24.) A lifting vehicle with $L/D = 0.5$ and $\frac{m}{C_D A} \approx 0.36$ slug/ft^2, but without terminal guidance, is also capable of achieving adequate communication times. These two approaches should be investigated further to determine the feasibility or desirability of such approaches in comparison with the minimum value of $\frac{m}{C_D A}$.

Parachute Deployment

A soft landing, which probably will require some type of parachute descent, is a desirable objective for future missions. For this reason, parachute-deployment conditions for Mars entry vehicles were obtained and are presented in figures 26 to 28. The effect of the atmospheric model on the altitude at which the parachute is deployed is demonstrated in figure 26 for both vertical and shallow entry and for a vehicle velocity of 1000 fps at deployment.

For vertical entry, parachute deployment in the two lower atmospheres, at reasonable altitudes (greater than or equal to 20 000 feet) requires very low values of $\frac{m}{C_D A}$ (less than 0.2 slug/ft^2). The densest atmosphere raises this

requirement significantly $\left(\frac{m}{C_DA} \approx 0.8\right)$. The alternative, shallow entry with terminal guidance, results in parachute deployment in the low-density atmosphere at an altitude of 20 000 feet with a $\frac{m}{C_DA}$ of about 0.66 slug/ft^2. As expected, relatively high values of $\frac{m}{C_DA}$ are feasible if atmosphere 1 is encountered.

The influence of lift is indicated in figure 27 for two nominal parachute-deployment velocities, 1000 and 3000 fps, corresponding to Mach numbers of approximately 1 and 3, respectively. For vertical entry, it is seen that the $\frac{m}{C_DA}$ requirement may be increased from 0.19 to 0.3 slug/ft^2 by the utilization of a vehicle with $L/D = 0.5$ for parachute deployment at an altitude of 20 000 feet and at a velocity of 1000 fps. On the other hand, increasing the velocity at deployment to supersonic values also allows an increase in the maximum $\frac{m}{C_DA}$. In fact, an increase in parachute-deployment velocity to about 3200 fps is equivalent to an increase in L/D from zero to 0.5 for vertical entry. For shallow entry, the lifting vehicle is far superior to the ballistic vehicle. Parachute deployment at an altitude of 20 000 feet and a velocity of 1000 fps is possible for a lifting vehicle with $\frac{m}{C_DA} \approx 0.9$ slug/ft^2, as compared with $\frac{m}{C_DA} \approx 0.66$ slug/ft^2 for the ballistic vehicle. Note that for a supersonic parachute deployment at a velocity of about 3000 fps, the deployment altitude is in excess of 130 000 feet for the range of $\frac{m}{C_DA}$ considered here. Parachute deployment at such high altitudes might be desirable for purposes of surface photography or extensive atmospheric sampling.

The effect of entry velocity on the parachute-deployment conditions is relatively minor, as indicated in figure 28. The greatest effect occurs at shallow entry angles for which an increase in $\frac{m}{C_DA}$ of approximately 0.09 slug/ft^2 may be obtained by reducing the entry velocity from 32 000 to 20 000 fps.

The advantages of terminal guidance and/or lift are shown to be pronounced and appear to be more desirable than the low $\frac{m}{C_DA}$ approach for soft-landing missions. The possibility of trading lift to obtain increased parachute-deployment velocities is also indicated. The desirability of a lifting vehicle with low parachute-deployment velocities as opposed to a ballistic vehicle with high-supersonic parachute-deployment velocities depends, to a great extent, on reliability considerations for the two systems. The present results do indicate, however, the desirability of more detailed systems studies of these approaches.

Relay Communication Between Fly-By Bus and Entry Capsule

One major problem in relay communication between the entry capsule and the fly-by bus is that of maintaining a clear line-of-sight transmission link between the two vehicles. Obviously, some entry angle exists for which the bus is on the horizon at the time of impact of the capsule. Any increase in entry angle will then result in an interruption in transmission prior to the capsule impact. The limiting entry angle can be expected to be greatly influenced by a variation of the trajectory parameters. Thus, the effect of such a variation has been determined for the particular case of an impacting atmospheric capsule with no terminal deceleration system.

Since the line-of-sight communication problem is greatest for the condition of a maximum flight time in the atmosphere, the emphasis is placed on entry into atmosphere 1 in this phase of the study. As shown in figure 29, fairly long atmospheric flight times can be obtained, particularly for the lower values of $\frac{m}{C_D A}$. The sum of the flight times of the capsule from bus-capsule separation to entry and from entry to impact then dictate the location of the bus at impact of the capsule. The procedure outlined in the analysis section of this report is then utilized to define the "limiting" condition.

A shallow entry angle actually presents little problem in communication line-of-sight maintenance since the capsule is on the same side of the planet as the bus. Steep entry would be expected to be somewhat more of a problem, however, as may be seen in the sketch in figure 30. In this figure, the effect of either an increase in the capsule separation velocity or a reduction in the bus velocity on the limiting entry angle for line-of-sight communication to capsule impact is demonstrated. The region to the left of any curve is available for clear line-of-sight communication to capsule impact. In the region to the right of any curve, communication is blocked by the Martian horizon prior to impact. For relay communication at the point of impact with minimum separation velocity, the limiting entry angle is denoted by the minimum $\Delta V_{s,c}$ curve and varies from -63° to -93° for the range of $\frac{m}{C_D A}$ considered. The numerical values of this minimum $\Delta V_{s,c}$ curve are obtained directly from figure 8 for a value of λ_s of 90° and are shown in the insert of figure 30. The entry angle limited by relay communication may be increased by either increasing the separation-velocity increment applied to the entry capsule above the minimum to achieve a given entry angle or by applying a propulsive velocity decrement $\Delta V_{s,b}$ to the bus in addition to the minimum capsule separation velocity.

The increase in $\Delta V_{s,c}$ to achieve an increased communication capability is denoted by lines of constant $\Delta V_{s,c}$. At the intersection of a constant $\Delta V_{s,c}$ curve with the minimum $\Delta V_{s,c}$ curve, the actual minimum $\Delta V_{s,c}$ is given $\left(\text{i.e., at } \frac{m}{C_D A} = 0.25, \quad (\Delta V_{s,c})_{min} = 175 \text{ fps}\right)$.

In comparing the two methods for increasing the communication time and, therefore, the entry angle available for the relay-communication mission, it

appears to be more efficient, in terms of the velocity increment, to increase $\Delta V_{s,c}$ rather than to apply a velocity decrement $\Delta V_{s,b}$ to the bus. For instance, at $\frac{m}{C_D A} = 0.15$ slug/ft^2, applying a $\Delta V_{s,b}$ of -50 fps increases the available entry angle for which line-of-sight communication is possible until the point of capsule impact from -73° to -91°. The same result is obtained by increasing the capsule separation velocity $\Delta V_{s,c}$ to about 200 fps. The minimum $\Delta V_{s,c}$ curve indicates that a $\Delta V_{s,c}$ of 190 fps is required to achieve a -90° entry angle without regard to the communication problem. Thus, the separation-velocity increment is increased by about 10 fps above the minimum for -90° entry or about 37 fps above the minimum for a -72° entry. On this basis, increased $\Delta V_{s,c}$ is definitely superior to applying retrothrust to the fly-by bus. It should also be noted that there is only a small influence of $\frac{m}{C_D A}$ on the $\Delta V_{s,c}$ required to achieve line-of-sight relay communication.

Atmosphere 1 is the worst atmosphere from the communications standpoint, as is demonstrated in figure 31 in which atmospheres 1 and 4 are compared for the nominal conditions and sufficient separation velocity to achieve the specified entry angle only.

It might be anticipated that a reduction in the distance between Mars and the spacecraft at the time of separation would somewhat alleviate the line-of-sight problem. This is not the case, however, as may be seen from figure 32. Here, only a 2° increase in entry angle is obtained by a reduction in separation distance from 700 to 50 Mars radii. On the other hand, the influence of the bus periapsis distance is shown in figure 33, to be most profound. Note that close passage to the planet greatly increases the communications problem. Thus, selection of the proper range of periapsis distances can reduce the problem of relay line-of-sight communications. Such gains are obtained, however, at the expense of an increased separation velocity, as was shown by figure 6. Figure 33 indicates that for $\frac{m}{C_D A} = 0.2$ slug/ft^2 an increase in the limiting entry angle from -78° to -85.5° causes an increase in the periapsis distance of 2 Mars radii. This same increase in periapsis distance is shown in figure 6 to require an increase in the separation velocity of 135 fps to maintain the same entry angle. Figure 30, however, demonstrates that the limiting entry angle for which relay communication from bus to capsule at impact is available can be increased from -78° to -90° for an increase in $\Delta V_{s,c}$ of only about 10 fps above the minimum required for vertical entry. Thus, velocity addition to the capsule is far superior to variations in spacecraft position insofar as gaining an increase in the entry-angle range available for line-of-sight communication between the capsule and the fly-by bus is concerned.

The effect of a reduction in the hyperbolic excess velocity is shown in figure 34 to increase the limiting entry angle for line-of-sight communication. Of course, a reduction in V_∞ or V_E was shown in figure 7 to reduce the separation velocity required to achieve a specific entry angle. A reduction in the hyperbolic excess velocity may then be one means of resolving the relay-communication problem. This parameter is dependent on the interplanetary

trajectory, however, and is not likely to be varied simply to achieve a small reduction in separation velocity.

The separation angles presented in figure 35 are the angles required to achieve a specified entry angle at the separation velocities $\Delta V_{s,c}$ of figure 30. Thus, the results of figure 35 are essentially the same as those of figure 30 and may be compared directly with the results of figure 8. The point to be made here is that an increase in λ_s of only 20° is required to insure relay communication for entry angles from -10° to -90° for the range of $\frac{m}{C_D A}$ considered. The penalty in $\Delta V_{s,c}$ which corresponds to this change in λ_s may be seen from figure 30 to be small (less than 15 fps) if a -90° entry angle is required.

One of the results of the entry analysis phase of this study was that the use of an entry capsule with $L/D = 0.5$ might alleviate some of the problems of entry. Figure 36 presents a comparison of the ballistic and lifting vehicles in terms of the line-of-sight communication requirements. Since a vehicle with $L/D = 0.5$ takes considerably longer to penetrate the atmosphere than a ballistic vehicle (fig. 29), the limiting entry angle for which line-of-sight communication is possible would be expected to be somewhat less for the lifting vehicle. As shown in figure 36, an increase in the separation velocity of less than about 15 fps above that required for ballistic entry is required, at the same conditions, for the vehicle with $L/D = 0.5$. It was pointed out previously, however, that the lifting capsule could utilize a higher value of $\frac{m}{C_D A}$ than the ballistic capsule for the same entry requirements. For instance, at an entry angle of -90°, a ballistic capsule requires a maximum value of $\frac{m}{C_D A}$ of 0.16 slug/ft^2 to attain a 60-second communication time, as opposed to a value of 0.36 slug/ft^2 for the $L/D = 0.5$ capsule. (See fig. 24.) A comparison of these two vehicles in figure 36 indicates that the maximum entry angle for which the two capsules can enter the atmosphere and communicate with the fly-by bus to impact is essentially the same for the same value of separation velocity. Thus, this aspect of the problem can be neglected in comparisons of the merits of a ballistic vehicle and a vehicle with $L/D = 0.5$.

APPLICATIONS TO ENTRY CAPSULE DESIGN

Design of an entry capsule for an unmanned Mars mission first requires a definition of mission objectives followed by a definition of mission restrictions. The basic mission may require either a hard or a soft landing with either direct or relay communication with Earth. Of primary importance to the entry capsule design are the restrictions on the characteristics of the entry capsule that are imposed by the presence of the Martian atmosphere in combination with the interplanetary navigation and guidance errors which dictate the arrival window at Mars. Another primary restriction placed on the capsule design is the size and weight limitation imposed by the capability of the launch vehicle.

It has been shown in figures 23 to 28 that the ballistic parameter $\frac{m}{C_D A}$ is of critical importance from the standpoint of communication for a hard-landing mission and of parachute deployment for a soft-landing mission. The size and weight restrictions are presented in figure 37 in terms of the ballistic parameter for the range of currently envisioned boosters which might be applicable to unmanned Mars missions. A diameter of 20 feet, the maximum indicated, would be approximately comparable to a Saturn class of launch vehicle. An Atlas-Centaur launch system would allow a maximum vehicle diameter of slightly less than 10 feet, and the Atlas-Agena D system, about 6 feet. Maximum payload capability placed on a Mars encounter trajectory is on the order of 1500 pounds for the Centaur system and about 600 pounds for the Agena system.

The results of the present study (fig. 24) indicate that, for ballistic entry with no terminal guidance capability, and a 1-minute communication time, the $\frac{m}{C_D A}$ for the entry capsule must be of the order of 0.2 slug/ft^2 or less for either hard- or soft-landing missions without supersonic parachute deployment. For this value of the ballistic parameter, the maximum entry-capsule weight is restricted to less than about 600 pounds for the Centaur system and less than about 200 pounds for the Agena system.

In comparison, a lifting vehicle ($L/D = 0.5$) was shown to require a value of the ballistic parameter of 0.3 slug/ft^2 or less from parachute deployment considerations. Figure 37 indicates that essentially all the Agena or Centaur capability could be utilized for the entry capsule if the $\frac{m}{C_D A}$ could be increased to 0.3 slug/ft^2. Thus, large gains appear to be available through the use of the lifting-vehicle concept.

The results of the Advanced Mariner and Voyager studies indicate that these weights are possibly adequate for early unmanned Mars missions. However, for sophisticated unmanned missions, such as the landing of an automated biological laboratory of the order of 5000 pounds, some type of terminal guidance appears to be required. This terminal guidance is necessary since, even with $L/D = 0.5$ and a Saturn-class launch vehicle, the maximum entry-vehicle weight would be of the order of 4000 pounds for vertical entry.

Another point in favor of the development of a terminal guidance system (or utilization of a lifting vehicle) is that a very low value of $\frac{m}{C_D A}$ is rather difficult to achieve with any significant payload-ratio capability. Thus, a new vehicle concept must be conceived and developed if ballistic entry without terminal guidance is accepted. On the other hand, well-developed shapes such as the Apollo configuration, or blunted cones, could be utilized for early Mars missions if a terminal guidance capability were to be developed or if aerodynamic lift were utilized.

Three general classes of entry vehicles may therefore be considered for unmanned Mars missions: ballistic vehicles, lifting vehicles, and vehicles with terminal guidance. Two of these, a ballistic vehicle without terminal guidance and a ballistic vehicle with terminal guidance, were compared on the

basis of the design requirements of the entry vehicle for a typical unmanned Mars mission. The typical mission selected for study requires:

(1) A soft landing

(2) Up to 1 hour of surface operation after landing

(3) Relay communication to Earth by way of a fly-by bus

(4) Compatibility with the Atlas-Centaur launch system

Parachute deployment is designed to occur in atmosphere 4 (the worst case) at an altitude of 15 000 feet and a Mach number of 0.9. It is assumed that the vehicle is decelerated to a velocity of 150 fps by parachute and is provided with retro-rockets to remove the residual velocity just prior to touchdown. In addition, the vehicle with terminal guidance is assumed to have an entry corridor width of 10°.

On the basis of these restrictions it was found that the ballistic vehicle with terminal guidance could be designed for an $\frac{m}{C_D A}$ of about 0.50 slug/ft^2. The actual value used in the calculations was 0.40 slug/ft^2, however, in order to reduce the stagnation-point heating loads and also to prevent the payload weight from exceeding the Centaur's capability, while the maximum available entry-vehicle diameter was maintained.

The ballistic vehicle without terminal guidance must be designed for a value of $\frac{m}{C_D A}$ of 0.18 slug/ft^2 or less. The maximum value was chosen for the calculations to obtain the best possible payload ratio.

The velocity required at separation of the bus and entry capsule to insure line-of-sight relay communication after impact is presented in figure 38 for the two vehicles considered. For the vehicle with terminal guidance, up to 24 minutes of surface operation is available without any increase in separation velocity. One hour of surface operation is available to this vehicle for a total separation velocity increment of 275 fps, an increase of 160 fps over the minimum. For the vehicle with no terminal guidance, a large velocity is required simply to assure entry over the required range of entry angle. Note that this vehicle has a surface operational lifetime of only 6 minutes for a total separation-velocity increment of 275 fps, which provided a 1-hour lifetime for the vehicle with terminal guidance. For a 1-hour operational lifetime on the surface, a separation velocity of 680 fps is required. Thus, a total velocity saving of 405 fps is possible by the use of terminal guidance. It is realized, of course, that the trade-off between the weights of the propulsion system and the terminal guidance system must be considered. The important point is, however, that a heavier payload with a more conventional shape may be landed in a smaller target area if terminal guidance is utilized. It should also be pointed out that the use of a lifting-vehicle system without terminal guidance would yield a significant increase in landed payload when compared with the ballistic system without terminal guidance. In addition, many

advantages may be foreseen for the combination of a terminal guidance capability with a vehicle having a controllable-lift capability.

CONCLUDING REMARKS

An unmanned ballistic entry vehicle capable of communication with the Earth between blackout and Mars impact or a vehicle capable of a soft landing with parachute deployment velocities of 1000 fps or less has been shown to require a value of the ballistic parameter of less than 0.2 slug/ft^2 if a vertical entry capability is required. The utilization of a vehicle with a lift-drag capability of 0.5 was shown to allow a significant increase in this requirement to values of the ballistic parameter of about 0.3 slug/ft^2. If a terminal guidance system is available for such missions, it may be possible to extend the maximum allowable values of the ballistic parameter to about 0.66 and 0.9 slug/ft^2 for ballistic and lifting vehicles, respectively.

On the basis of the present stagnation-point heating analysis, convective heating appears to be the dominant heating mode at the entry velocities associated with unmanned missions.

The problem of communication between the fly-by bus and the capsule was shown to be minimized if shallow entry angles are utilized. Also, minimum hyperbolic excess velocity, bus-capsule separation at maximum distances from the planet, and application of the separation thrust at essentially right angles to the flight path appear to be desirable.

The comparison of two ballistic vehicles, one without terminal guidance and one with terminal guidance, indicates that a 1-hour surface operation with a line-of-sight relay-communications link can be obtained for the terminally guided vehicle at the same cost in separation velocity as a 6-minute surface operation for the vertical-entry vehicle.

On the basis of the results of the present report, the use of a ballistic vehicle with a terminal guidance capability, a lifting vehicle, or a combination of both concepts appears to be superior for early unmanned missions to Mars to the use of a vehicle with a low ballistic-parameter value without terminal guidance. It is believed that these concepts therefore merit further, more detailed, investigation.

Langley Research Center,
National Aeronautics and Space Administration,
Langley Station, Hampton, Va., February 1, 1965.

APPENDIX

HYPERBOLIC EQUATIONS

Bus Trajectory

For trajectories confined to the encounter of a planet, a two-body analysis can be performed. The planet is considered the central force, and all other perturbing effects are neglected as a vehicle approaches the planet. The hyperbolic equations required to define the characteristics of these trajectories have been developed (ref. 5), hence they will be presented here with a minimum of description.

Periapsis velocity of the bus:

$$V_p^2 = V_\infty^2 + \frac{2\mu}{r_p} \qquad \left(\frac{2\mu}{r_\infty} \approx 0\right) \tag{A1}$$

Semimajor axis:

$$a = \frac{\mu r_p}{r_p V_p^2 - 2\mu} \tag{A2}$$

Semilatus rectum:

$$p = \frac{r_p}{a}\left(r_p + 2a\right) \tag{A3}$$

Eccentricity:

$$e = \frac{r_p}{a} + 1 \tag{A4}$$

Local velocity:

$$V^2 = \mu\left(\frac{2}{r} + \frac{1}{a}\right) \tag{A5}$$

Flight-path angle:

$$\gamma = \cos^{-1}\left(\frac{1 + e\cos\theta}{\sqrt{1 + 2e\cos\theta + e^2}}\right) \tag{A6}$$

Orbital central angle:

$$\theta = \cos^{-1}\left(\frac{p - r}{er}\right) \tag{A7}$$

APPENDIX

Time from periapsis passage:

$$t_p = \sqrt{\frac{p^3}{\mu}}\left(\frac{1}{e^2 - 1}\right)\left[\frac{e \sin\theta}{1 + e\cos\theta} - \frac{1}{\sqrt{e^2 - 1}} \ln\left(\frac{e + \cos\theta + \sin\theta\sqrt{e^2 - 1}}{1 + e\cos\theta}\right)\right] \quad (A8)$$

For convenience, the reference point of time was transferred from the periapsis point to the bus-capsule separation point.

Capsule Trajectory

At some distance from Mars it has been assumed that a capsule will be separated from a fly-by bus and will enter the Martian atmosphere as illustrated in figure 1. Some of the possible hyperbolic encounter trajectories for this type of vehicle have been calculated through the use of the following equations.

Capsule entry velocity:

$$V_E^2 = V_{s,c}^2 - \frac{2\mu}{r_s} + \frac{2\mu}{r_E} \quad (A9)$$

Semimajor axis:

$$a = \frac{\mu r_E}{r_E V_E^2 - 2\mu} \quad (A10)$$

Semilatus rectum:

$$p = \frac{r_E^2 V_E^2 \cos^2\gamma_E}{\mu} \quad (A11)$$

Periapsis distance:

$$r_p = a\sqrt{1 + \frac{r_E V_E^2 \cos^2\gamma_E}{\mu^2}\left(r_E V_E^2 - 2\mu\right)} - a \quad (A12)$$

The eccentricity, local velocity, and flight-path angle for the capsule were obtained from the general equations (A4) to (A6). The orbital central angle for the capsule was calculated from equation (A7). The reference axis was then transferred to the bus periapsis radius.

The elapsed time of travel of the capsule from separation to the edge of the Martian atmosphere was determined by utilizing equation (A8), except for $\gamma_E = -90^\circ$ for which equation (A8) becomes indeterminant (since $e = 1$). For

this case, the required expression for time, measured from separation, is easily obtained since the centrifugal forces are zero:

$$(t_s)_{\gamma=-90^\circ} = \frac{1}{\sqrt{2}\left(\frac{V_{s,c}^2}{2} - \frac{\mu}{r_s}\right)} \left\{ \sqrt{\mu r_s + \left(\frac{V_{s,c}^2}{2} - \frac{\mu}{r_s}\right) r_s^2} - \sqrt{\mu r + \left(\frac{V_{s,c}^2}{2} - \frac{\mu}{r_s}\right) r^2} \right.$$

$$\left. + \frac{\mu}{\sqrt{\frac{V_{s,c}^2}{2} - \frac{\mu}{r_s}}} \ln \left[\frac{\sqrt{\left(\frac{V_{s,c}^2}{2} - \frac{\mu}{r_s}\right) r} + \sqrt{\mu + \left(\frac{V_{s,c}^2}{2} - \frac{\mu}{r_s}\right) r}}{\sqrt{\left(\frac{V_{s,c}^2}{2} - \frac{\mu}{r_s}\right) r_s} + \sqrt{\mu + \left(\frac{V_{s,c}^2}{2} - \frac{\mu}{r_s}\right) r_s}} \right] \right\} \tag{A13}$$

The velocity increment required to separate the entry capsule from the fly-by bus is

$$\Delta V_{s,c} = \sqrt{V_{s,b}^2 + V_{s,c}^2 - 2V_{s,b}V_{s,c} \cos \Delta\gamma_s} \tag{A14}$$

where $\Delta\gamma_s = \gamma_{s,c} - \gamma_{s,b}$. The angle at which this velocity increment is applied is determined from

$$\lambda_s = \sin^{-1}\left(\frac{V_{s,c}}{\Delta V_{s,c}} \sin \Delta\gamma_s\right) \tag{A15}$$

It should be noted that for cases in which $\lambda_s = 90^\circ$, the resultant velocity of the capsule at separation was calculated instead of using this velocity as a given condition. In this case, the expression used to calculate $V_{s,c}$ is

$$V_{s,c}^2 = V_{s,b}^2 + \left\{ - \frac{r_s^2 V_{s,b} \cos \gamma_{s,b} \sin \gamma_{s,b}}{r_E^2 \cos^2 \gamma_E - r_s^2 \sin^2 \gamma_{s,b}} \right.$$

$$\left. + \frac{\sqrt{\left(r_s^2 V_{s,b} \cos \gamma_{s,b} \sin \gamma_{s,b}\right)^2 - \left(r_E^2 \cos^2 \gamma_E - r_s^2 \sin^2 \gamma_{s,b}\right)\left[r_E^2 \cos^2 \gamma_E \left(V_{s,b}^2 - \frac{2\mu}{r_s} + \frac{2\mu}{r_E}\right) - r_s^2 V_{s,b}^2 \cos^2 \gamma_{s,b}\right]}}{r_E^2 \cos^2 \gamma_E - r_s^2 \sin^2 \gamma_{s,b}} \right\}^2 \tag{A16}$$

APPENDIX

Equation (A16) is based on equation (A9) and the identity

$$r_E^2 V_E^2 \cos^2 \gamma_E \equiv r_s^2 V_{s,c}^2 \cos^2 \gamma_{s,c} \tag{A17}$$

as well as the fundamental relationships of a right triangle.

REFERENCES

1. Kaplan, Lewis D.; Münch, Guido; and Spinrad, Hyron: An Analysis of the Spectrum of Mars. Astrophys. J., vol. 139, no. 1, Jan. 1964, pp. 1-15.

2. Seiff, Alvin: Developments in Entry Vehicle Technology. AIAA Paper No. 64-528, Am. Inst. Aeron. Astronaut., July 1964.

3. Beuf, F. G.: A Simple Entry System Experiment for Martian Atmospheric Measurements. AIAA Paper No. 64-292, Am. Inst. Aeron. Astronaut., June 1964.

4. Woestemeyer, F. B.: Guidance Requirements for an Unmanned Planet Landing. Paper No. 64-645, Am. Inst. Aeron. Astronaut., Aug. 1964.

5. Jensen, J.; Kraft, J. D.; and Townsend, G. E., Jr.: Orbital Mechanics. Orbital Flight Handbook. Part 1 - Basic Techniques and Data, NASA SP 33, pt. 1, 1963, pp. III-1 - III-87.

6. Knip, Gerald, Jr.; and Zola, Charles L.: Three-Dimensional Trajectory Analysis for Round-Trip Missions to Mars. NASA TN D-1316, 1962.

7. Levin, George M.; Evans, Dallas E.; and Stevens, Victor: NASA Engineering Models of the Mars Atmosphere for Entry Vehicle Design. NASA TN D-2525, 1964.

8. Demele, Fred A.: A Study of the Convective and Radiative Heating of Shapes Entering the Atmospheres of Venus and Mars at Superorbital Speeds. NASA TN D-2064, 1963.

9. James, Carlton S.: Experimental Study of Radiative Transport From Hot Gases Simulating in Composition the Atmospheres of Mars and Venus. [Preprint] 63-455, presented at AIAA Conference on Physics of Entry Am. Inst. Aeron. Astronaut., Aug. 1963.

10. Woestemeyer, F. B.: Approach Phase Guidance for Interplanetary Missions. Paper No. 64-655, Am. Inst. Aeron. Astronaut., Aug. 1964.

11. Allen, H. Julian; and Eggers, A. J., Jr.: A Study of the Motion and Aerodynamic Heating of Ballistic Missiles Entering the Earth's Atmosphere at High Supersonic Speeds. NACA Rept. 1381, 1958. (Supersedes NACA TN 4047.)

12. Roberts, Leonard: Entry Into Planetary Atmospheres. Astronaut. and Aeron., vol. 2, no. 10, Oct. 1964, pp. 22-29.

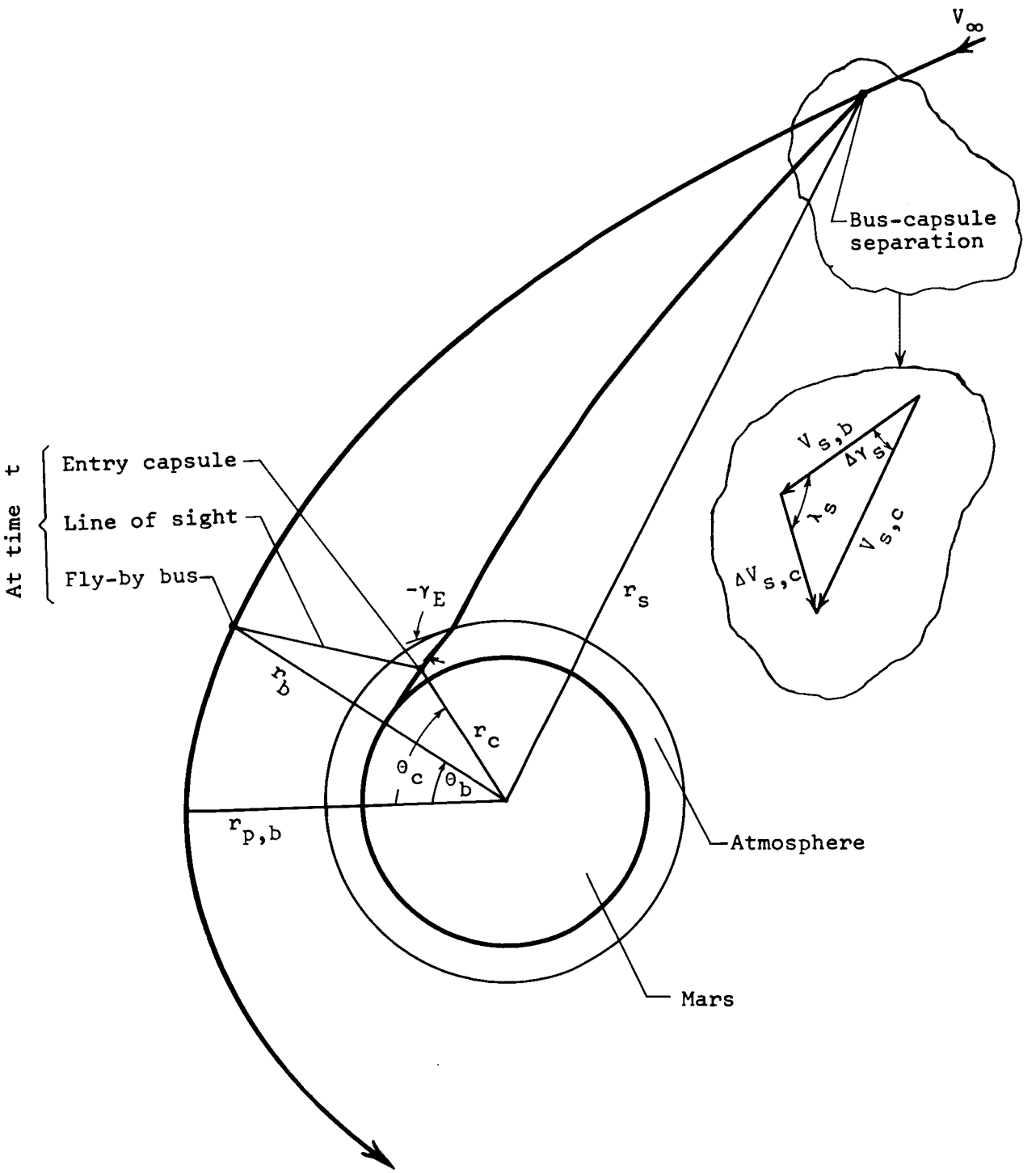

Figure 1.- Relative position of bus and capsule at separation and at encounter of Mars.

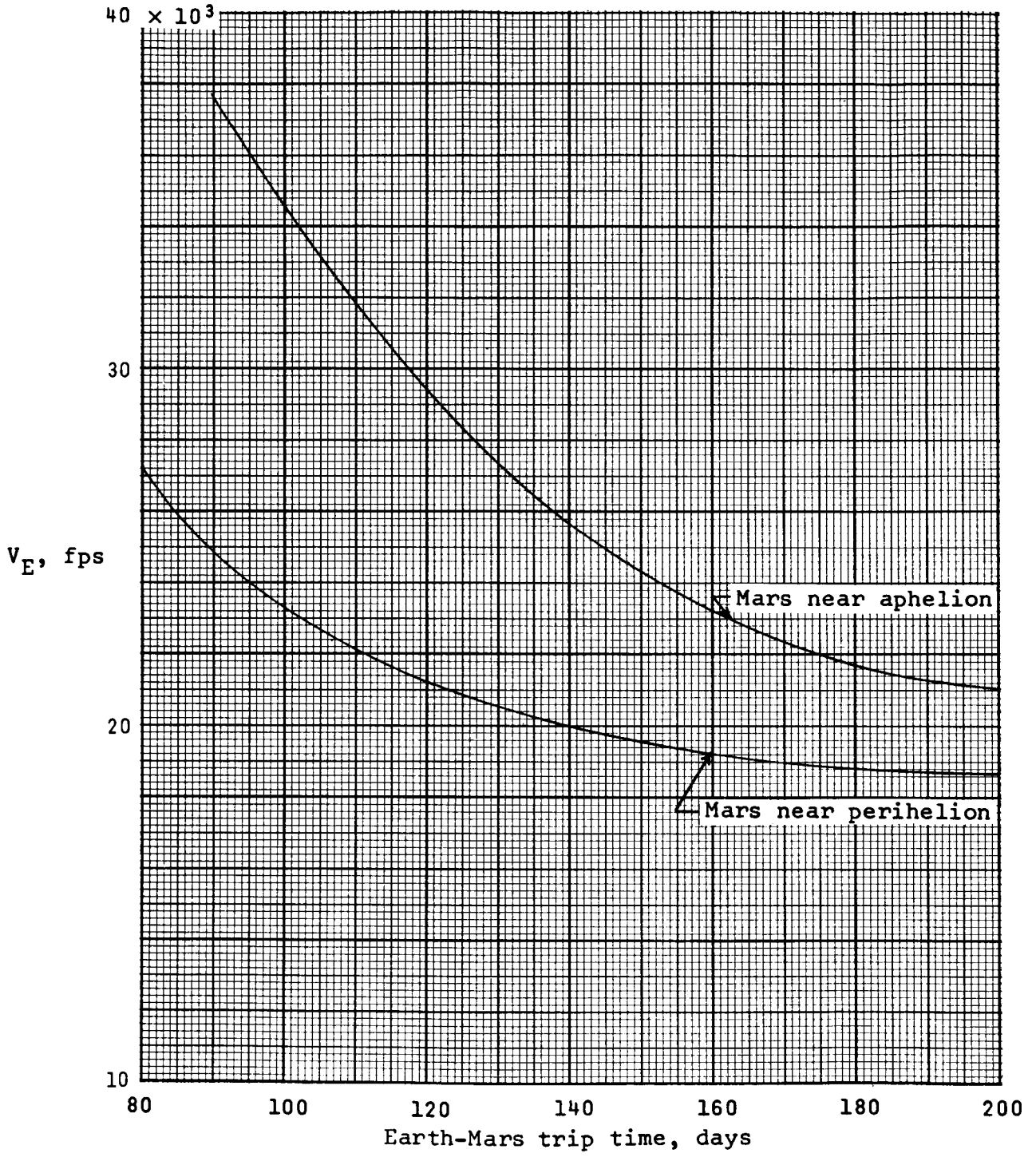

Figure 2.- Typical Mars entry velocities.

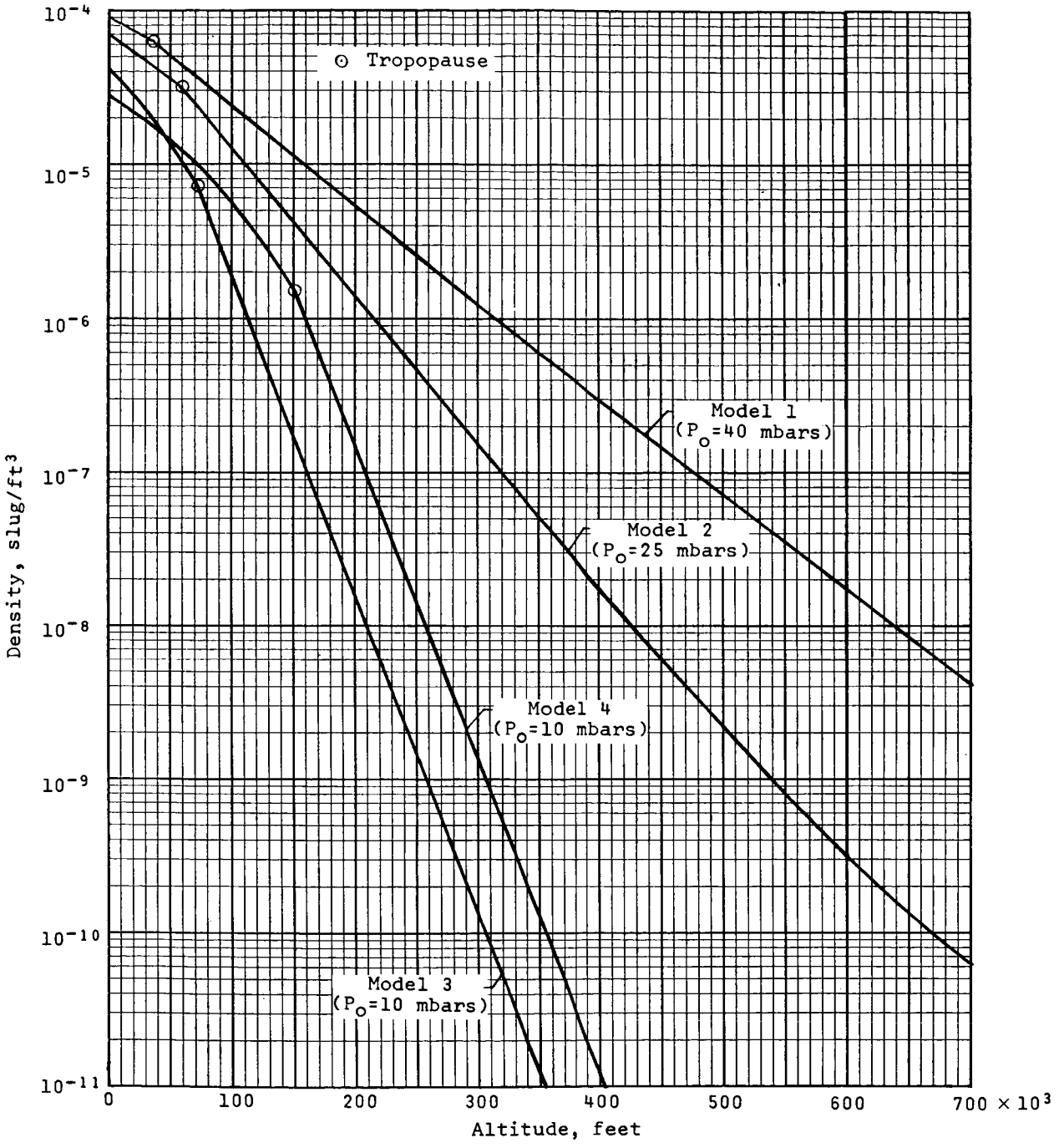

(a) Density profile.

Figure 3.- Proposed NASA Mars model atmospheres.

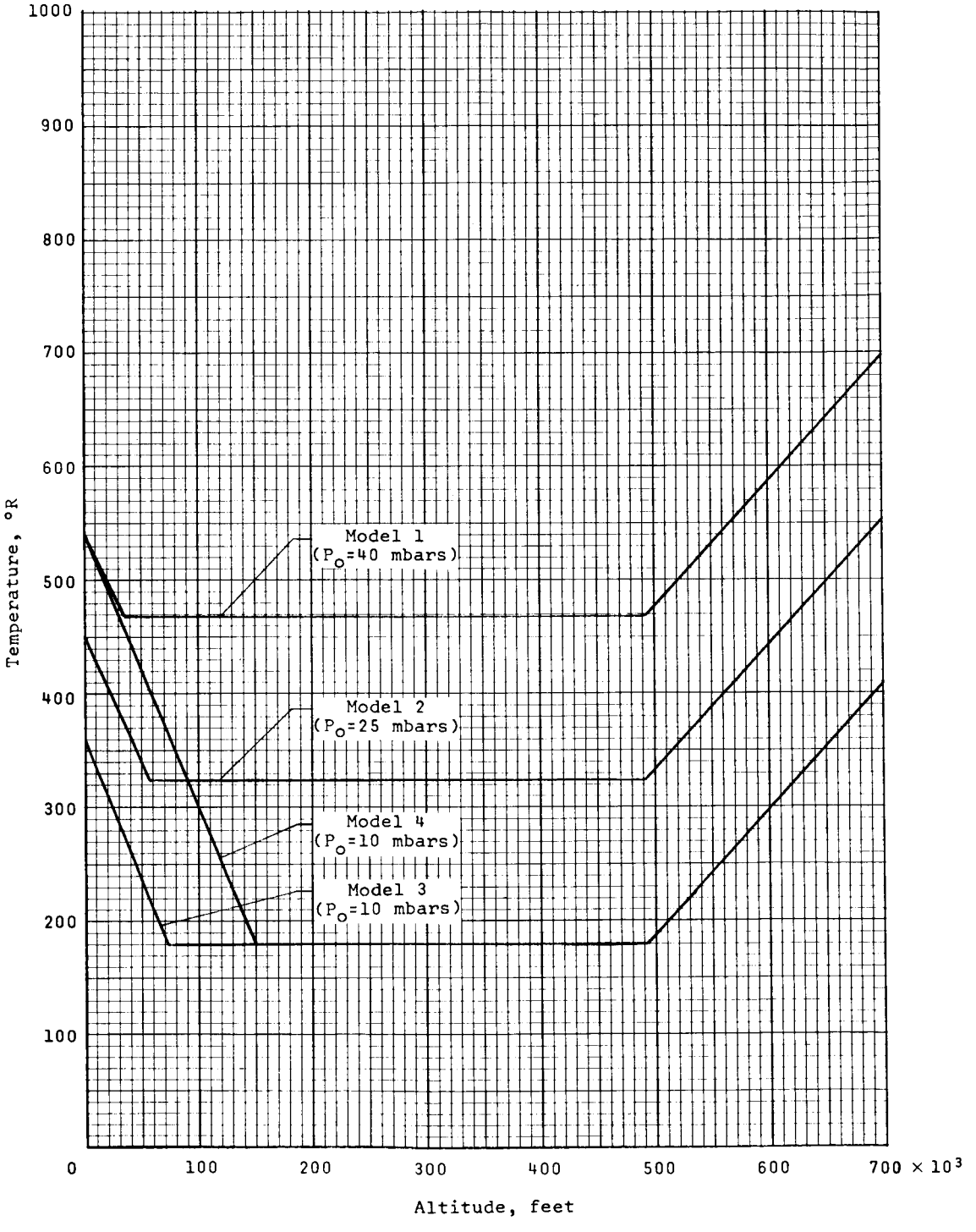

(b) Temperature profile.

Figure 3.- Concluded.

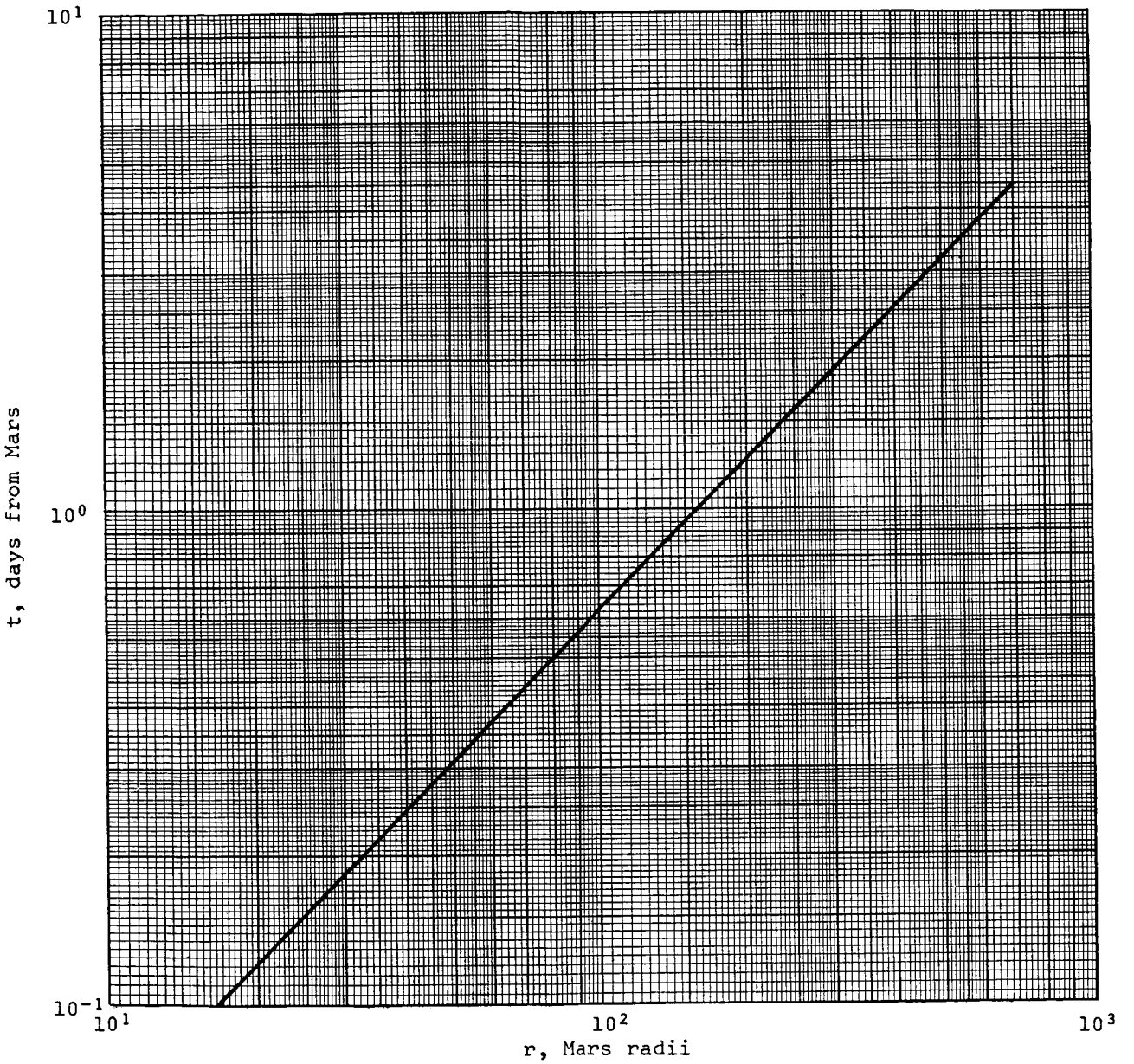

Figure 4.- Typical time-distance schedule for fly-by bus. V_∞ = 20 323 fps; $r_{p,b}$ = 2.5 Mars radii (Mars radius = 2113 int. statute miles).

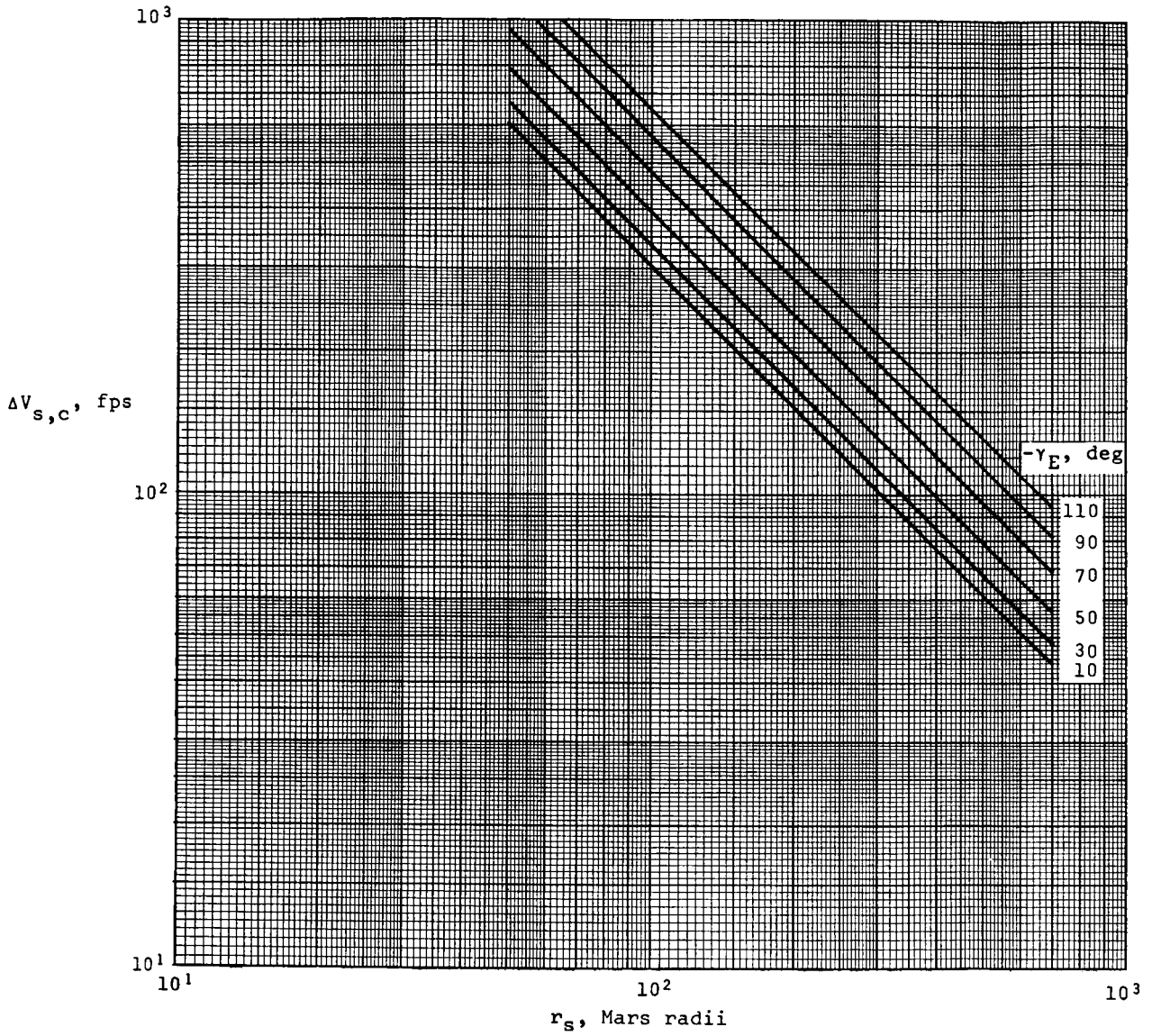

Figure 5.- Effect of separation distance on separation velocity. V_∞ = 20 323 fps; $\lambda_s = 90^\circ$; $r_{p,b}$ = 2.5 Mars radii (Mars radius = 2113 int. statute miles).

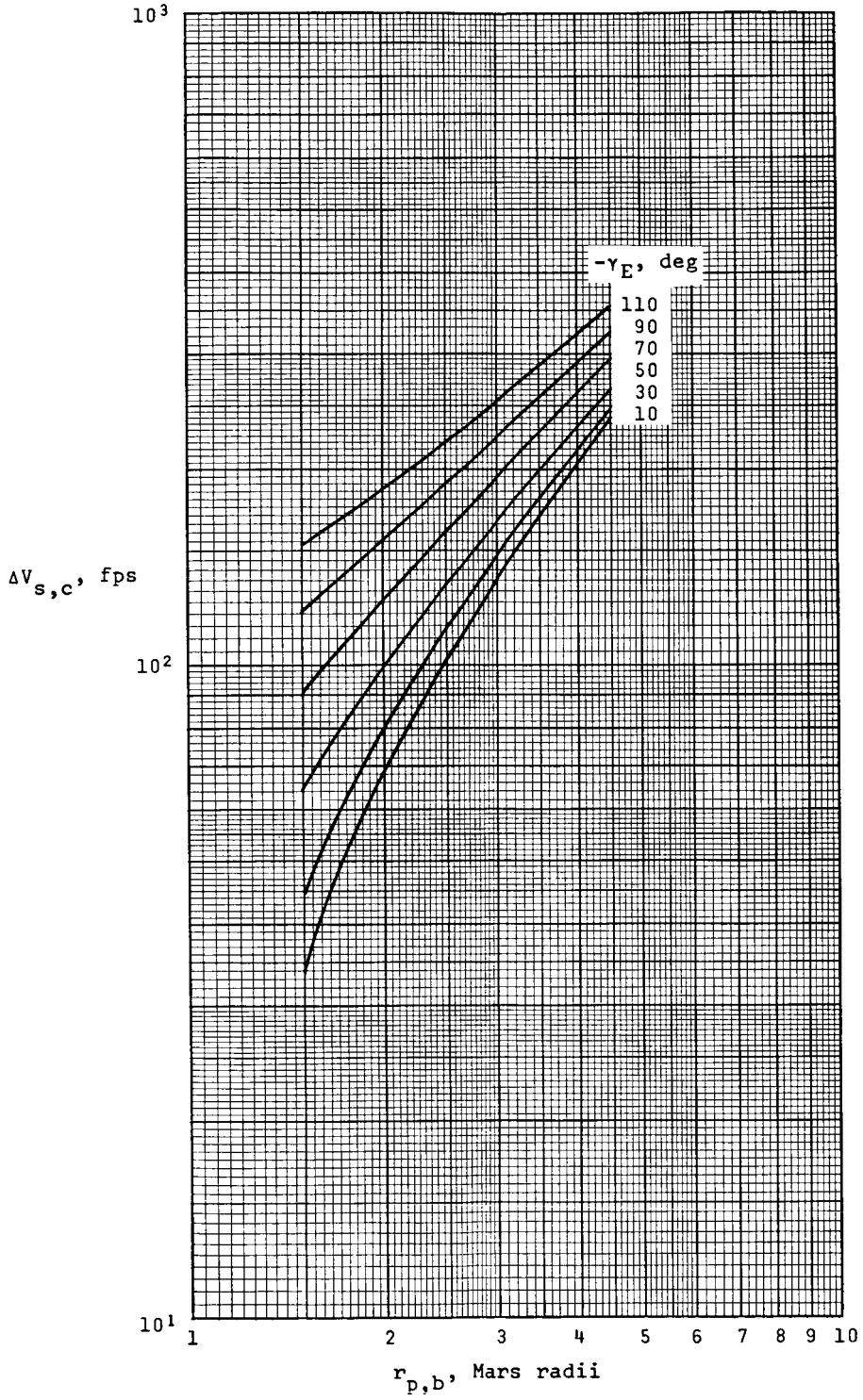

Figure 6.- Effect of bus periapsis distance on separation velocity. V_∞ = 20 323 fps; $\lambda_S = 90^\circ$; r_S = 300 Mars radii (Mars radius = 2113 int. statute miles).

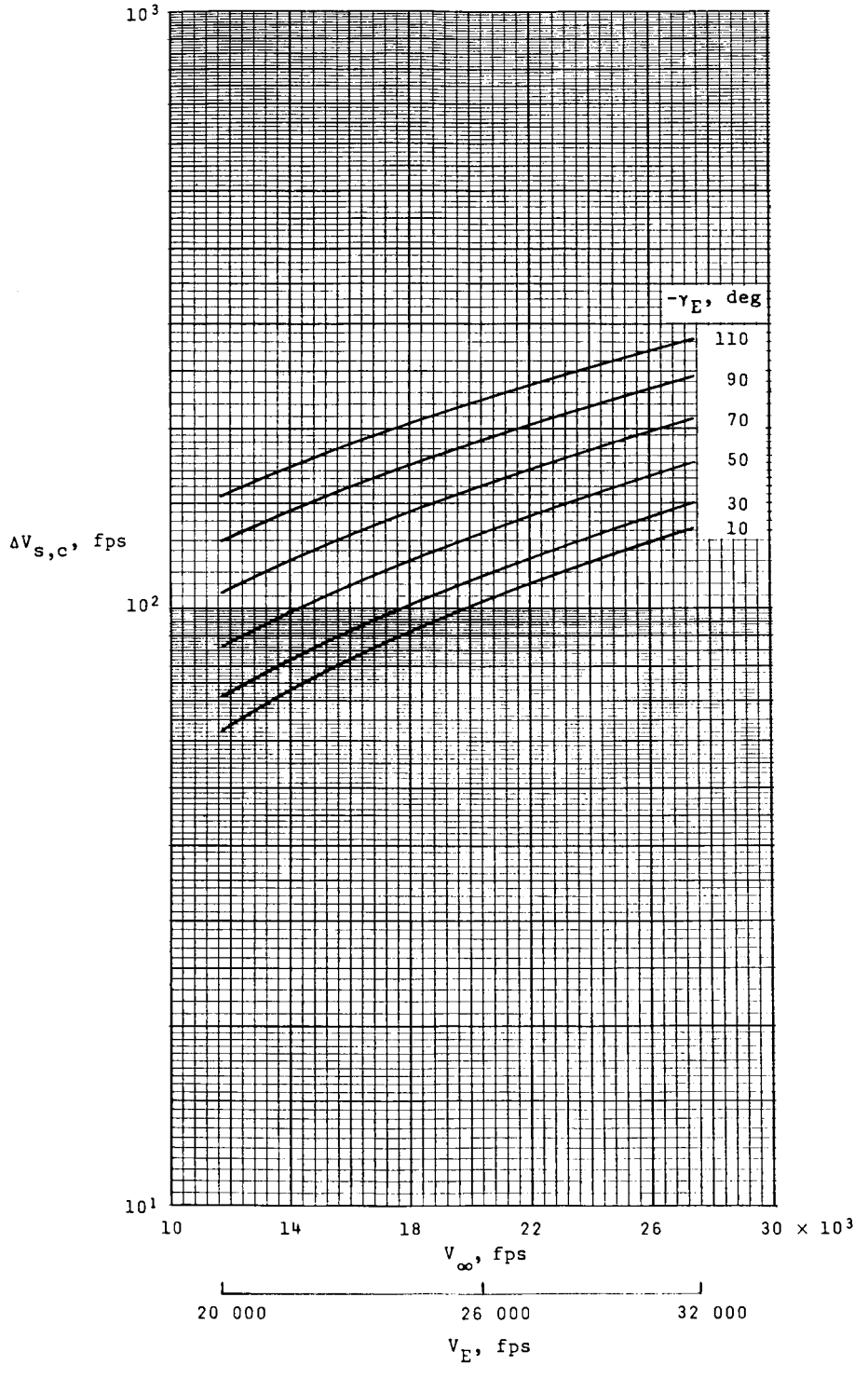

Figure 7.- Effect of hyperbolic excess velocity on separation velocity. $\lambda_s = 90^\circ$; $r_s = 300$ Mars radii; $r_{p,b} = 2.5$ Mars radii.

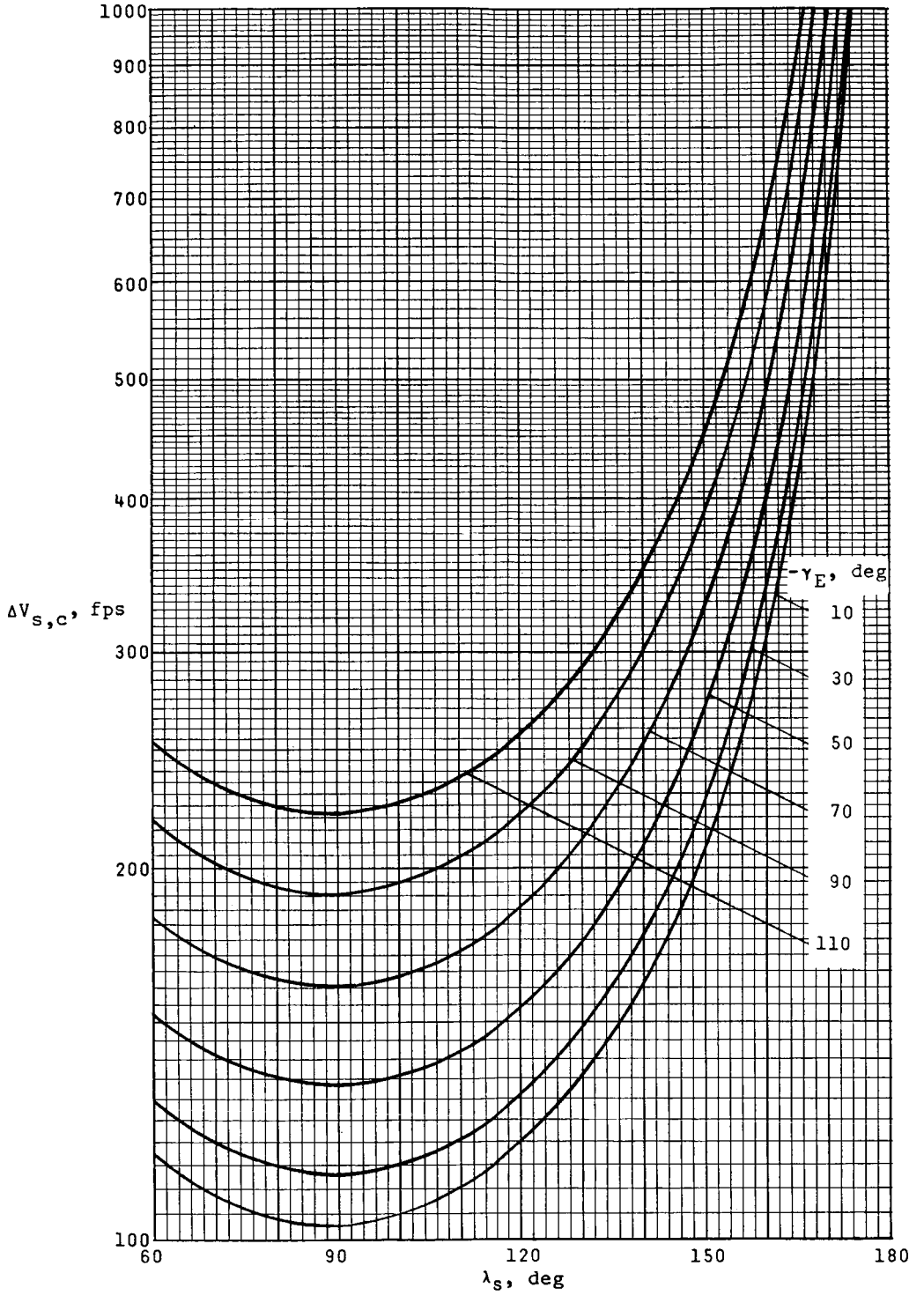

Figure 8.- Effect of separation angle on separation velocity. V_∞ = 20 323 fps; r_s = 300 Mars radii; $r_{p,b}$ = 2.5 Mars radii.

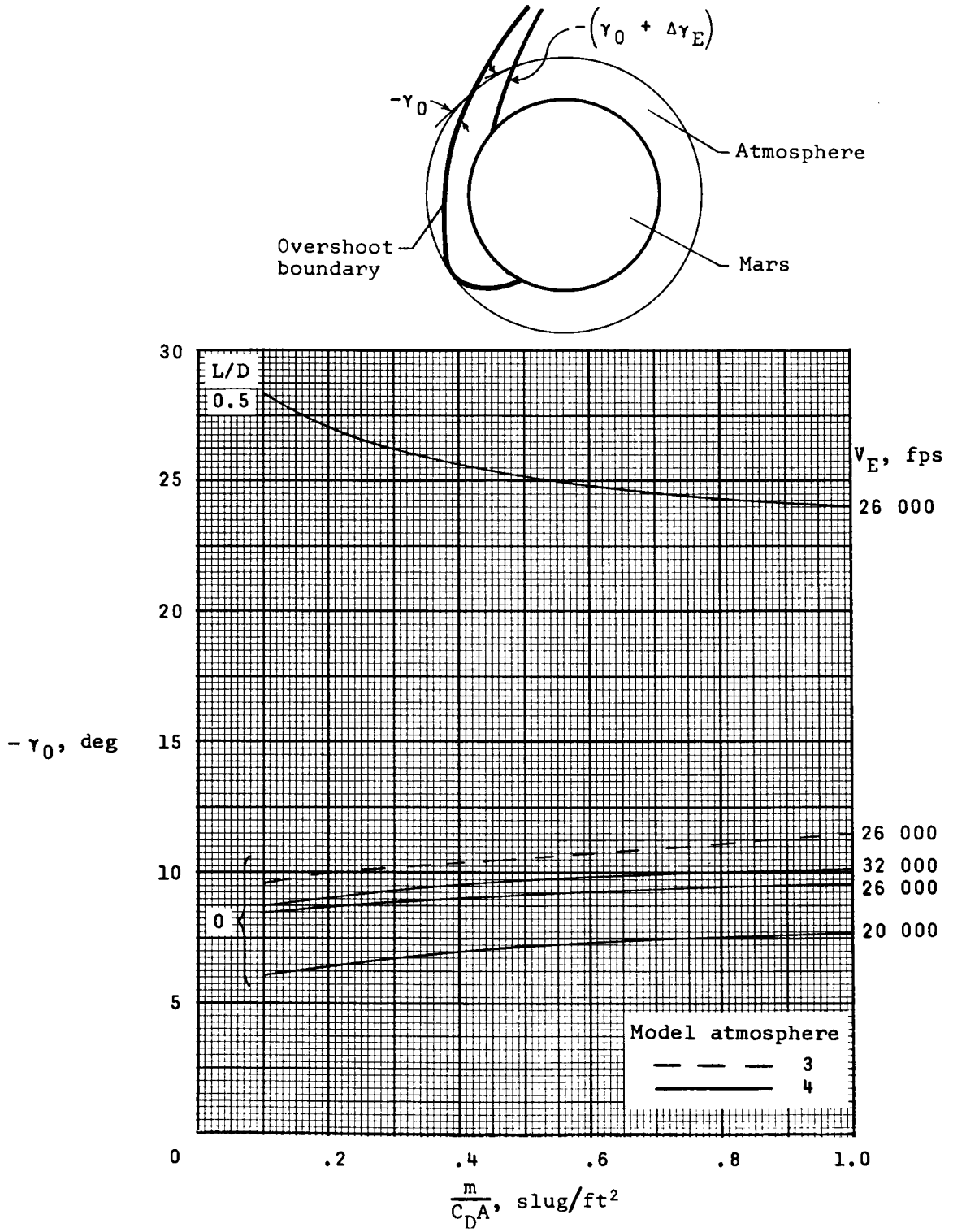

Figure 9.- Overshoot-boundary entry angle.

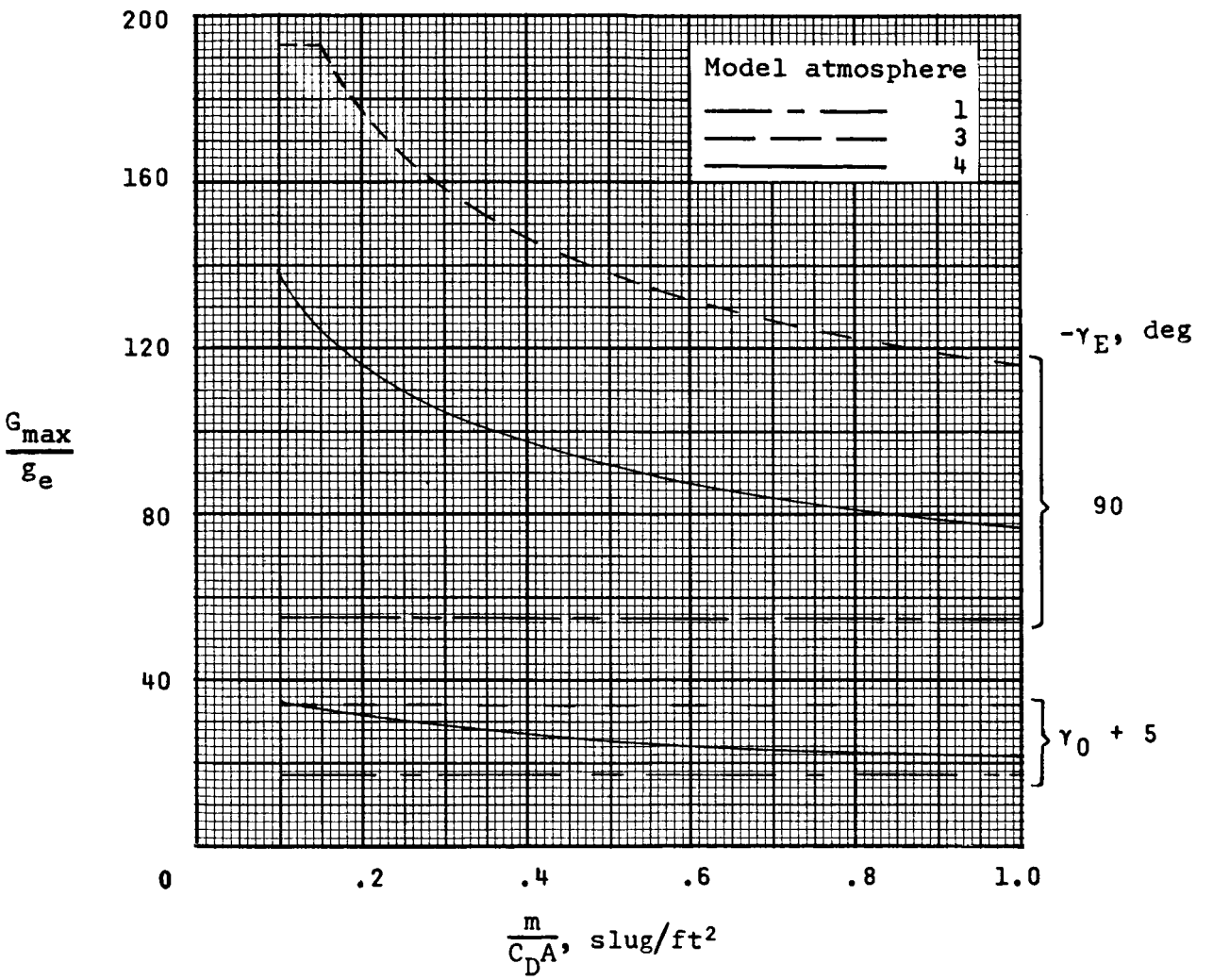

Figure 10.- Effect of atmospheric model on maximum deceleration loads for steep and shallow entry. L/D = 0; V_E = 26 000 fps. (γ_0 = Overshoot boundary; see fig. 9.)

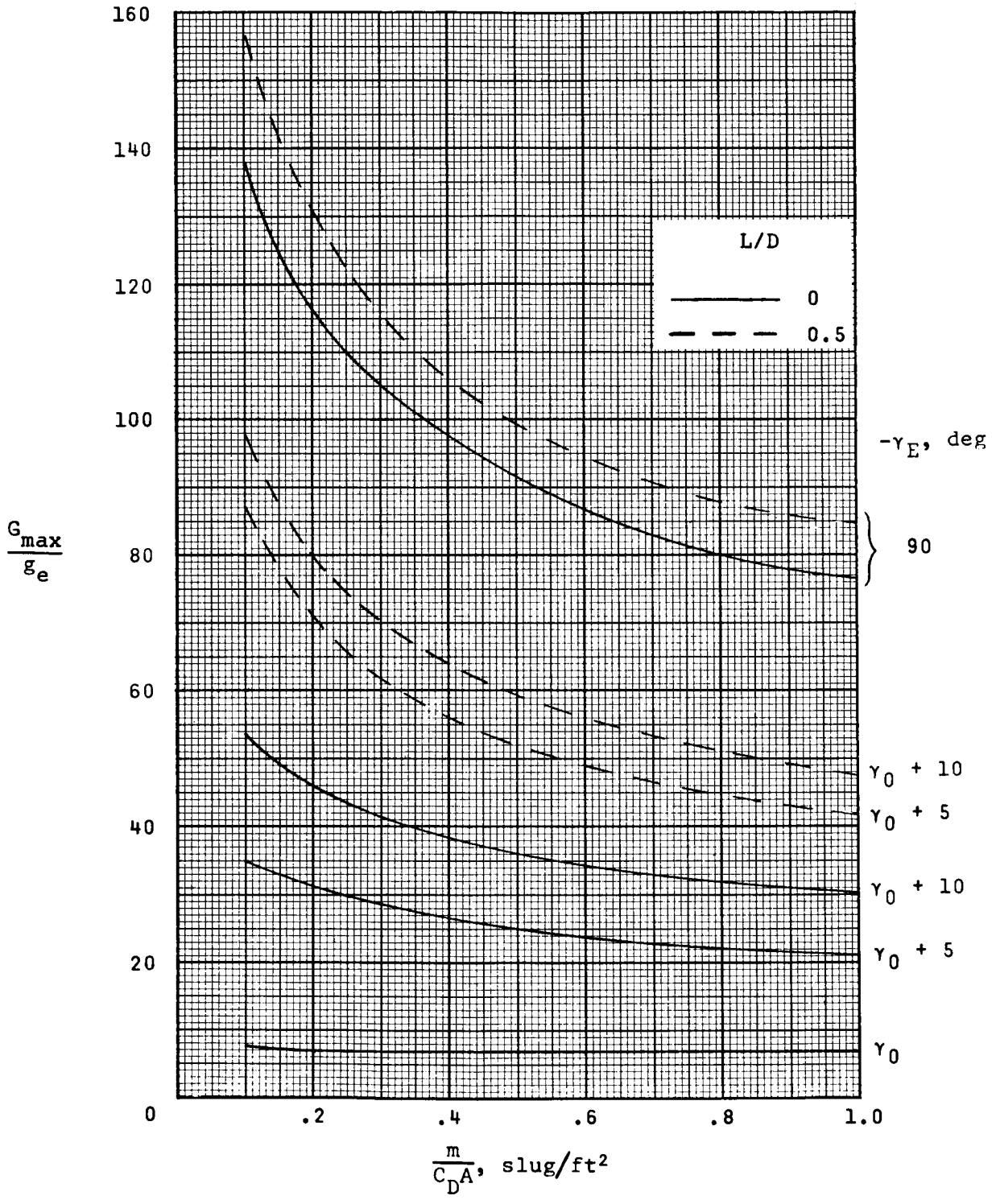

Figure 11.- Effect of lift on maximum deceleration loads for steep and shallow entry in model atmosphere 4 at V_E = 26 000 fps. (γ_0 = Overshoot boundary; see fig. 9.)

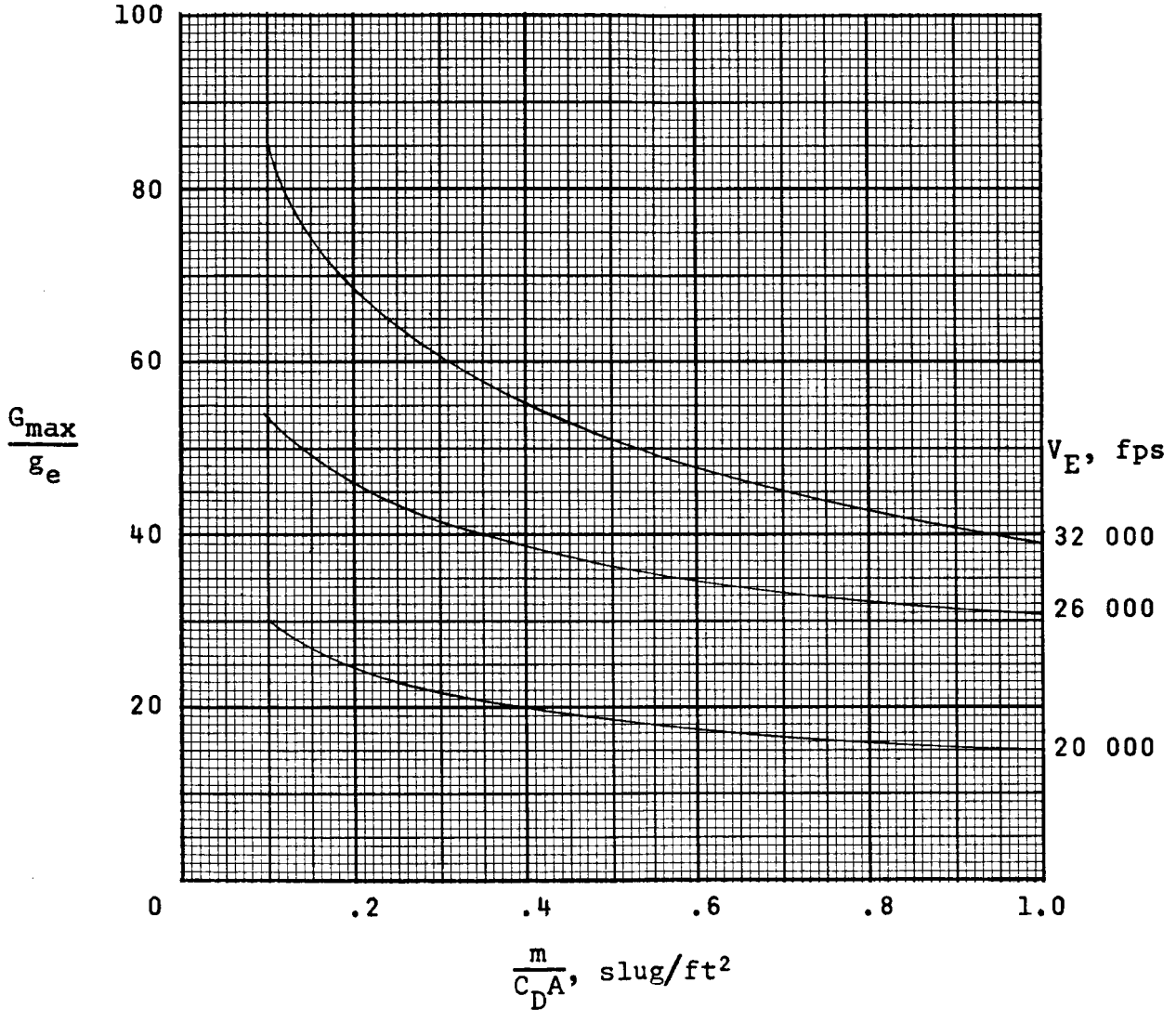

Figure 12.- Effect of entry velocity on maximum deceleration loads in model atmosphere 4. $L/D = 0$; $-\gamma_E = \gamma_0 + 10^o$.

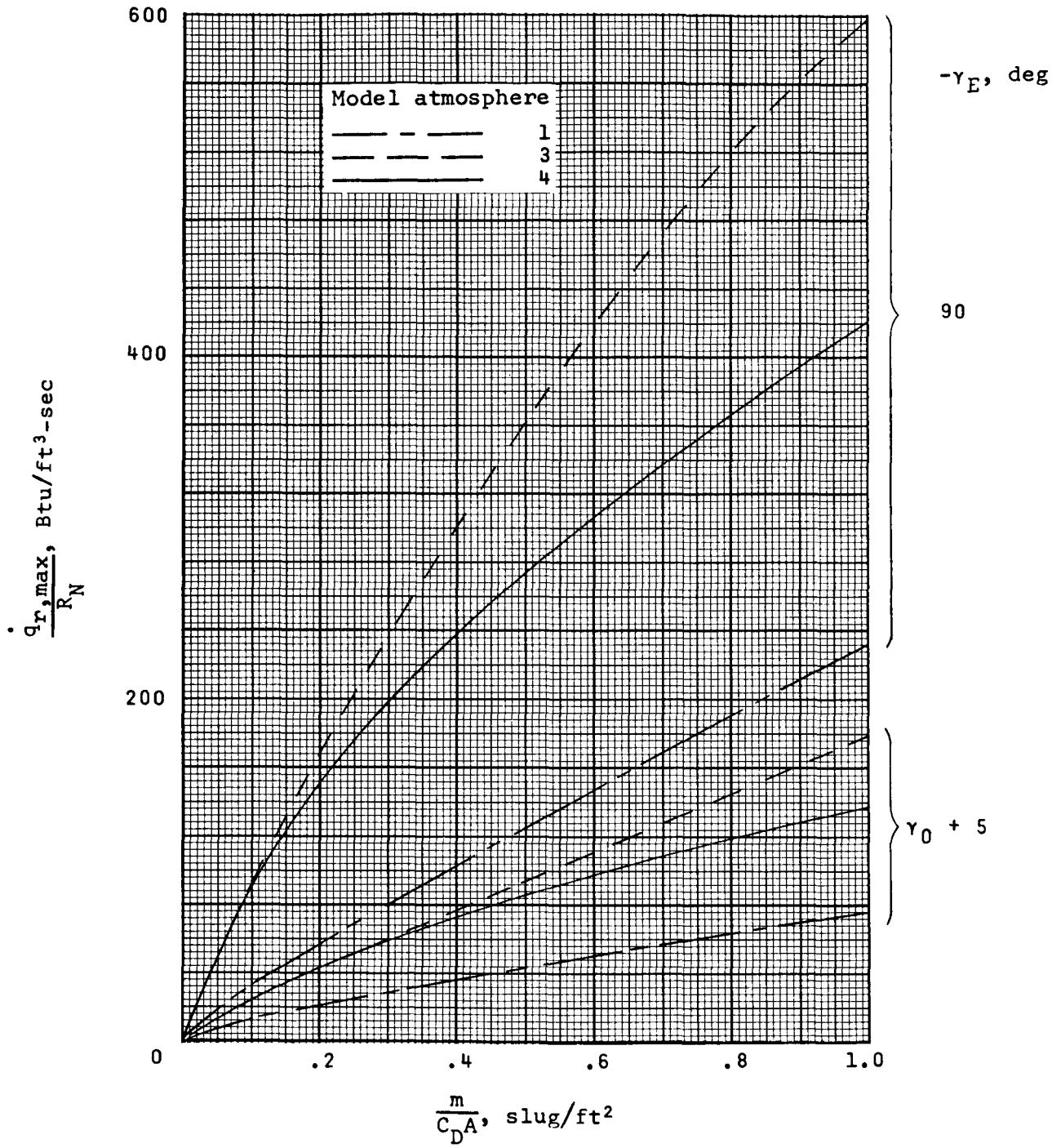

Figure 13.- Effect of atmospheric model on maximum radiative heating rates for steep and shallow entry. L/D = 0; V_E = 26 000 fps. (γ_0 = Overshoot boundary; see fig. 9.)

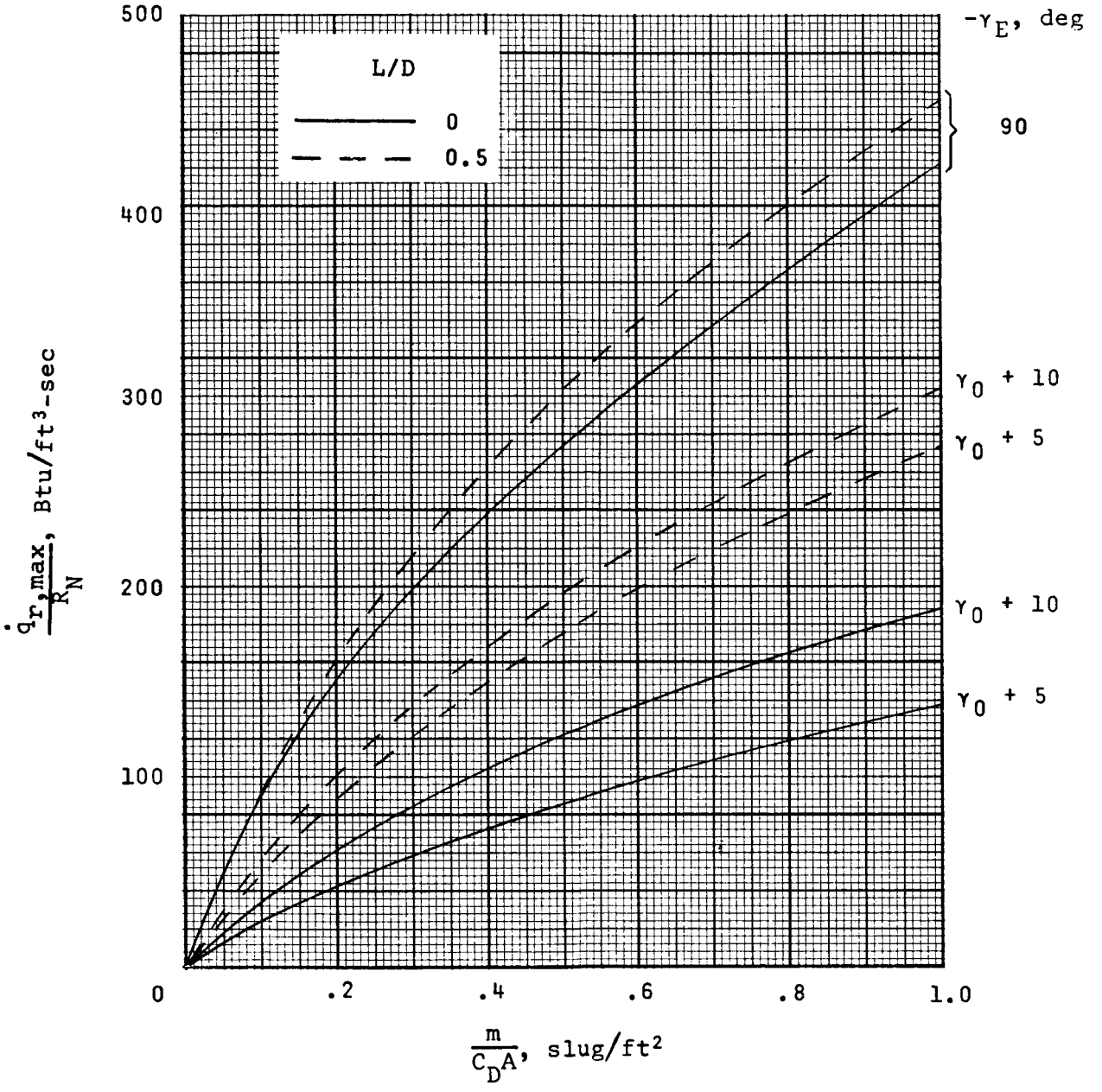

Figure 14.- Effect of lift on maximum radiative heating rates for steep and shallow entry in model atmosphere 4 at V_E = 26 000 fps. (γ_0 = Overshoot boundary; see fig. 9.)

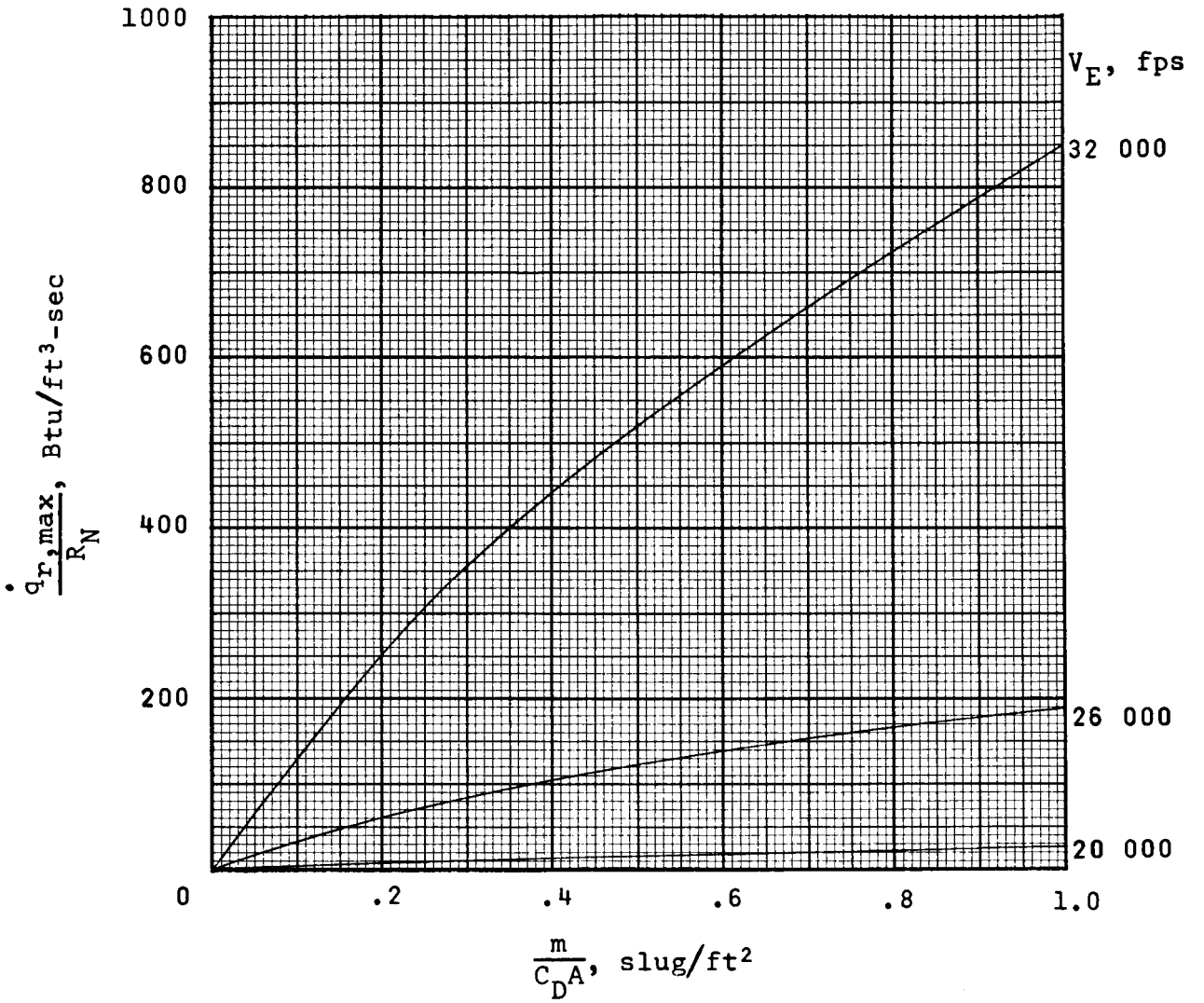

Figure 15.- Effect of entry velocity on maximum radiative heating rates in model atmosphere 4. L/D = 0; $-\gamma_E = \gamma_0 + 10^\circ$.

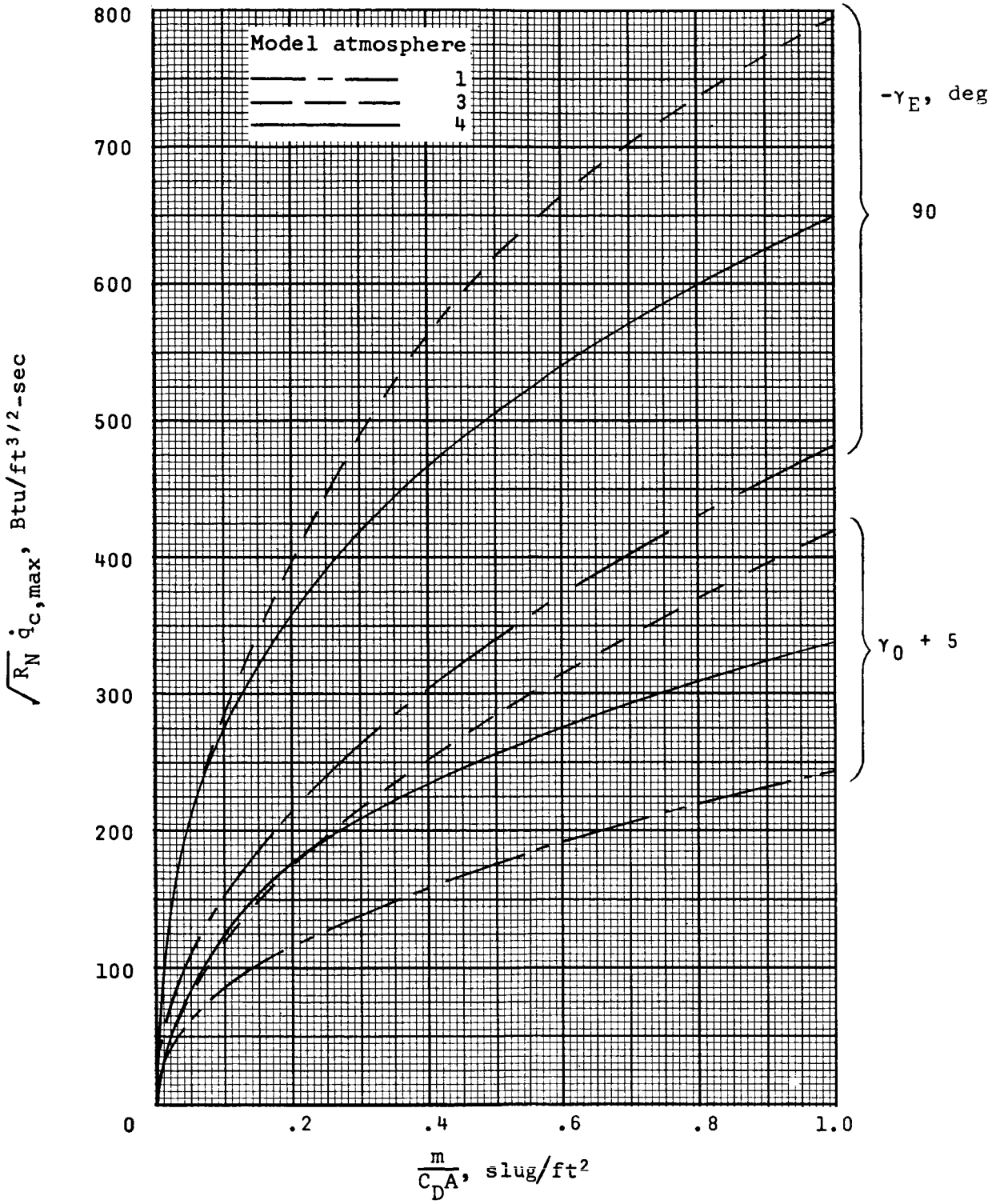

Figure 16.- Effect of atmospheric model on maximum convective heating rates for steep and shallow entry. L/D = 0; V_E = 26 000 fps. (γ_O = Overshoot boundary; see fig. 9.)

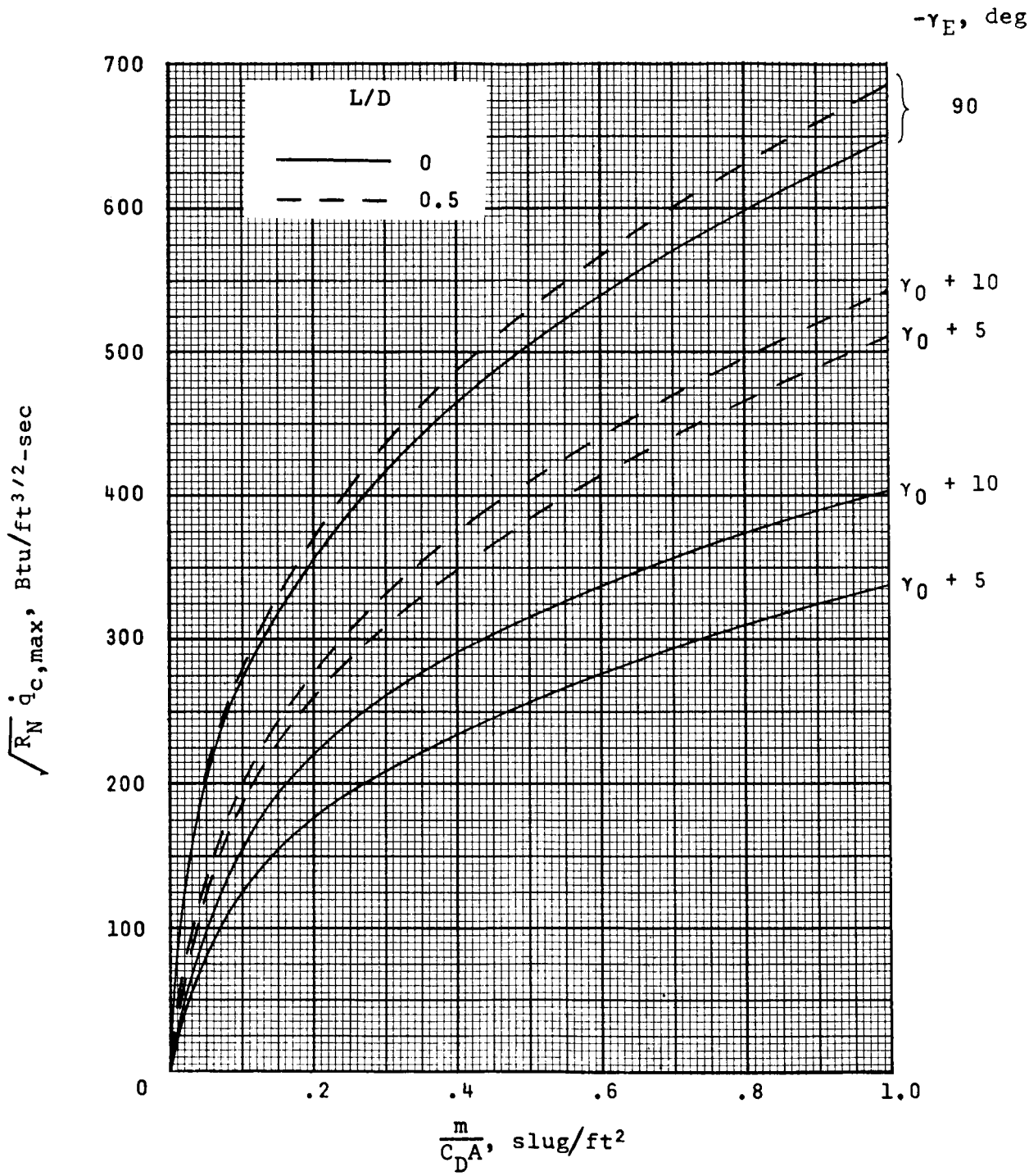

Figure 17.- Effect of lift on maximum convective heating rates for steep and shallow entry in model atmosphere 4 at V_E = 26 000 fps. (γ_0 = Overshoot boundary; see fig. 9.)

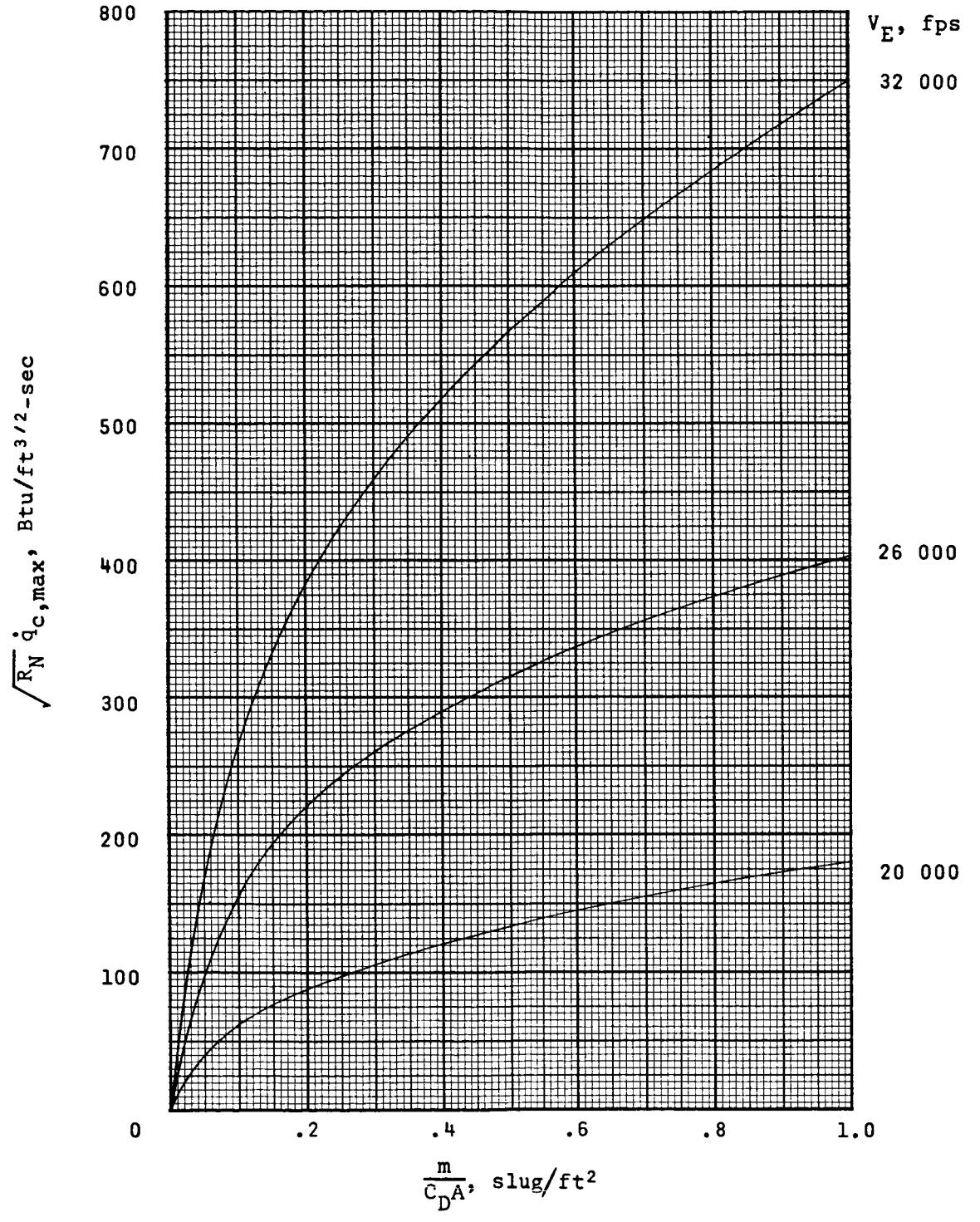

Figure 18.- Effect of entry velocity on maximum convective heating rates in model atmosphere 4. L/D = 0; $-\gamma_E = \gamma_0 + 10^o$.

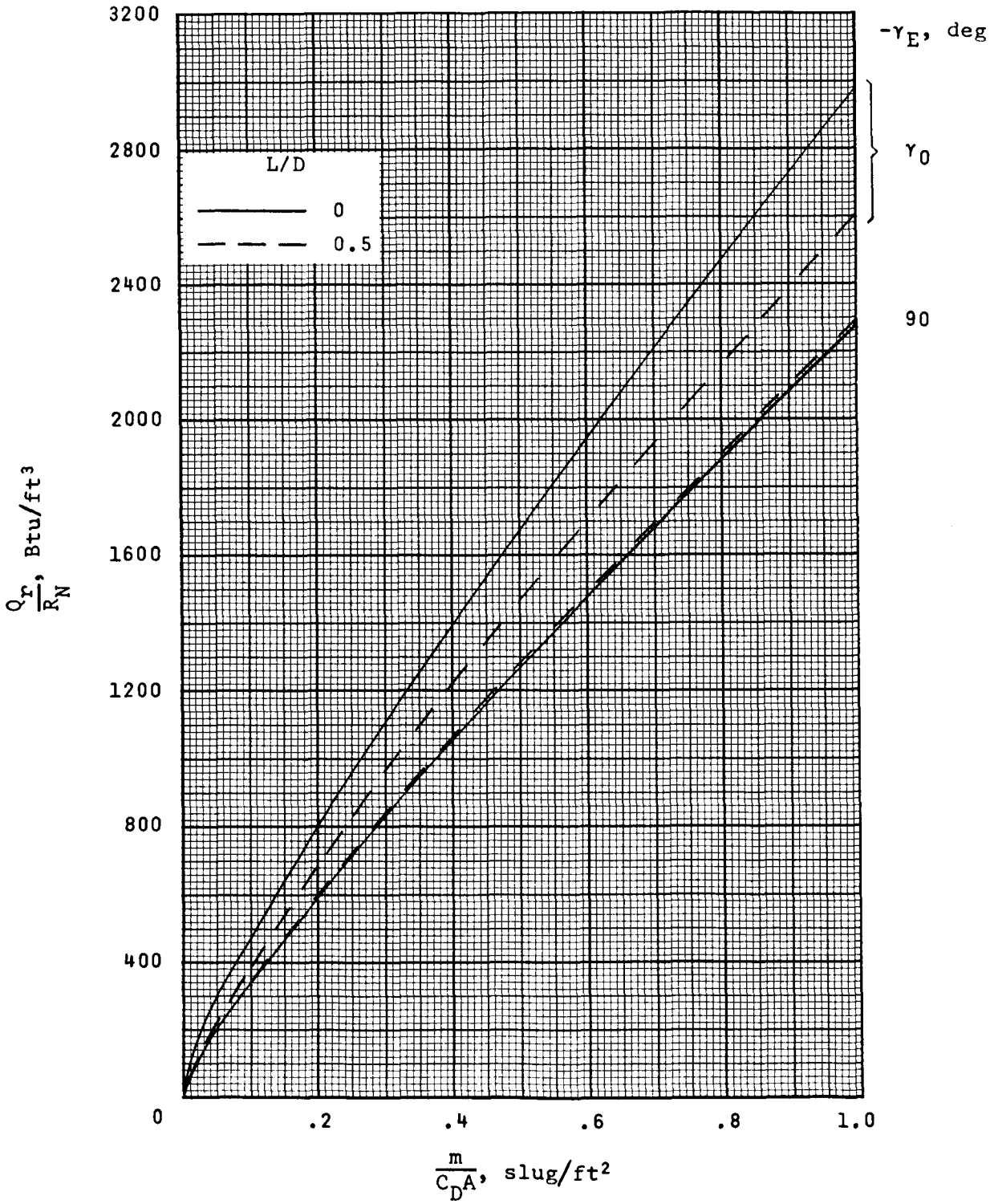

Figure 19.- Effect of lift on radiative heating load for steep and shallow entry in model atmosphere 1 at V_E = 26 000 fps. (γ_0 = Overshoot boundary; see fig. 9.)

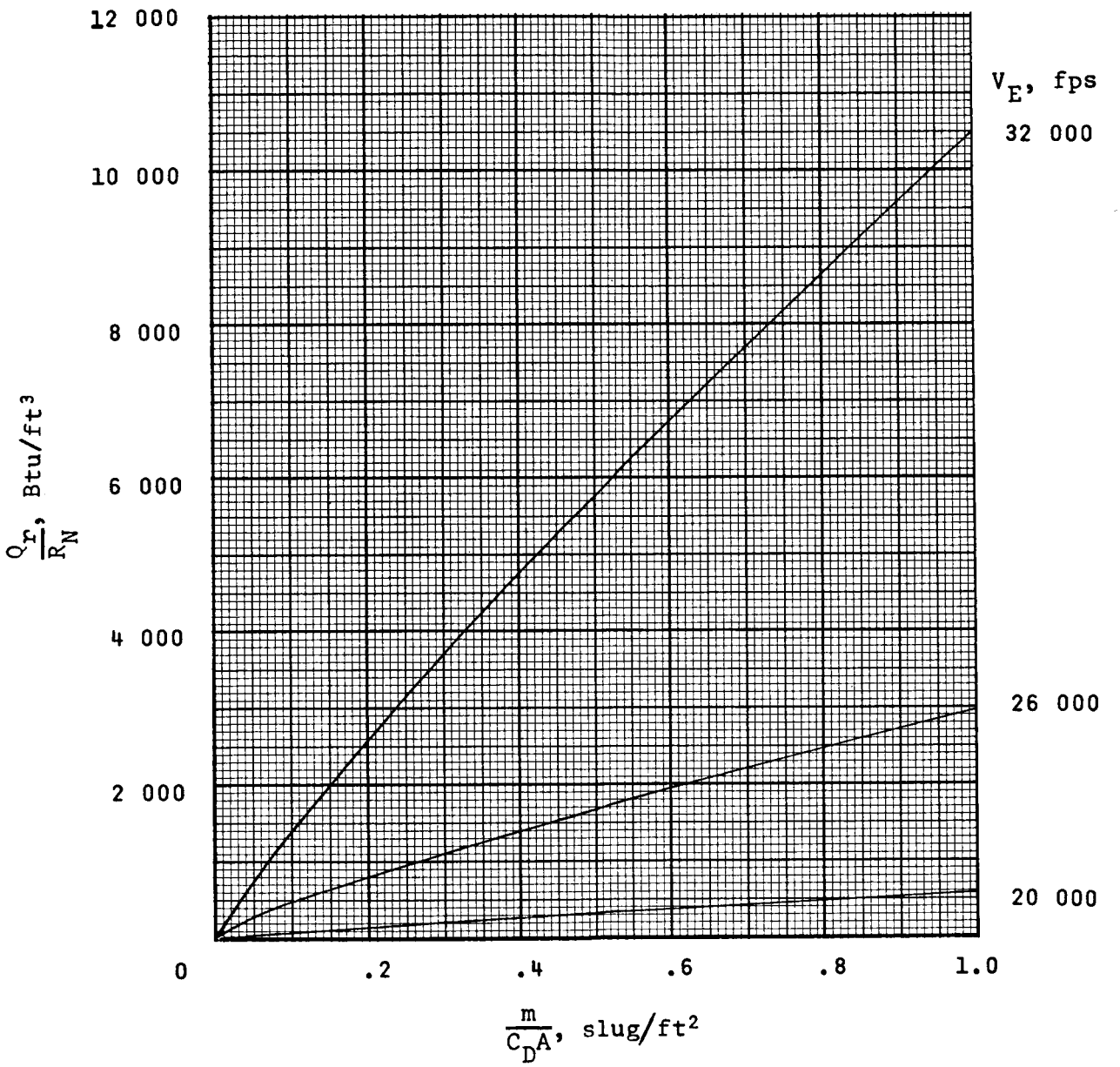

Figure 20.- Effect of entry velocity on radiative heating load for entry at overshoot boundary in model atmosphere 1. L/D = 0.

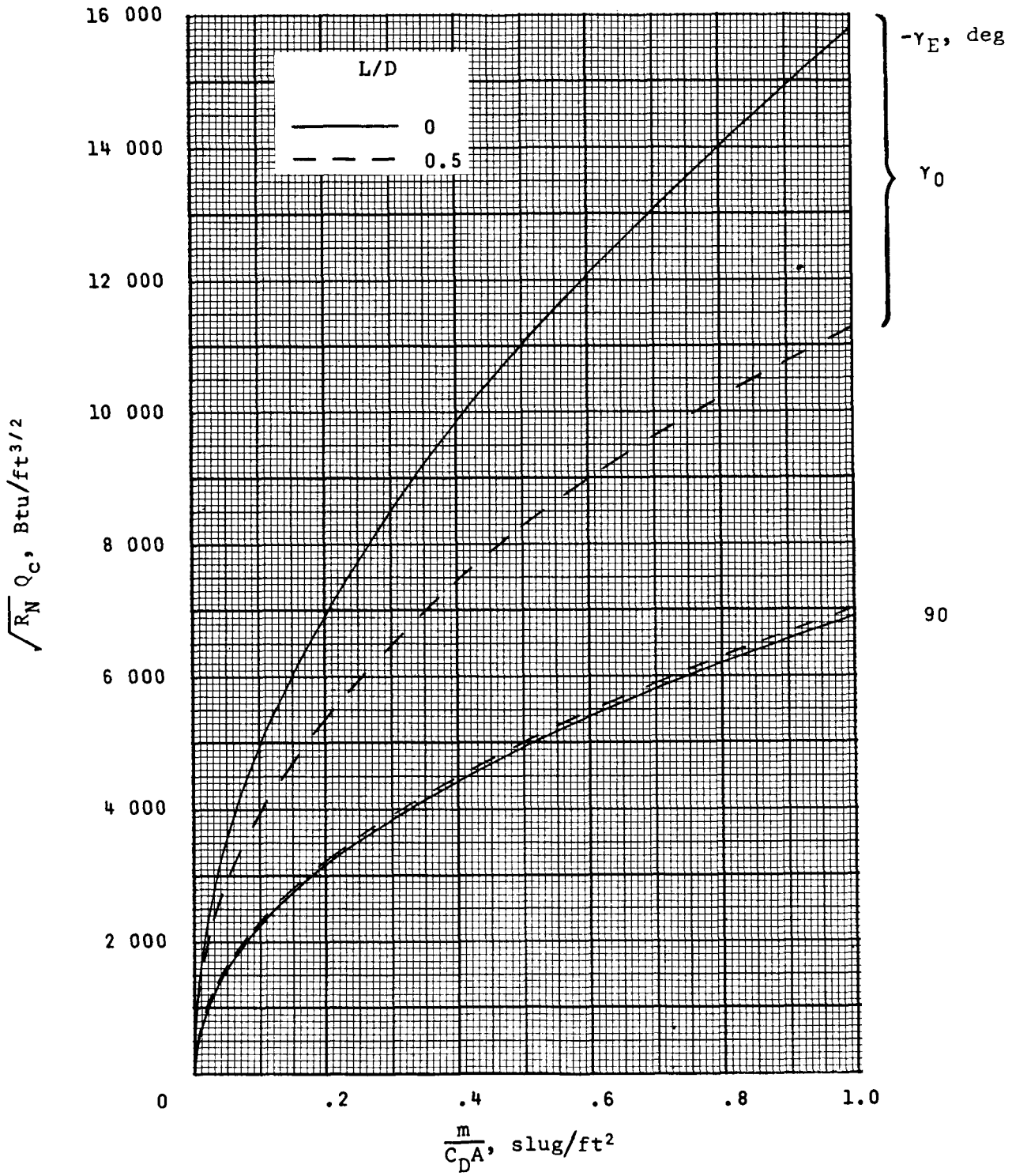

Figure 21.- Effect of lift on convective heating load for steep and shallow entry in model atmosphere 1 at V_E = 26 000 fps. (γ_0 = Overshoot boundary; see fig. 9.)

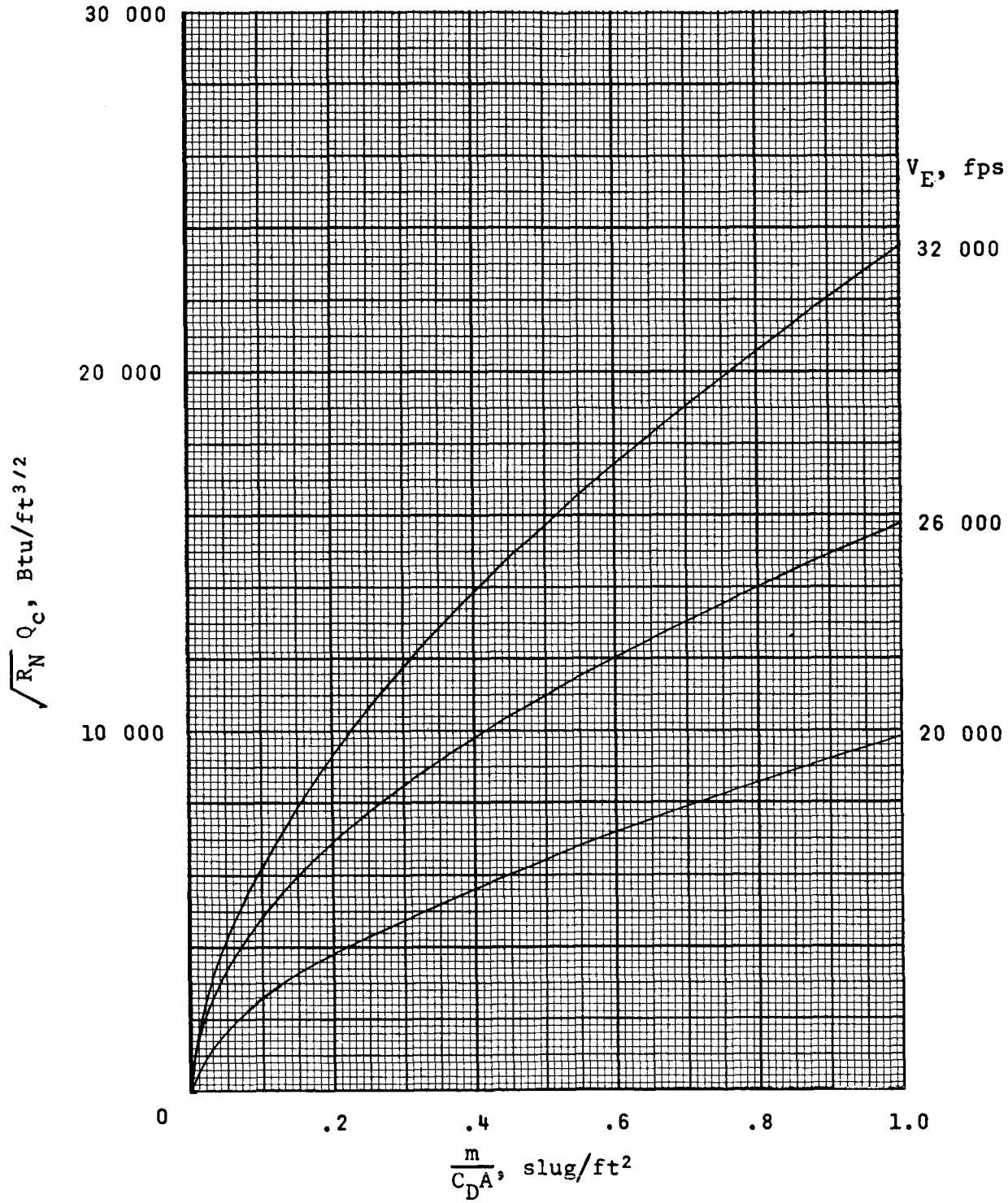

Figure 22.- Effect of entry velocity on convective heating load for entry at overshoot boundary in model atmosphere 1. L/D = 0.

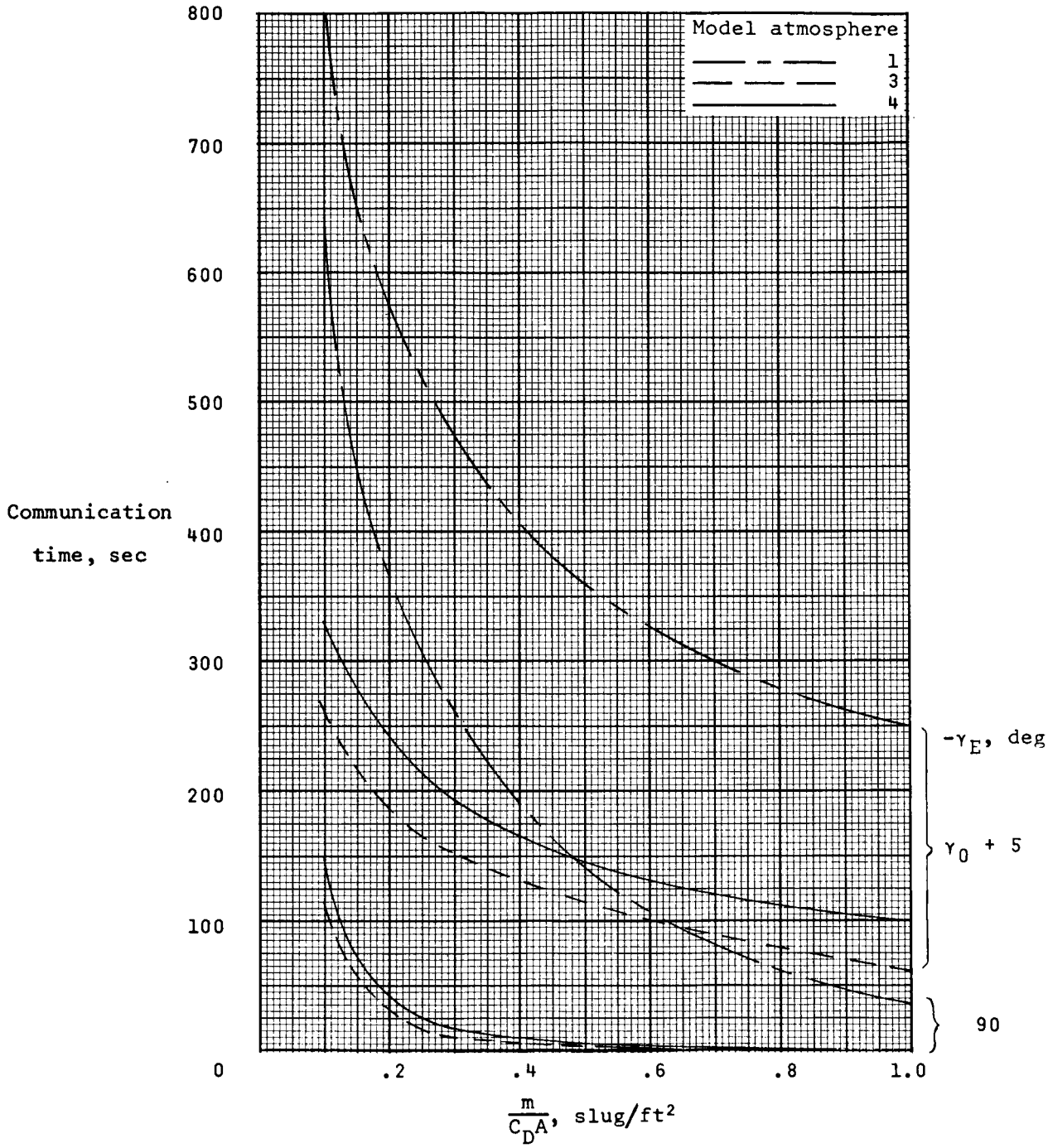

Figure 23.- Effect of atmospheric model on communication time for an atmospheric probe. L/D = 0; V_E = 26 000 fps. (γ_0 = Overshoot boundary; see fig. 9.)

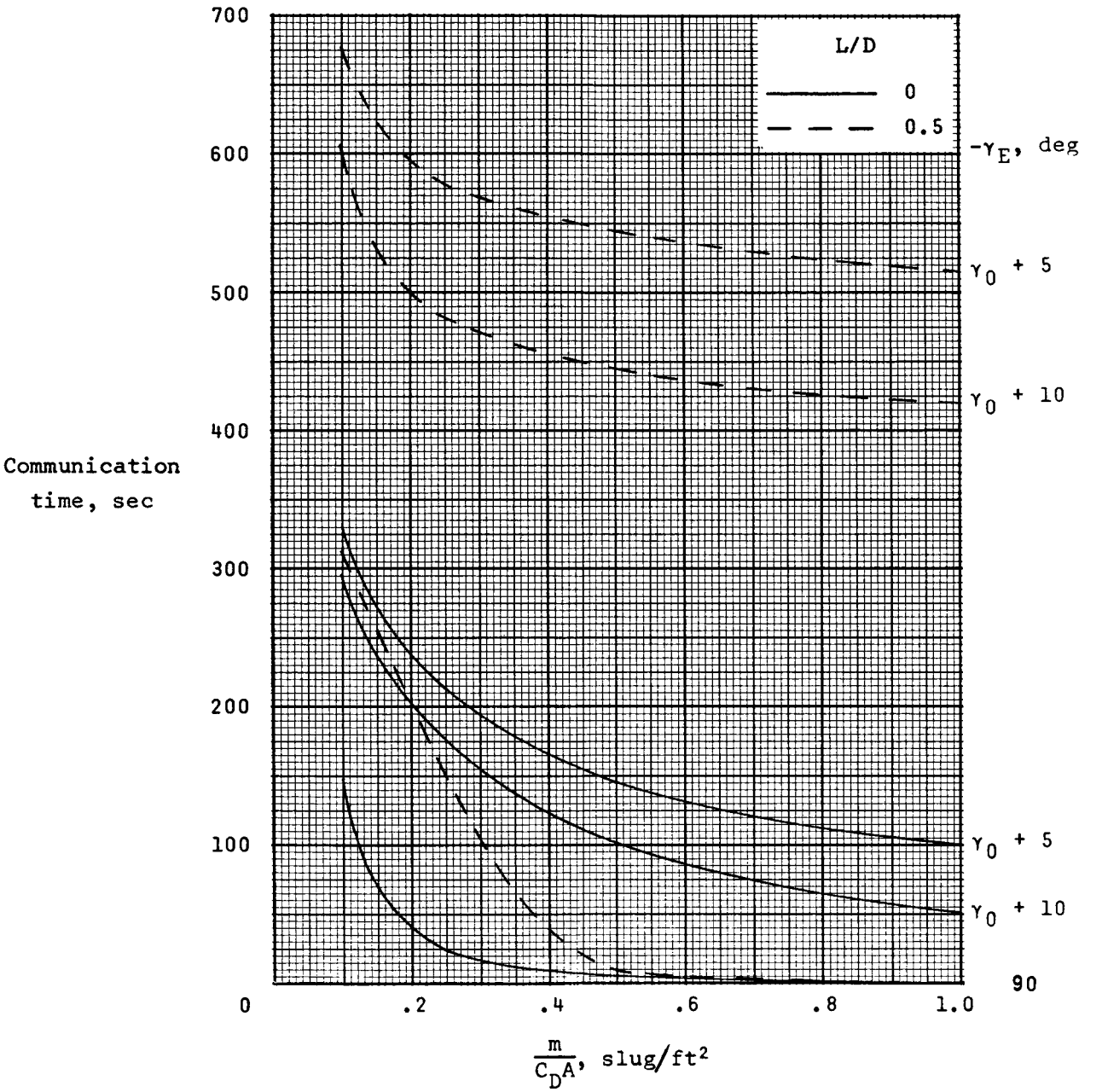

Figure 24.- Effect of lift on communication time for an atmospheric probe in model atmosphere 4 at V_E = 26 000 fps. (γ_0 = Overshoot boundary; see fig. 9.)

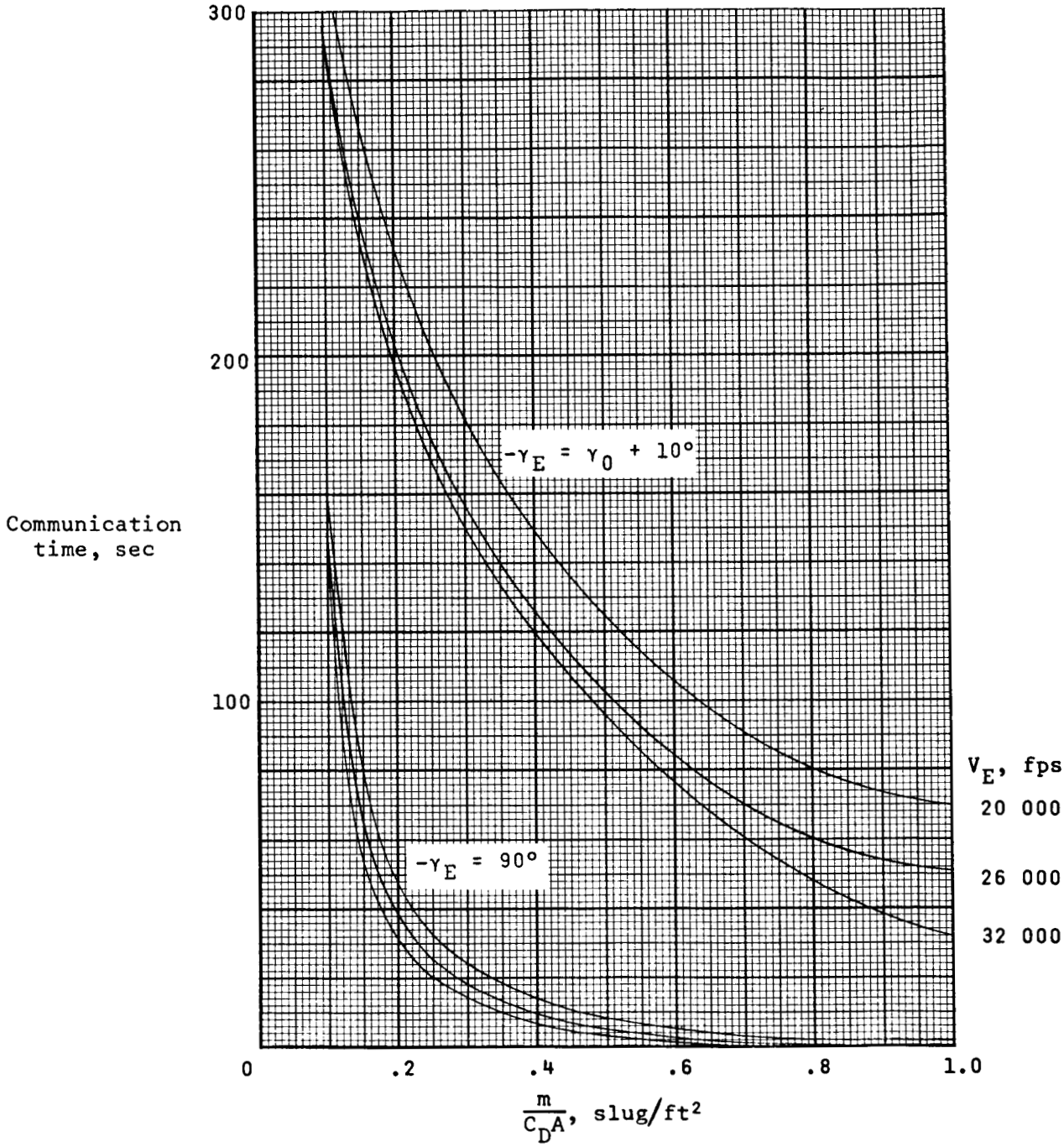

Figure 25.- Effect of entry velocity on communication time for an atmospheric probe in model atmosphere 4. L/D = 0. (γ_0 = Overshoot boundary; see fig. 9.)

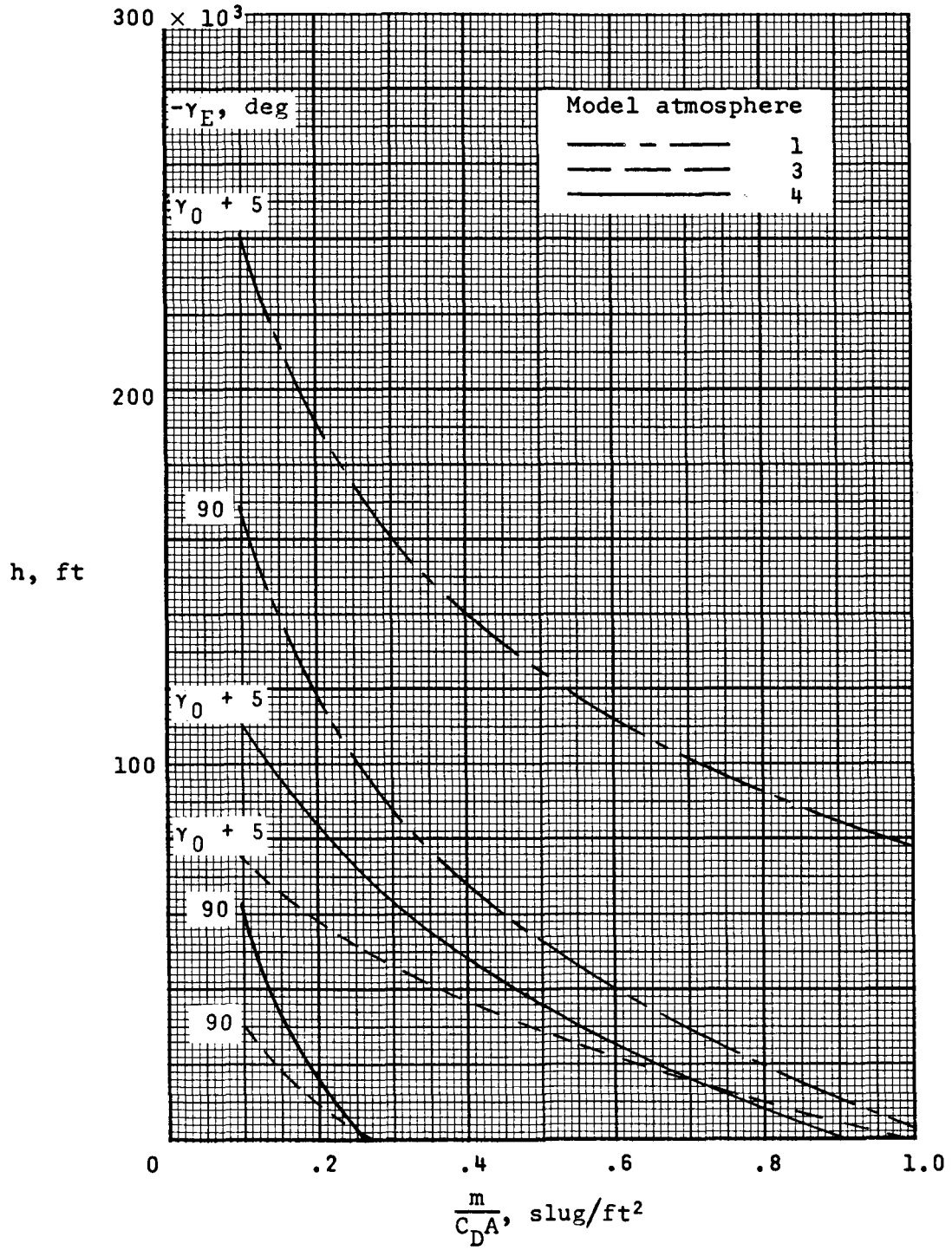

Figure 26.- Effect of atmospheric model on parachute deployment altitude for steep and shallow entry. L/D = 0; V_d = 1000 fps; V_E = 26 000 fps. (γ_0 = Overshoot boundary; see fig. 9.)

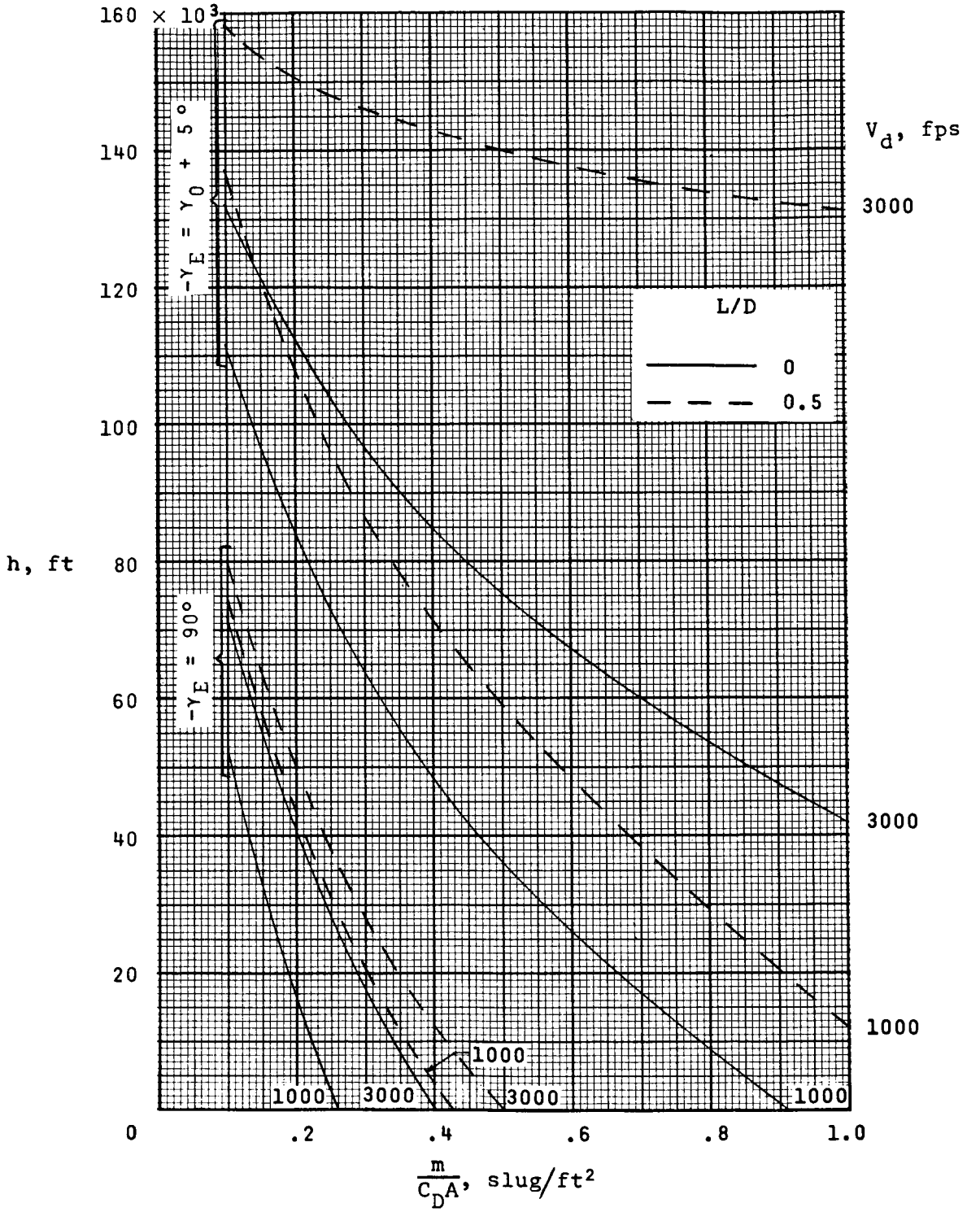

Figure 27.- Effect of lift on parachute deployment altitude for steep and shallow entry in model atmosphere 4 at V_E = 26 000 fps. (γ_O = Overshoot boundary; see fig. 9.)

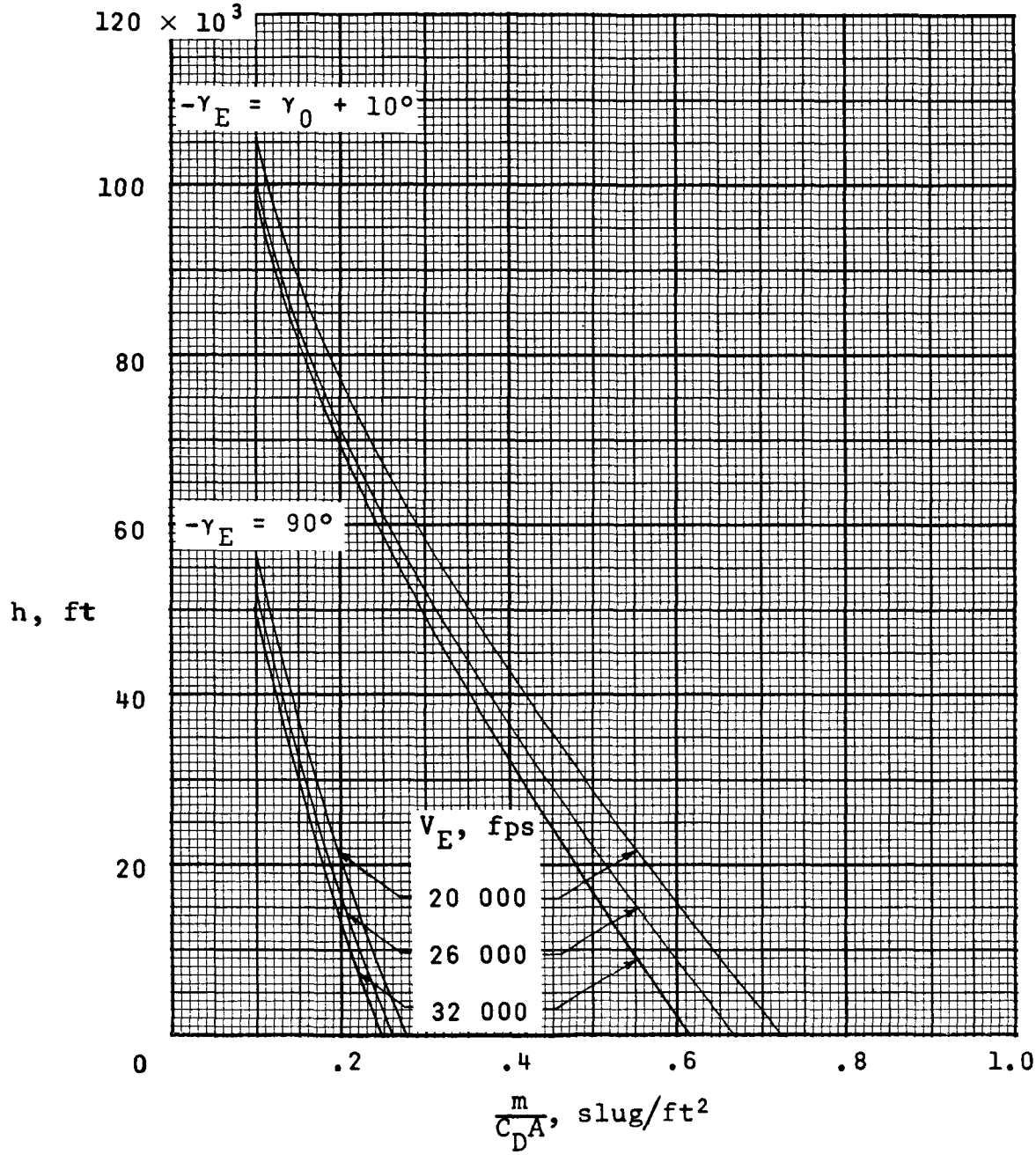

Figure 28.- Effect of entry velocity on parachute deployment altitude for steep and shallow entry in model atmosphere 4. V_d = 1000 fps; L/D = 0. (γ_0 = Overshoot boundary; see fig. 9.)

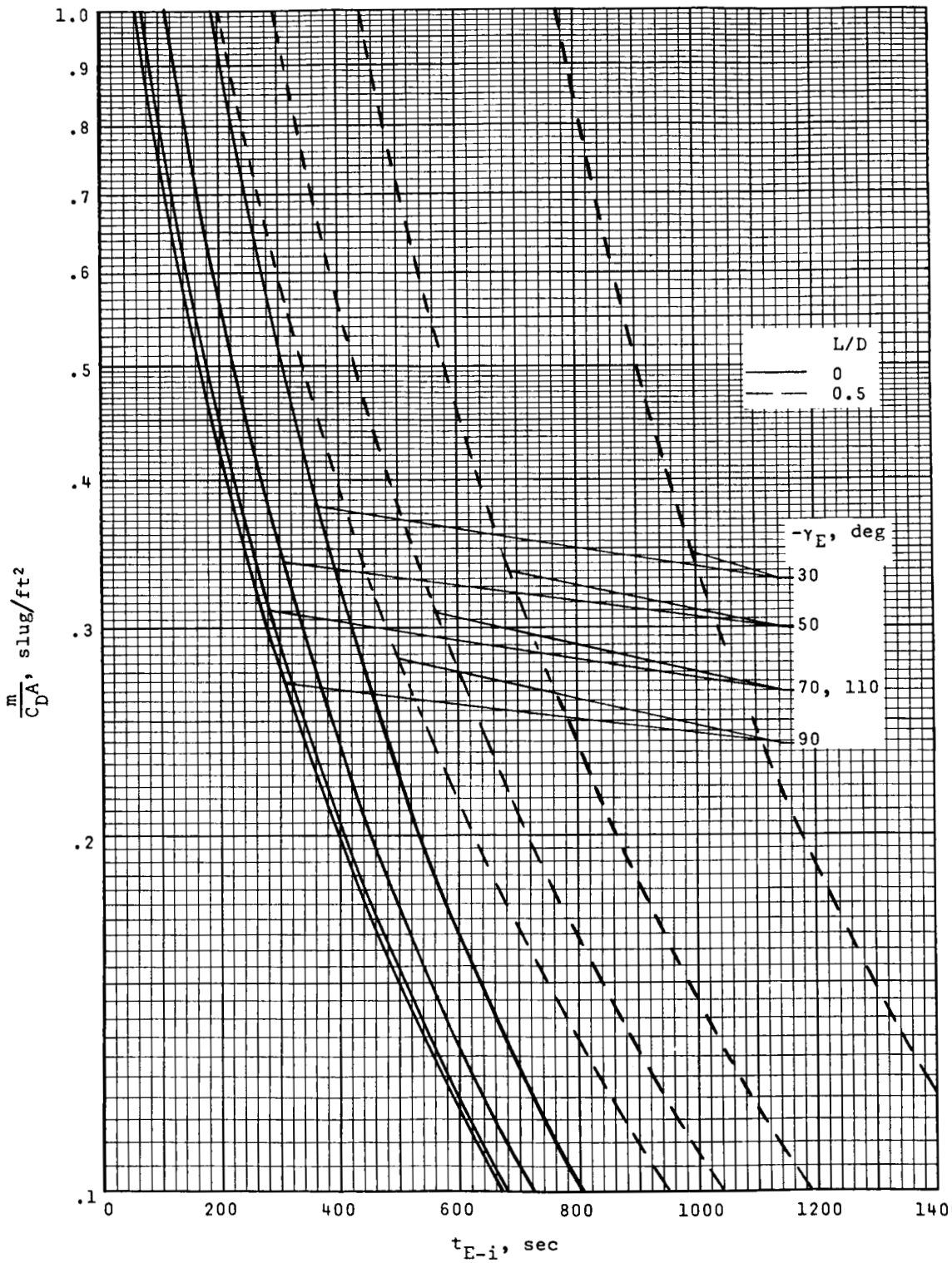

Figure 29.- Elapsed time from entry into model atmosphere 1 to impact. V_E = 26 000 fps.

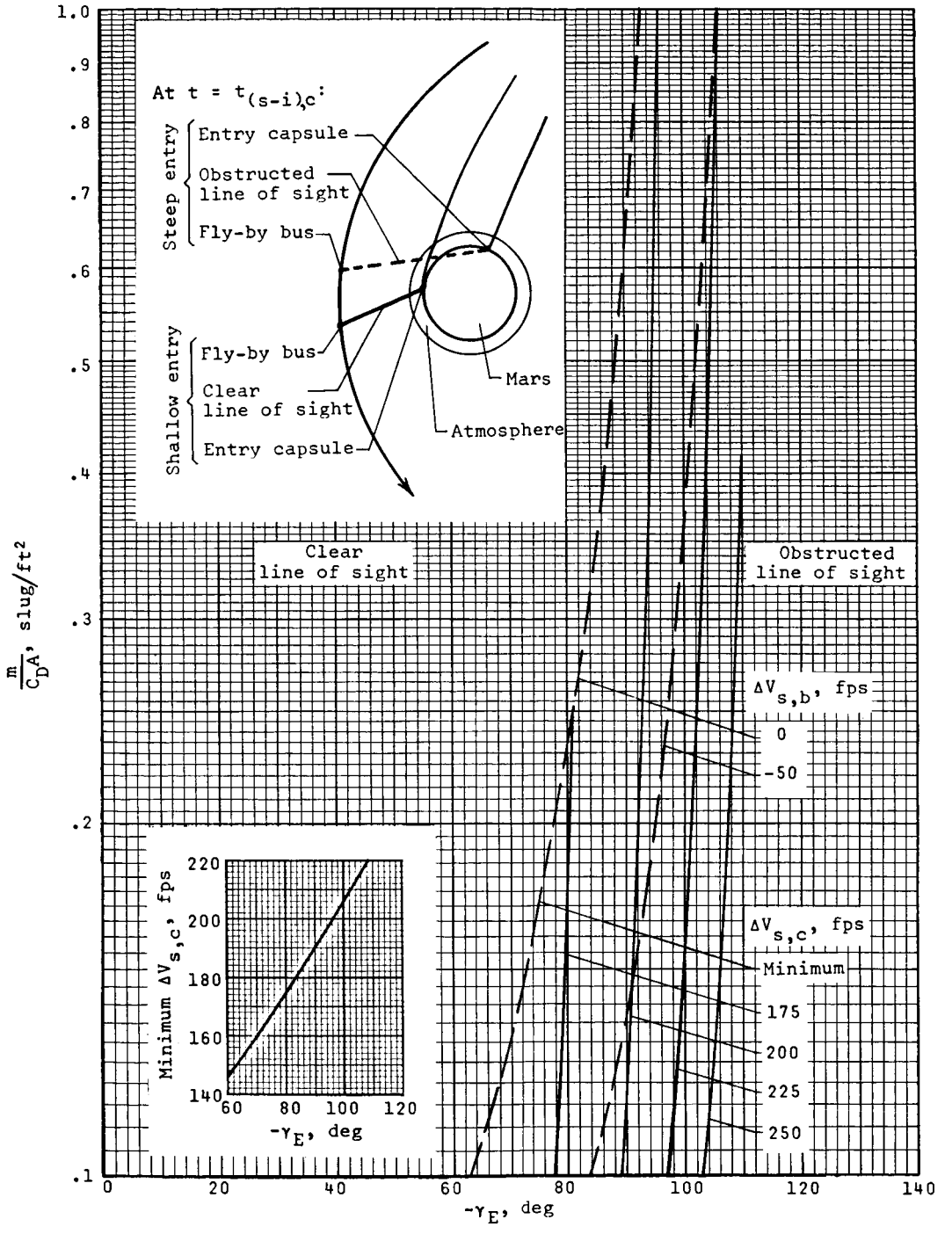

Figure 30.- Effect of separation velocity on line-of-sight communication requirements at impact for model atmosphere 1. L/D = 0; $r_{p,b}$ = 2.5 Mars radii (except when $\Delta V_{s,b}$ = -50 fps, then $r_{p,b}$ = 3.2 Mars radii); r_s = 300 Mars radii; V_∞ = 20 323 fps ($V_E \approx$ 26 000 fps).

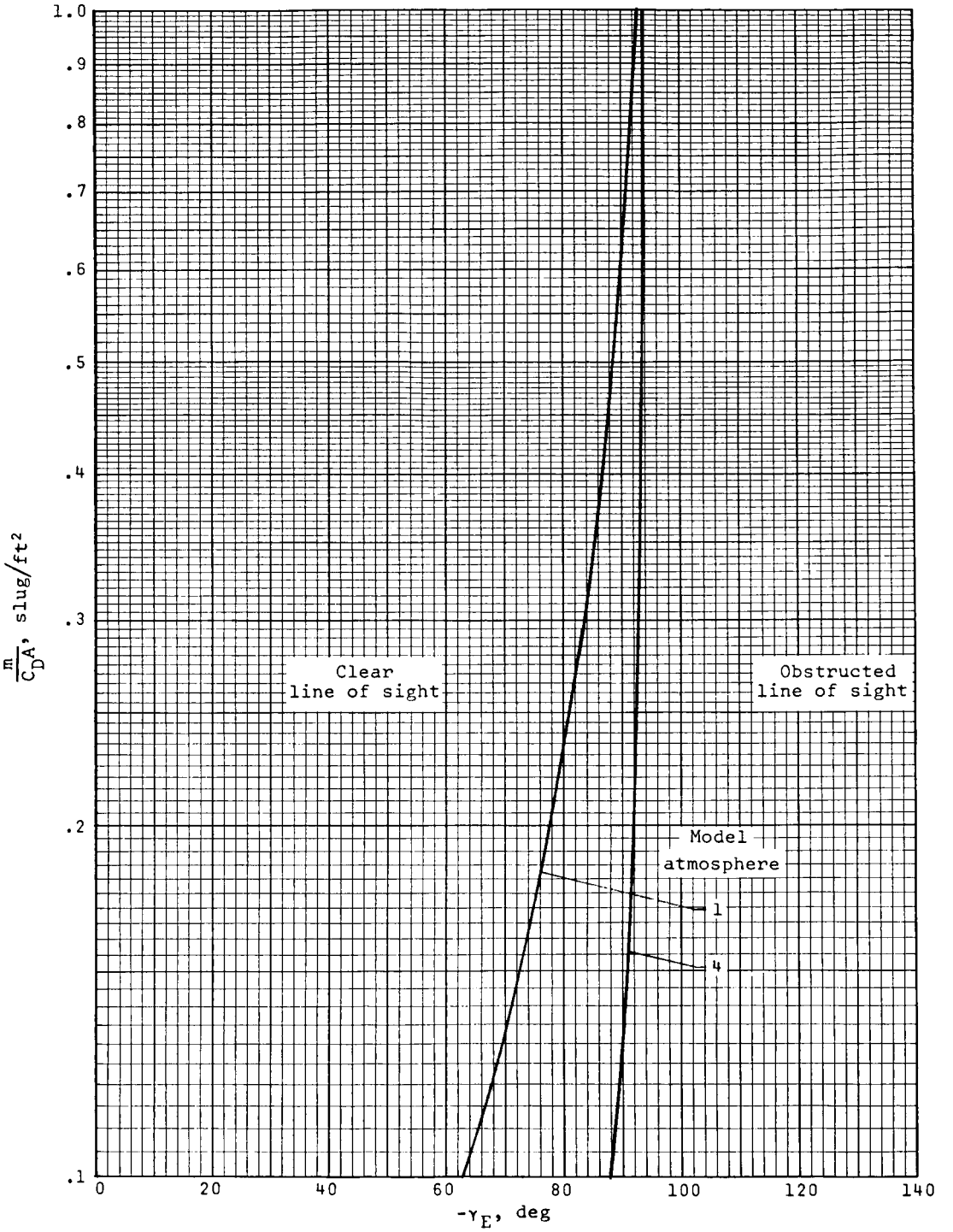

Figure 31.- Effect of atmospheric characteristics on line-of-sight communication requirements at impact. L/D = 0; $r_{p,b}$ = 2.5 Mars radii; r_s = 300 Mars radii; V_∞ = 20 323 fps ($V_E \approx$ 26 000 fps); $\lambda_s = 90^\circ$.

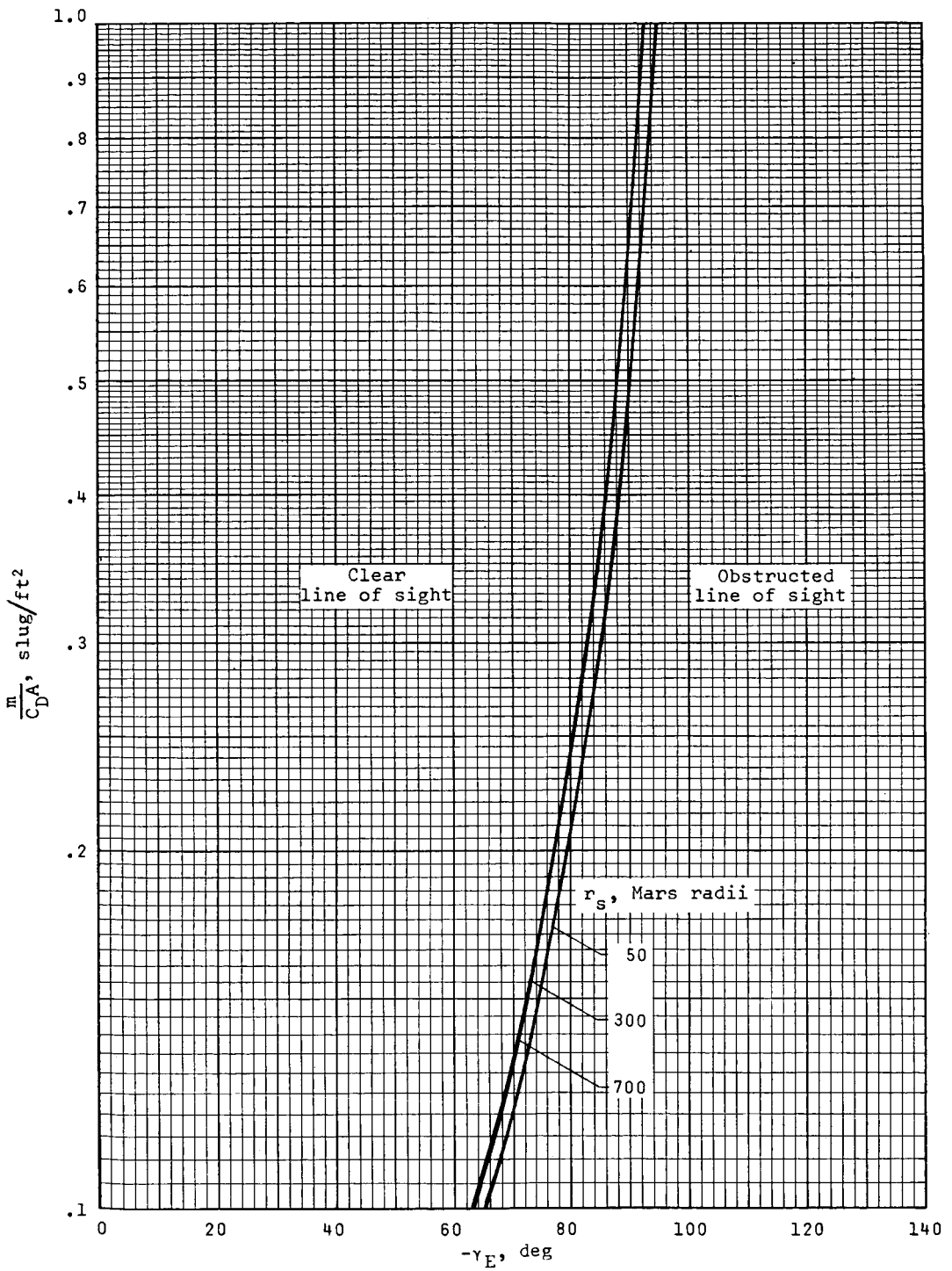

Figure 32.- Effect of separation distance on line-of-sight communication requirements at impact for model atmosphere 1. $L/D = 0$; $r_{p,b} = 2.5$ Mars radii; $V_\infty = 20\ 323$ fps ($V_E \approx 26\ 000$ fps); $\lambda_s = 90^\circ$.

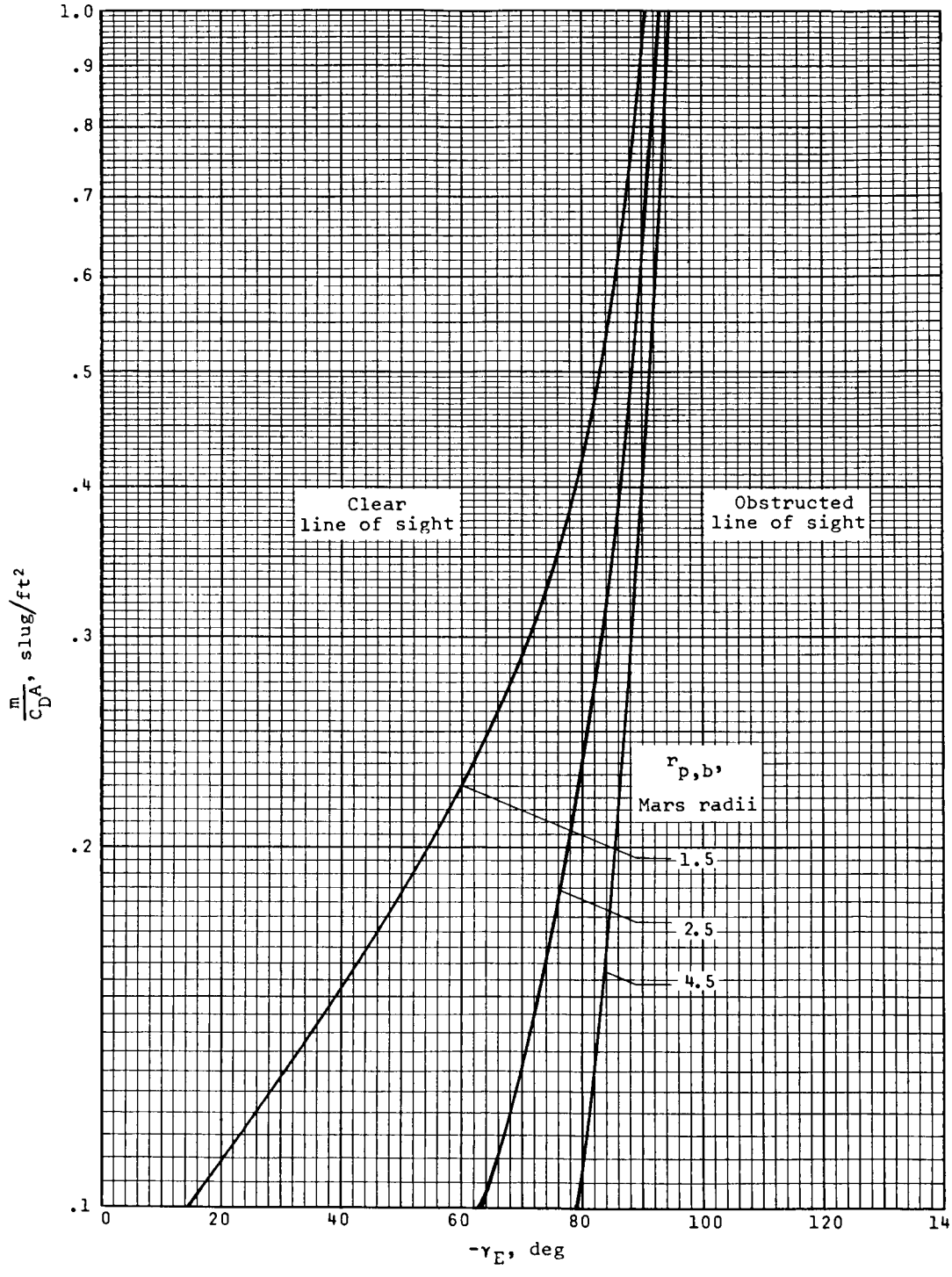

Figure 33.- Effect of bus periapsis distance on line-of-sight communication requirements at impact for model atmosphere 1. L/D = 0; r_s = 300 Mars radii; V_∞ = 20 323 fps ($V_E \approx$ 26 000 fps); $\lambda_s = 90^\circ$.

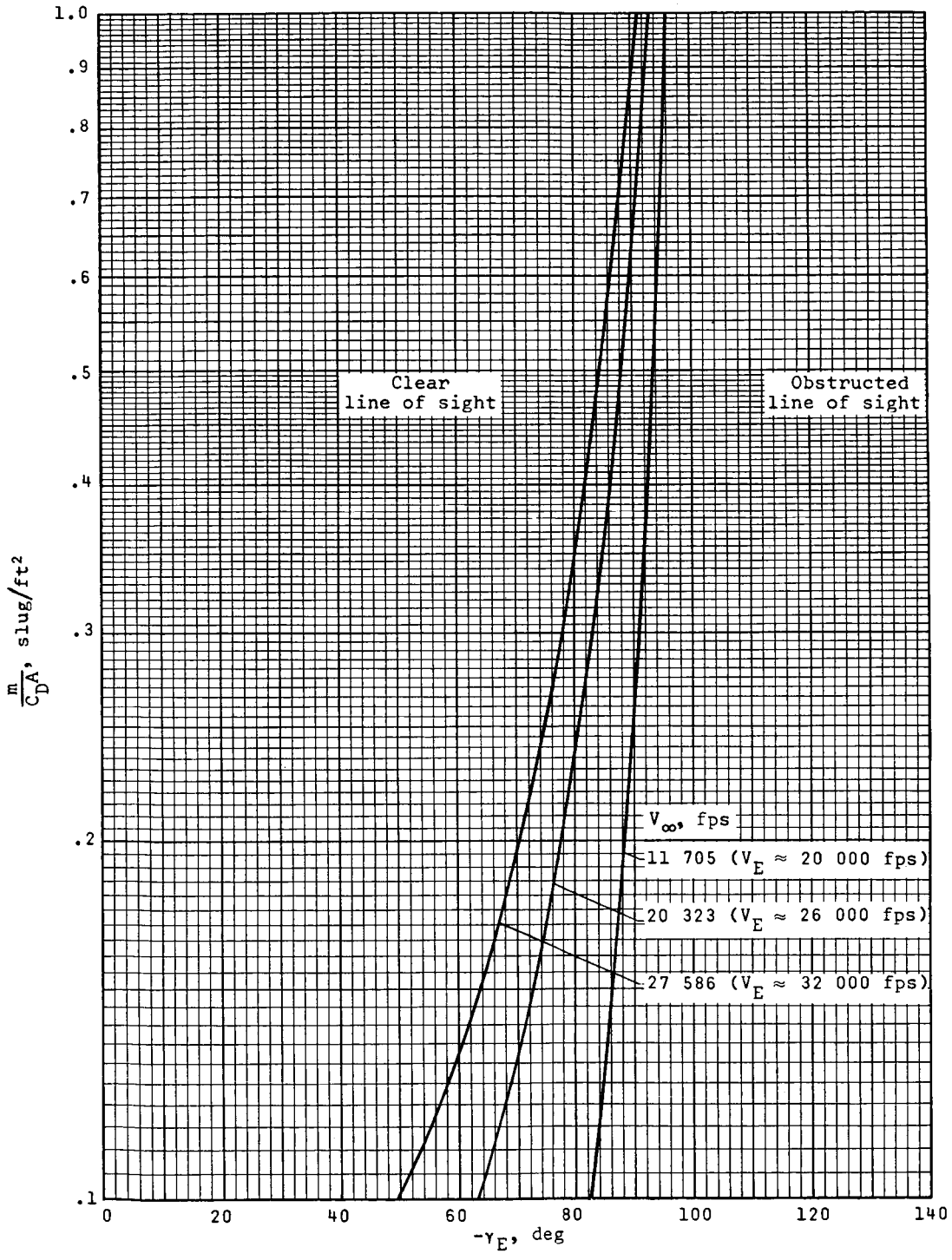

Figure 34.- Effect of hyperbolic excess velocity on line-of-sight communication requirements at impact for model atmosphere 1. L/D = 0; $r_{p,b}$ = 2.5 Mars radii; r_s = 300 Mars radii; $\lambda_s = 90^\circ$.

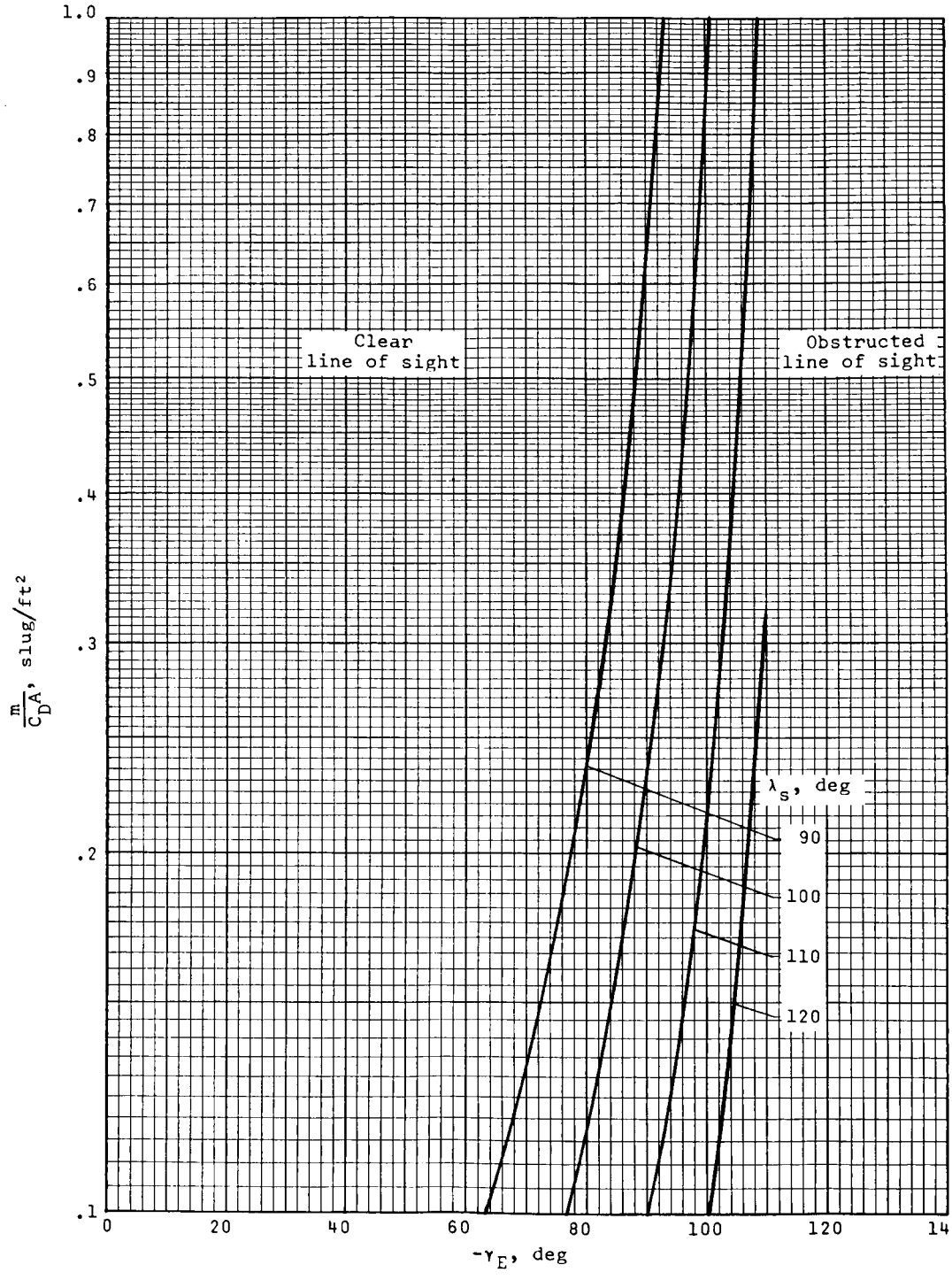

Figure 35.- Effect of separation angle on line-of-sight communication requirements at impact for model atmosphere 1. L/D = 0; $r_{p,b}$ = 2.5 Mars radii; r_s = 300 Mars radii; V_∞ = 20 323 fps ($V_E \approx$ 26 000 fps).

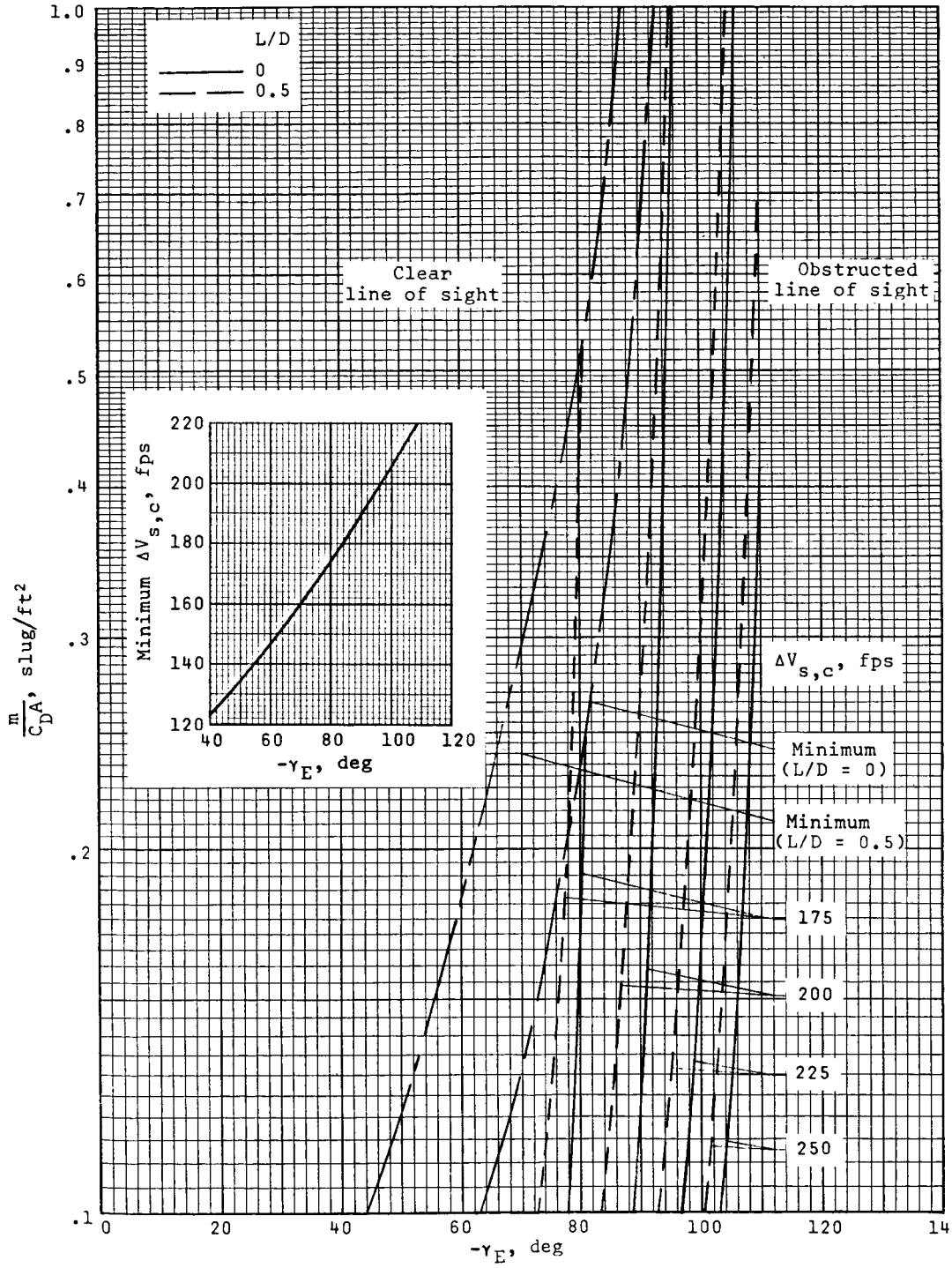

Figure 36.- Comparison of ballistic and lifting capsules in model atmosphere 1 in terms of line-of-sight communications at impact. $r_{p,b}$ = 2.5 Mars radii; r_s = 300 Mars radii; V_∞ = 20 323 fps ($V_E \approx$ 26 000 fps).

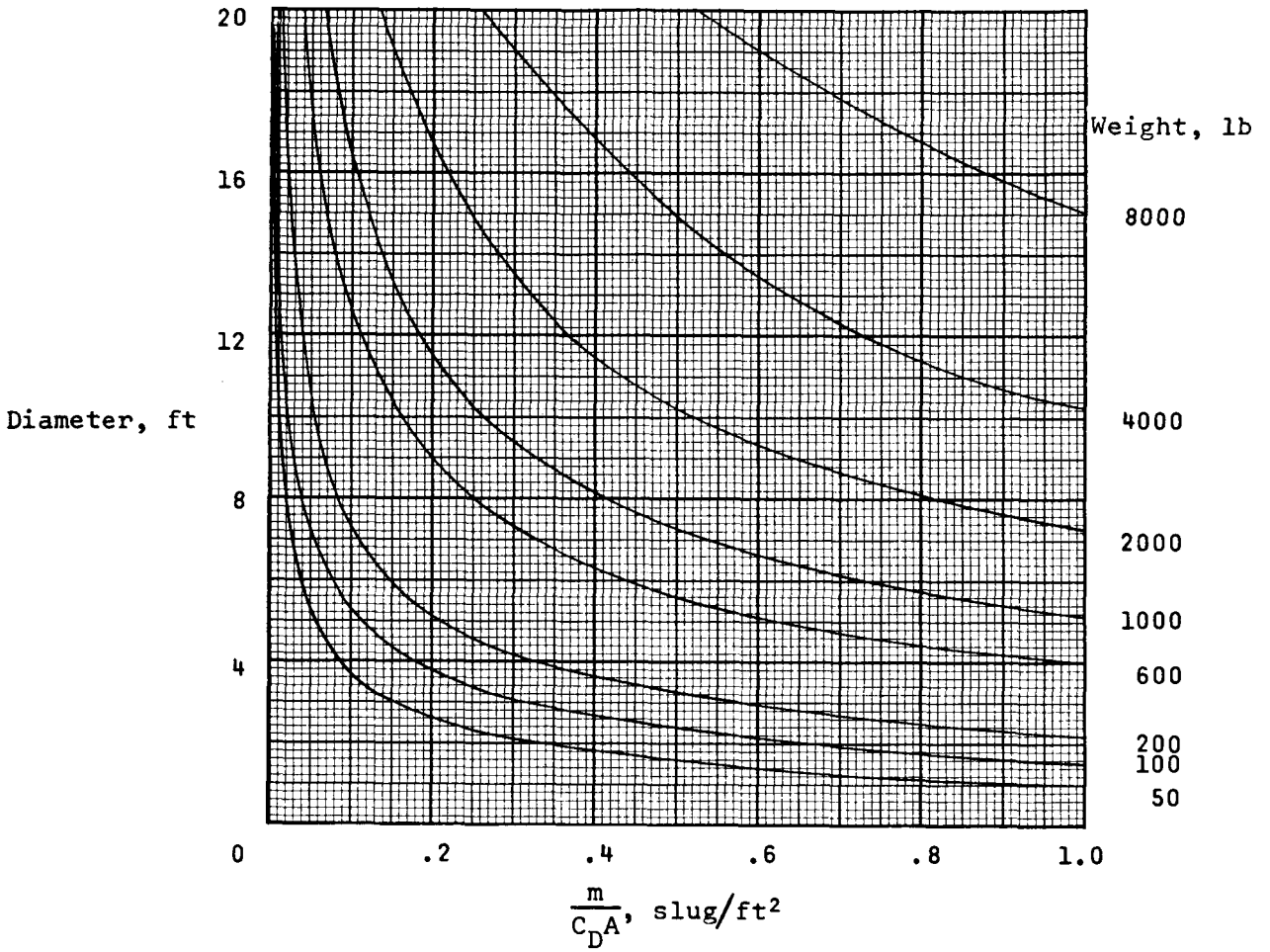

Figure 37.- Typical effects of weight and size on ballistic parameter. $C_D = 1.5$.

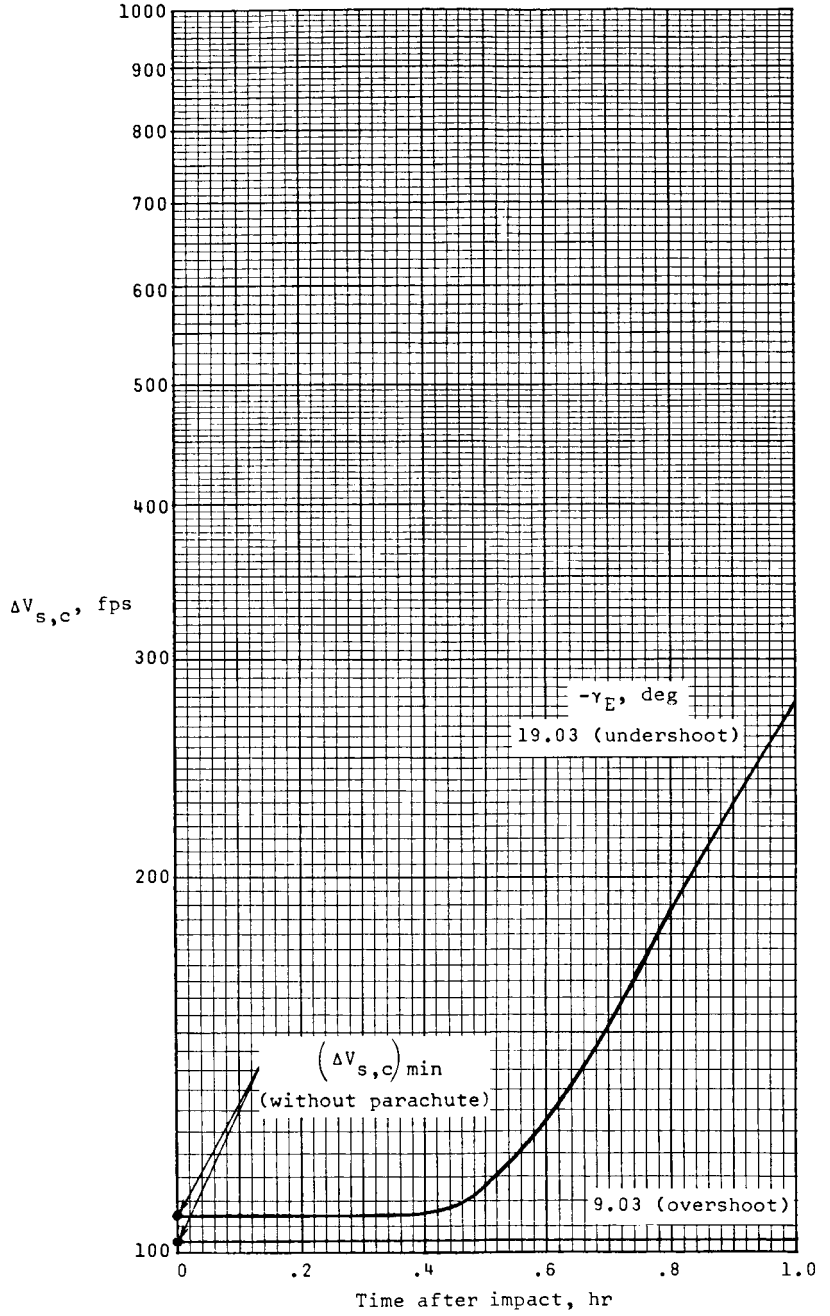

(a) $\frac{m}{C_D A} = 0.40$ slug/ft^2.

Figure 38.- Separation velocity for a particular mission requiring a clear line of sight after impact for model atmosphere 1. L/D = 0; $r_{p,b}$ = 2.5 Mars radii; r_s = 300 Mars radii; V_∞ = 20 323 fps ($V_E \approx$ 26 000 fps).

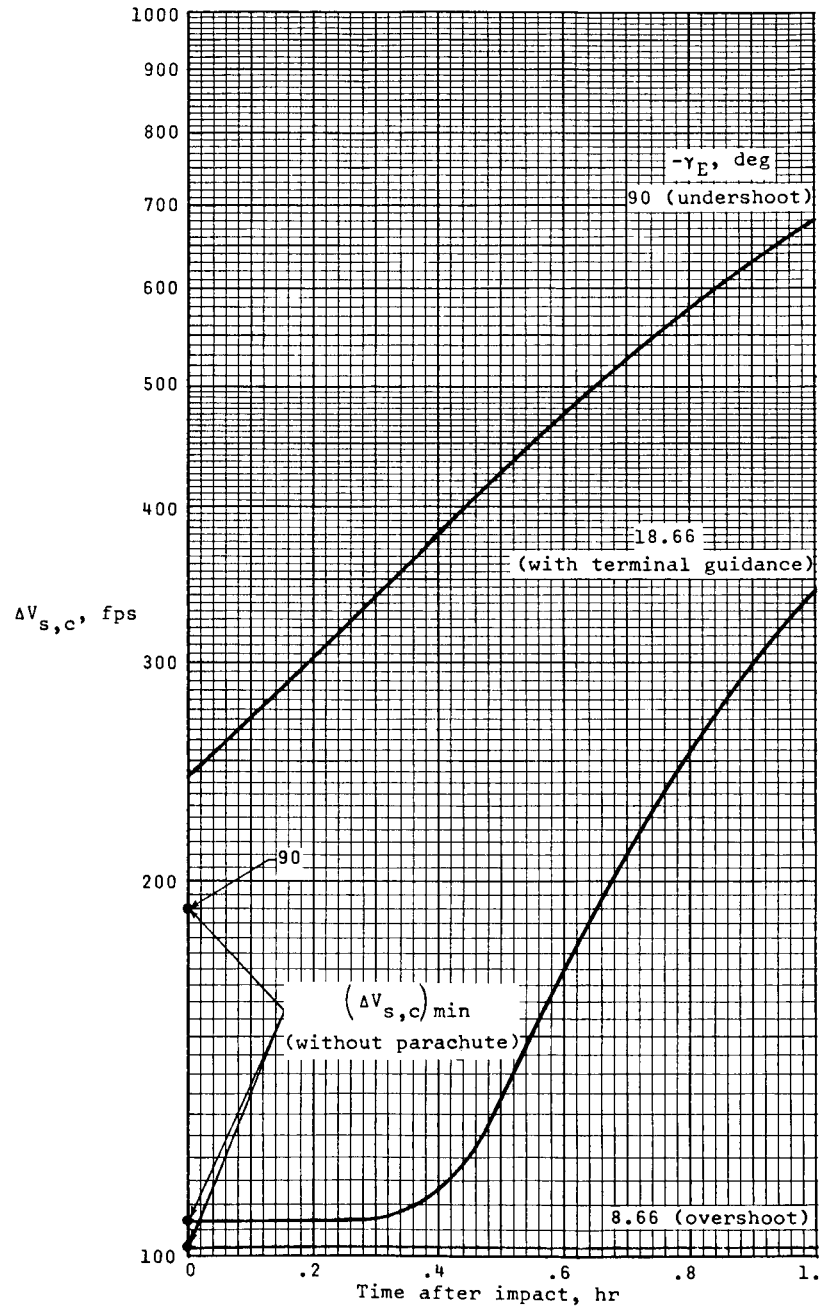

(b) $\frac{m}{C_D A} = 0.18$ slug/ft^2.

Figure 38.- Concluded.